WVMP SAR Reference 3-26

Thermodynamics of the Liquid State: Generalized Predictions of Properties," K. M. Watson, Ind. Eng. Chem., 35(4), 398-406, 1943

Thermodynamics of the Liquid State

GENERALIZED PREDICTION OF PROPERTIES

K. M. Watson
UNIVERSITY OF WISCONSIN, MADISON, WIS.

On the basis of a modified application of the theorem of corresponding states, new methods are presented for the general prediction of the following thermodynamic properties of liquids: thermal expansion and compressibility, pressure correction to enthalpy, pressure correction to entropy, pressure correction to heat capacity at constant pressure, heat of vaporization, difference between heat capacity of a saturated liquid and its ideal gas, and difference between heat capacity of saturated liquid and heat capacity at constant pressure. The only data required are the boiling point, the critical temperature, critical pressure, and the liquid density at some one temperature.

Like all applications of the theorem of corresponding states, these relations are not rigorously correct. However, deviations from the available experimental data on a variety of compounds, both polar and nonpolar, are sufficiently small to warrant their use for many process problems where reliable data are not available, and for rationalizing fragmentary experimental data.

DURING the past ten years much attention has been directed (*2, 4, 7, 8, 10, 23–26*) toward the development of generalized relations which permit prediction of the thermodynamic properties of the gaseous state, even at extreme conditions of temperature and pressure, with accuracy sufficient for general engineering purposes. The similar properties of the liquid state have received little attention because of their lesser importance and because of the failure of the theorem of corresponding states to directly correlate liquid properties with accuracy. However, by a modified application of this theorem it is possible to correlate liquid properties with a degree of accuracy similar to the correlations of the gas phase.

THERMAL EXPANSION AND COMPRESSIBILITY

The equation of state for the gaseous phase is ordinarily written,

$$pv = zRT \tag{1}$$

where z, the compressibility factor, is a function of reduced temperature and pressure, approximately the same for all substances. If this relation were applied to the liquid state, an expression for liquid density might be written,

$$\rho = \frac{pM}{zRT} = \left(\frac{p_r}{zRT_r}\right)\frac{P_cM}{T_c} = \omega\frac{P_cM}{T_c} \tag{2}$$

where ω, which might be termed the "expansion" factor, would be a function only of reduced temperature and pressure.

Unfortunately it is found that factor ω of Equation 2 is not a generalized function of reduced conditions. Values of ω at the same reduced conditions may vary by more than 20 per cent for different compounds. Accordingly, Equation 2 is a rough approximation useful only where no direct liquid density data of any type are available.

Since at least one value of liquid density is available for almost any compound, a more useful relation results by applying Equation 2 to obtain an expression for the ratio of the density at any given condition to that at some reference state designated by subscript 1:

$$\frac{\rho}{\rho_1} = \frac{\omega}{\omega_1}$$

$$\text{or } \rho = \frac{\rho_1}{\omega_1}\omega \tag{3}$$

It has been found that if ω is evaluated as a function of reduced temperature and reduced pressure for one compound on which complete data are available, Equation 3 may be used with satisfactory accuracy for predicting the densities of any other compound for which one liquid density value is available to establish ρ_1/ω_1.

Table I. Values of Expansion Factor ω

	Expansion Factor ω							
T_r	$P_r = 0$	$P_r = 0.4$	$P_r = 0.8$	$P_r = 1.0$	$P_r = 1.5$	$P_r = 2$	$P_r = 3$	$P_r = 5$
0.5	(0.1328)	....	....	0.1332	....	0.1338	....	0.1350
0.6	0.1242	....	....	0.1250	....	0.1258	....	0.1275
0.7	0.1144	0.1150	....	0.1158	....	0.1170	0.1182	0.1202
0.8	0.1028	0.1042	0.1050	0.1056	0.1070	0.1077	0.1098	0.1125
0.9	....	0.0900	0.0915	0.0926	0.0949	0.0968	0.1002	0.1043
0.95	....	....	0.0810	0.0831	0.0872	0.0902	0.0943	0.1000
1.0	....	....	....	0.0440	0.0764	0.0818	0.0875	0.0954

Figure 1 and Table I give values of ω for isopentane, calculated from the measurements of Young (*11*) and extended to higher pressures by the data of Sage and Lacey (*16, 18*) on propane and *n*-pentane and Equation 3. Tables II and III compare liquid densities calculated from these curves and Equation 3 with experimental data from the indicated sources for compressed and saturated liquids of various polar and nonpolar types. The agreement is reasonably good with deviations, in general, less than 5 per cent, even for the case of water at 100° C. and above. The anomalous density changes of water at low temperature are not in agreement with the correlation, and selection of 4° C. as the reference conditions instead of 100° C. would increase the maximum deviations in the high-temperature range to approximately 10 per cent. In general, it is desirable to use the highest temperature at which data are available as the reference state, particularly when the high-temperature behavior of polar substances such as water are being calculated.

PRESSURE CORRECTION TO ENTHALPY

The effect of pressure on the enthalpy of any substance is expressed by the rigorous thermodynamic equation:

$$J\left(\frac{\partial H}{\partial p}\right)_T = V - T\left(\frac{\partial V}{\partial T}\right)_p \qquad (4)$$

Rearranging in terms of reduced conditions,

$$\frac{J}{P_c}\left(\frac{\partial H}{\partial p_r}\right)_T = V - T_r\left(\frac{\partial V}{\partial T_r}\right)_p \qquad (5)$$

Combining Equations 3 and 5,

$$\frac{J\rho_1}{P_c\omega_1}\left(\frac{\partial H}{\partial p_r}\right)_T = \frac{1}{\omega} - T_r\left(\frac{\partial \frac{1}{\omega}}{\partial T_r}\right)_p \qquad (6)$$

Through Equation 6 the group

$$\frac{J\rho_1}{P_c\omega_1}\left(\frac{\partial H}{\partial p_r}\right)_T$$

may be expressed as a general function of reduced temperature and pressure by the graphical differentiation of Figure 1, remembering that $\partial(1/\omega) = -(\partial\omega/\omega^2)$. The results of this operation are summarized in Figure 2 and Table IV for the range of conditions not close to the critical point.

The effect of pressure on enthalpy may be expressed in a more useful form by graphically integrating Equation 6 to obtain the differences between the enthalpy of a liquid under

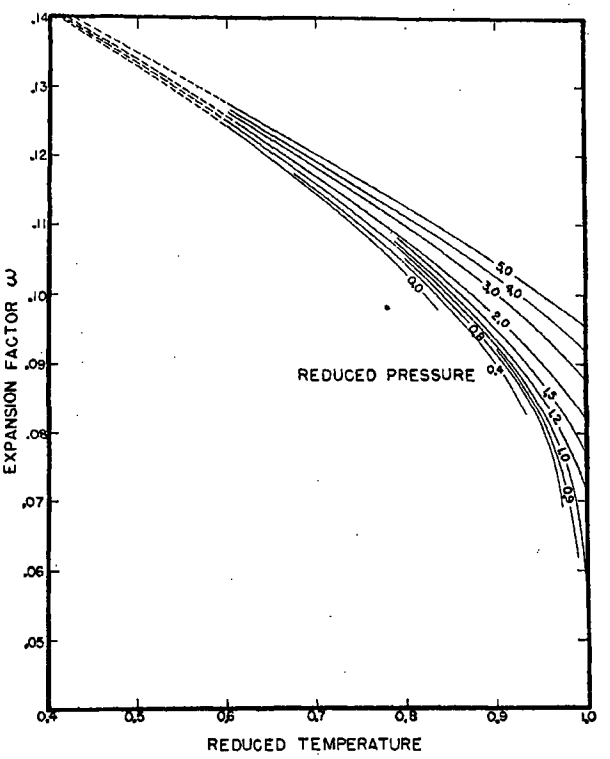

Figure 1. Thermal Expansion and Compressibility of Liquids

Table II. Densities of Compressed Liquids

Pressure, Lb./Sq. In.	Reduced Pressure	Density, Gram/Cc. Calcd.	Exptl.	Calcd.	Exptl.	Calcd.	Exptl.
WATER (*18*): $\rho_1/\omega_1 = 7.586$ AT 100° C., 1 ATM.		204.4° C., $T_r = 0.738$		348.9° C., $T_r = 0.961$		374.3° C., $T_r = 1.0$	
1000	0.312	0.842	0.864	....	....	....	....
3206	1.0	0.851	0.874	0.611	0.616	0.326	0.318
4000	1.248	0.854	0.878	0.633	0.639	0.551	0.543
5500	1.715	0.858	0.885	0.658	0.660	0.603	0.603
PROPANE (*17*): $\rho_1/\omega_1 = 4.807$ AT 21.0° C., 200 LB./SQ. IN.		54.5° C., $T_r = 0.878$		71.1° C., $T_r = 0.921$		87.9° C., $T_r = 0.966$	
300	0.466	0.453	0.447	....	....	....	....
600	0.934	0.460	0.458	0.416	0.422	0.374	0.368
1500	2.35	0.485	0.482	0.460	0.458	0.431	0.430
3000	4.66	0.508	0.506	0.489	0.489	0.469	0.470
BUTANE (*18*): $\rho_1/\omega_1 = 5.037$ AT 21.1° C., 250 LB./SQ. IN.		71.1° C., $T_r = 0.809$		104.4° C., $T_r = 0.887$		121.1° C., $T_r = 0.926$	
250	0.462	0.521	0.522	0.467	0.461	0.427	0.411
500	0.945	0.526	0.527	0.475	0.472	0.438	0.434
1500	2.84	0.546	0.545	0.508	0.501	0.487	0.475
3000	5.67	0.567	0.564	0.536	0.528	0.521	0.507

Table III. Densities of Saturated Liquids

Temperature, ° C.	Density, G./Cc. Calcd.	Exptl.	Temperature, ° C.	Density, G./Cc. Calcd.	Exptl.
AMMONIA (*21*): $\rho_1/\omega_1 = 5.463$ AT −33.3° C., SATD. PRESSURE					
−73.3	0.729	0.730	37.8	0.586	0.584
−45.6	0.698	0.699	93.3	0.488	0.475
−17.8	0.664	0.664	121	0.388	0.380
+10	0.626	0.625	133 (T_c)	0.240	0.234
ETHYL ALCOHOL (*11*): $\rho_1/\omega_1 = 6.210$ AT 20° C., SATD. PRESSURE					
0	0.809	0.806	60	0.746	0.755
40	0.768	0.772	80	0.721	0.735
			243.1 (T_c)	0.273	0.275

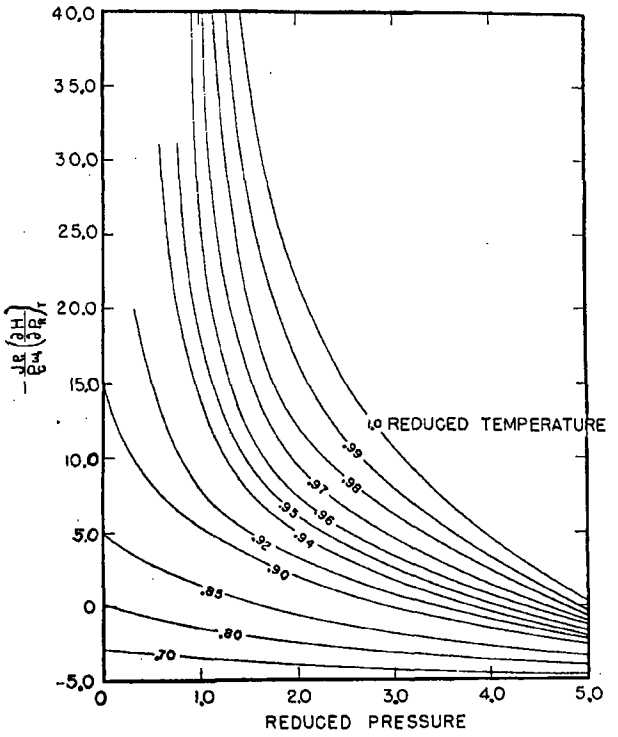

Figure 2. Differential Effect of Pressure on Enthalpy of Liquids

its critical pressure and the enthalpy at the same temperature and other pressures:

$$\frac{J\rho_1}{P_c\omega_1}(H_{cp} - H)_T = \int_{p_r}^{1.0} \frac{J\rho_1}{P_c\omega_1}\left(\frac{\partial H}{\partial p_r}\right)_T dp_r \qquad (7)$$

The results of this integration are summarized in Figure 3 and Table V.

Unfortunately few data are available with which to compare the enthalpy corrections calculated from Figure 3. Table VI compares the calculated values and those experimentally evaluated for water and propane. The agreement is reasonably good for both compounds. In view of the fact that the pressure correction is relatively small as compared to the enthalpy changes ordinarily encountered in industrial operations, it is believed that Figure 3 may be safely used for many engineering applications. The fact that a relation based on data for pentane is in even fair agreement with such dissimilar materials as water and propane is reassuring as to its generality.

PRESSURE CORRECTION TO ENTROPY

The effect of pressure on the entropy of any substance is expressed by the rigorous thermodynamic equation:

$$J\left(\frac{\partial S}{\partial p}\right)_T = -\left(\frac{\partial V}{\partial T}\right)_p \qquad (8)$$

Expressing in terms of reduced conditions and combining with Equation 3,

$$\frac{J\rho_1 T_c}{\omega_1 P_c}\left(\frac{\partial S}{\partial p_r}\right)_T = -\left(\frac{\partial \frac{1}{\omega}}{\partial T_r}\right)_p \qquad (9)$$

Equation 9 may be integrated to obtain a useful correction chart relating the difference between entropy under the critical pressure and entropy at any other pressure under the same temperature:

$$\frac{J\rho_1 T_c}{\omega_1 P_c}(S_{cp} - S)_T = \int_{p_r}^{1.0} -\left(\frac{\partial \frac{1}{\omega}}{\partial T_r}\right)_p dp_r \qquad (10)$$

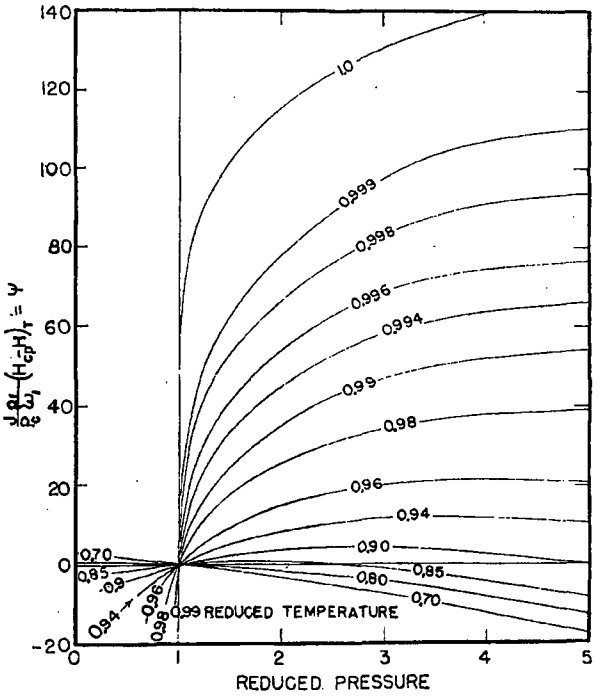

Figure 3. Pressure Correction to Enthalpy of Liquids

Table IV. Values of $-\frac{J\rho_1}{P_c\omega_1}\left(\frac{\partial H}{\partial P_r}\right)_T$

T_r	$P_r = 0$	$P_r = 0.4$	$P_r = 0.8$	$P_r = 1.0$	$P_r = 1.5$	$P_r = 2$	$P_r = 3$	$P_r = 5$
0.7	− 3.0	−3.2	− 3.4	− 3.5	− 3.8	− 4.0	− 4.4	−4.7
0.8	+ 0.1	−0.6	− 1.3	− 1.6	− 2.2	− 2.6	− 3.3	−4.1
0.85	+ 5.0	+3.1	+ 1.8	+ 1.3	+ 0.2	− 0.7	− 1.9	−3.4
0.90	+15.0	+9.1	+ 6.3	+ 5.3	+ 3.4	+ 1.9	− 0.2	−2.7
0.94	....	...	+19.0	+14.0	+ 7.7	+ 4.9	+ 1.7	−2.0
0.98	....	...	....	....	+20.3	+12.1	+ 6.2	−0.7
1.0	....	...	....	....	+36.0	+21.8	+10.7	+0.4

Table V. Values of $\frac{J\rho_1}{P_c\omega_1}(H_{cp} - H)_T = \psi$

T_r	$P_r = 0$	$P_r = 0.4$	$P_r = 0.8$	$P_r = 1.2$	$P_r = 1.5$	$P_r = 2$	$P_r = 3$	$P_r = 5$
0.7	+3.1	+2	+0.8	− 0.7	− 1.8	− 3.4	− 7.3	− 17.2
0.8	+0.8	+0.5	+0.1	− 0.2	− 0.7	− 1.4	− 4.0	− 12.3
0.85	−3.2	−1.8	−0.5	+ 0.4	+ 0.9	+ 1.0	− 0.9	− 8.0
0.9	...	−5.0	−1.7	+ 1.0	+ 2.2	+ 3.7	+ 4.4	+ 0.2
0.94	...	...	−3.5	+ 2.1	+ 5.2	+ 8.2	+ 11.8	+ 10.8
0.98	...	...	...	+10.0	+ 18	+ 25.8	+ 20.2	+ 39.3
0.99	...	...	...	+15.0	+ 24.9	+ 35.0	+ 47	+ 54.1
0.999	...	...	...	+46.5	+ 62.5	+ 77.8	+ 97.6	+110.3
1.0	...	...	...	+87.0	+101.5	+115.2	+130.5	.....

Values $[\partial(1/\omega)/\partial T_r]_p$ were obtained from Figure 1 in deriving Figure 2. The resulting integrated pressure correction to entropy is plotted against reduced temperature and pressure in Figure 4 and summarized in Table VII. Table VIII compares values calculated from Figure 4 with experimental values for water and propane. The agreement appears to be somewhat better than that of the enthalpy correction, indicating that generalization is sufficiently sound for useful application.

PRESSURE CORRECTION TO HEAT CAPACITY AT CONSTANT PRESSURE

A useful expression for the effect of pressure on heat capacity at constant pressure may be derived by designating the right-hand side of Equation 7 as ψ, a function of reduced temperature and pressure:

$$\frac{J\rho_1}{P_c\omega_1}(H_{cp} - H)_T = \psi \qquad (11)$$

Upon differentiation at constant pressure,

$$\frac{J\rho_1}{P_c\omega_1}\left[\left(\frac{\partial H_{cp}}{\partial T}\right)_p - \left(\frac{\partial H}{\partial T}\right)_p\right]_T = \frac{1}{T_c}\left(\frac{\partial \psi}{\partial T_r}\right)_p$$

or $$\frac{J\rho_1 T_c}{\omega_1 P_c}(C_{cp} - C_p)_T = \left(\frac{\partial \psi}{\partial T_r}\right)_p \qquad (12)$$

The results of graphically differentiating Figure 3 in accordance with Equation 12 are summarized in Figure 5 and Table IX. A comparison of values calculated from Figure 5 with those derived from experimental data for water is shown in Table X. Additional data for testing this relation are scanty, but the agreement with the data on water is sufficiently good to indicate that the generalization did not lose greatly in accuracy through the series of manipulations employed in deriving Figure 5.

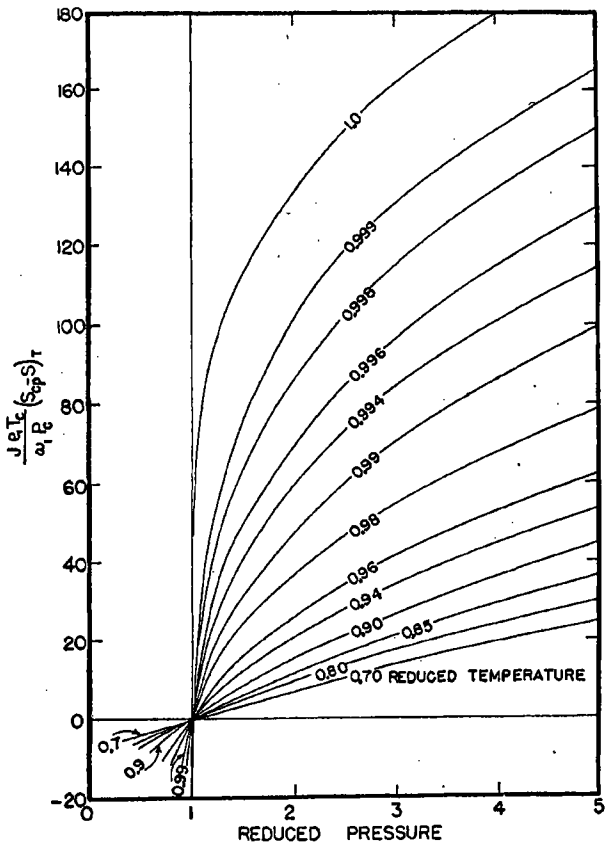

Figure 4. Pressure Correction to Entropy of Liquids

Table VI. Pressure Correction to Enthalpy

Pressure, Lb./Sq. In.	$(H_{cp} - H)_T$, cal./gram mole: 204.4° C. Calcd.	204.4° C. Exptl.	348.9° C. Calcd.	348.9° C. Exptl.	374.3° C. Calcd.	374.3° C. Exptl.
			WATER (*12*)			
1000	23	28	...	...	....	....
2500	8	10	−107	−115	....	....
4000	− 8	− 9	+ 75	+ 79	+1130	+1266
5500	−26	−32	+164	+172	+1370	1526
			PROPANE (*17*)			
	54.5° C. Calcd.	54.5° C. Exptl.	71.1° C. Calcd.	71.1° C. Exptl.	87.9° C. Calcd.	87.9° C. Exptl.
300	−29	−25	...	...	....	....
1500	+18	+12	+68	+63	+205	+200
3000	−28	−21	+58	+45	+260	+256

Table VII. Values of $\frac{J\rho_1 T_c}{\omega_1 P_c}(S_{cp} - S)_T$

T_r	$P_r = 0.4$	$P_r = 0.8$	$P_r = 1.2$	$P_r = 1.5$	$P_r = 2$	$P_r = 3$	$P_r = 5$
0.7	−4.6	−1.7	+ 1.1	+ 3.2	+ 6.9	+ 13.8	+ 25.0
0.9	...	−3.6	+ 3.8	+ 8.5	+ 15.5	+ 26.9	+ 44.9
0.94	...	−7.1	+ 5.6	+ 12.2	+ 20.8	+ 34.7	+ 53.8
0.98	...	...	+13.2	+ 24.6	+ 37.3	+ 55.1	+ 79.0
0.99	...	...	+18.3	+ 31.9	+ 47.7	+ 71.0	+ 99.9
0.996	...	...	+32.1	+ 50.0	+ 70.2	+ 96.9	+130.0
0.999	...	...	+50.7	+ 76.9	+102.0	+130.9	+165.6
1.0	...	...	+93.2	+118.0	+134.0	+161.5	.....

HEAT OF VAPORIZATION

An empirical graphical generalization was developed by the author (*22*) which satisfactorily represents the effect of temperature on the heat of vaporization of a variety of polar and nonpolar compounds. A curve, based on the available data for all materials, was presented from which the heat of vaporization at any reduced temperature can be calculated if one value at a known reduced temperature is available. The Kistiakowsky equation offers a satisfactory method of estimating heats of vaporization at the normal boiling points for nonpolar compounds but does not apply to polar materials.

A satisfactory generalized method for estimating the heat of vaporization of any substance at any temperature was developed by Meissner (*14*). This method shows good agreement with experimental results, particularly at high temperatures. It becomes somewhat unsound at low reduced temperatures, but even in this range the errors are not ordinarily serious. The method here presented is an alternate to Meiss-

Table VIII. Pressure Correction to Entropy

Pressure, Lb./Sq. In.	$(S_{cp} - S) \times 10^3$ cal./gram mole/° K.: 204.4° C. Calcd.	204.4° C. Exptl.	348.9° C. Calcd.	348.9° C. Exptl.	374.3° C. Calcd.	374.3° C. Exptl.
			WATER (*12*)			
1000	−115	−100	....	...	....	....
2500	− 37	− 32	− 249	−242	.....	.....
4000	+ 88	+ 83	+ 194	187	1900	2030
5500	+112	+ 96	+ 430	445	2400	2545
			PROPANE (*17*)			
	54.5° C. Calcd.	54.5° C. Exptl.	71.1° C. Calcd.	71.1° C. Exptl.	87.9° C. Calcd.	87.9° C. Exptl.
300	−235	−238	...	...	.....	.....
1500	+470	+442	+630	591	+915	+970
3000	+990	+984	+1215	1200	+1670	+1790

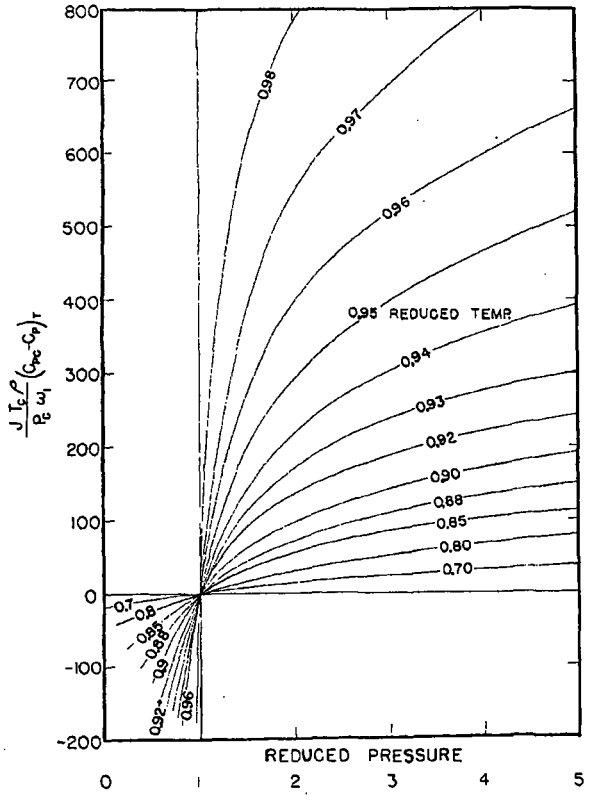

Figure 5. Pressure Correction to Heat Capacity at Constant Pressure of Liquids

ner's method, with the advantage of not involving any graphical relations and consequently being adaptable to mathematical manipulation for the derivation of other thermodynamic functions. It is perhaps somewhat more dependable than Meissner's method at low reduced temperatures.

It has been found that the general curve, referred to above (*22*) and expressing the relation between heat of vaporization and reduced temperature, is represented by the following empirical equation:

$$\lambda = \lambda_1 \left(\frac{1 - T_r}{1 - T_{r_1}}\right)^{0.38} \tag{13}$$

This equation is more convenient to use than the original curve and gives considerably more reproducible results, particularly at temperatures near the critical. It is in good agreement with the available data with the exception of water at low temperatures, below the normal boiling point. As previously mentioned, water is unusual in many of its characteristics in this region.

Heats of vaporization ma y be accurately calculated at any temperature from the rigorously correct Clapeyron equation:

$$\frac{dp_s}{dT} = \frac{\lambda}{T(v_g - v_l)} \tag{14}$$

The molal volume of the vapor, v_g, may be calculated from the generalized gas compressibility factors while the volume of the liquid, v_l, is obtained from Equation 3 and Figure 1. Where complete vapor pressure data are not available, excellent approximations can be obtained from only the boiling point and the critical temperature and pressure by use of a reference substance method of plot ting such as that introduced

Table IX. Values of $\frac{JT_c\rho_1}{P_c\omega_1}(C_{cp} - C_p)_T$

T_r	$P_r = 0.4$	$P_r = 0.8$	$P_r = 1.2$	$P_r = 1.5$	$P_r = 2$	$P_r = 3$	$P_r = 5$
0.7	− 9	− 3	+ 3	+ 7	+ 14	+ 23	+ 38
0.8	−28	− 9	+ 6	+ 16	+ 30	+ 52	+ 80
0.9	..	− 42	+ 30	+ 62	+ 98	+142	+192
0.94	..	− 75	+ 70	+143	+216	+303	+392
0.96	..	−190	+146	+272	+400	+518	+662
0.97	..	...	+208	+387	+550	+695	...
0.98	..	...	+385	+608	+778	...	...

by Cox (*5*) which permits ready determination of dp_s/dT from the corresponding values for the reference substance. However, this method is rather tedious, and the added labor is frequently not warranted by the improved accuracy obtained.

If the application of Equation 14 is restricted to the normal boiling point, a reasonably good approximation is obtained with the following modified form of the Clausius-Clapeyron equation in which the factor 0.95 represents the average deviation of the vapor from the ideal gas laws at these conditions, together with the effect of the liquid volume:

$$\left(\frac{dp_s}{dT}\right)_B = \frac{p_B\lambda_B}{0.95RT_B^2} \tag{15}$$

A simple relation between temperature and vapor pressure was developed by Calingaert and Davis (*3*) as a result of a study of the Cox method of vapor-pressure plotting:

$$\ln p_s = A - \frac{B}{T - 43} \tag{16}$$

where T is expressed in degrees Kelvin. This equation is not particularly reliable for many materials and is not recommended as a general method of predicting vapor pressures where considerable accuracy is required. However, it can be used satisfactorily for evaluating dp/dT for generalized thermodynamic relations where a high order of accuracy is not required or inherent in the other relations. Thus, differentiating Equation 16,

$$\frac{dp_s}{dT} = \frac{p_sB}{(T - 43)^2} \tag{17}$$

The constant B may be determined from any two vapor pressure values, such as the boiling point and critical point:

$$B = \frac{\ln \frac{p_c}{p_B}}{\frac{1}{T_B - 43} - \frac{1}{T_c - 43}} \tag{18}$$

Combining Equations 12 and 14,

$$\lambda_B = 0.95RB\left(\frac{T_B}{T_B - 43}\right)^2 \tag{19}$$

Table X. Pressure Correction to Heat Capacity of Water at Constant Volume (*12*)

	$(C_{cp} - C_p)_T$ cal./gram mole/° K.					
	260° C., $T_r = 0.824$		315.6° C., $T_r = 0.910$		337.8° C., $T_r = 0.943$	
Pressure, Lb./Sq. In.	Calcd.	Exptl.	Calcd.	Exptl.	Calcd.	Exptl.
1000	−0.88	−0.81	....	....	....	....
2000	−0.46	−0.38	−1.98	−1.93	....	....
2500	−0.27	−0.23	−1.15	−0.99	−2.48	−2.61
4000	+0.25	+0.27	+0.87	+0.90	+1.94	+2.02
6000	+0.74	+0.86	+2.18	+2.32	+4.40	+4.41

This equation gives results generally not differing from reliable experimental values by so much as 5 per cent when constant B is determined from the critical point and boiling point. Somewhat better results are obtained if B is evaluated from a vapor pressure value less distant from the normal boiling point than the critical temperature, and if the actual compressibility factor of the vapor is used instead of the average value of 0.95.

HEAT CAPACITY DIFFERENCE BETWEEN SATURATED LIQUID AND ITS IDEAL GAS

By combining the equations developed above with the generalized expression for the effect of pressure on the enthalpy of gases, it is possible to derive a generalized thermodynamic method for calculating the difference between the heat capacity of a saturated liquid and the same material as an ideal gas at the same temperature and zero pressure. Such a

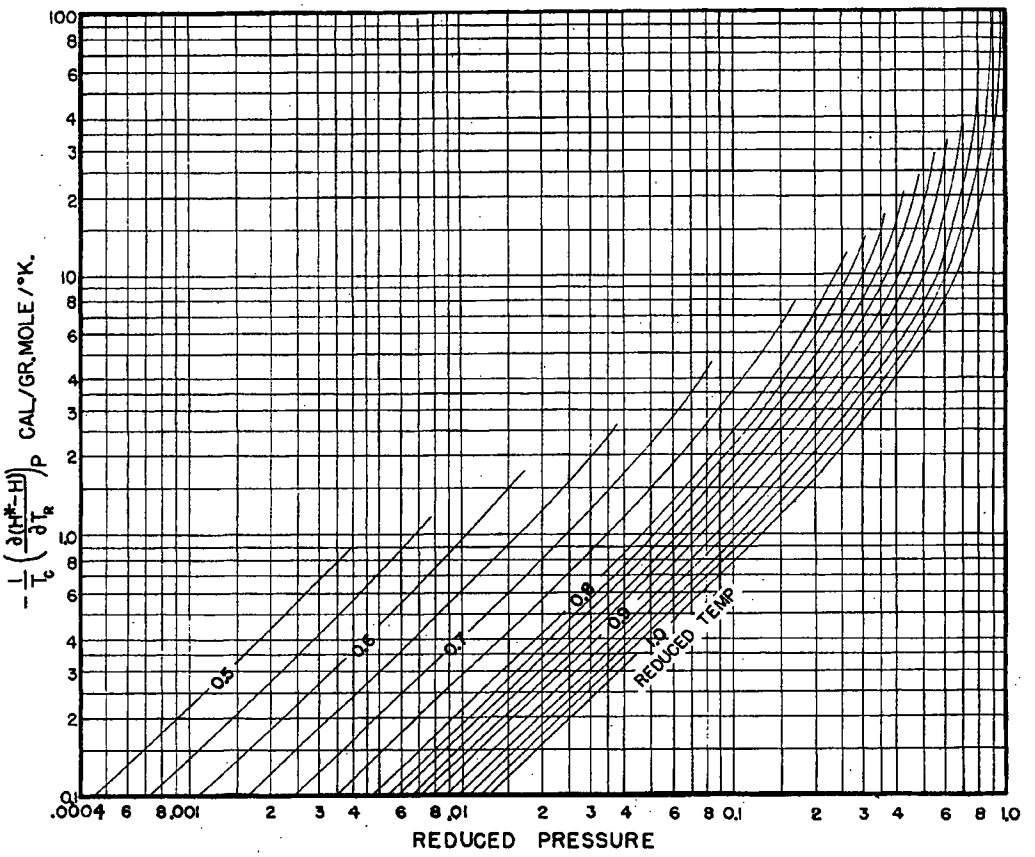

Figure 6. Differential Pressure Correction to Enthalpy of Gases

Combining Equations 13 and 19, an expression is obtained which permits calculation of the heat of vaporization of any substance at all conditions from a knowledge merely of the boiling point and critical temperature and pressure, since B is also found from T_c and P_c:

$$\lambda = 0.95RB\left(\frac{T_B}{T_B - 43}\right)^2\left(\frac{1 - T_r}{1 - T_{rB}}\right)^{0.38} \qquad (20)$$

Table XI compares values calculated from Equation 20 with experimental data for several compounds on which measurements were made at elevated temperatures. The deviations are of the same order as shown by Meissner's method; they are greater in some cases and less in others. Further comparisons indicated that the major source of error is Equation 19 rather than Equation 13, and the over-all accuracy is improved by using the actual compressibility factor at the boiling point instead of the average value of 0.95.

method is of considerable value because of the scarcity and general unreliability of heat capacity data. Recent development of generalized statistical methods (*1*, *6*) derived from spectroscopic observations permits reasonably satisfactory prediction of the heat capacities of the more simple molecules in the ideal gaseous state. These methods, combined with a thermodynamic relation between gaseous and liquid heat capacities and the relations for thermodynamic properties of liquids developed above, will permit complete prediction of heat capacities at all conditions, both liquid and gaseous. Conversely, for complex high-boiling liquids on which liquid heat capacity measurements have been made, such a thermodynamic relation may offer a more reliable method of estimating gaseous heat capacities than the statistical methods. The relation will also be useful in rationalizing experimental observations of gaseous and liquid heat capacities and making them consistent with each other.

There are several methods by which a saturated liquid at temperature T_1 may be converted into a saturated vapor at a

higher temperature T_2. One is to heat the liquid (maintaining saturation) to T_2 and vaporize it. Another is to vaporize the liquid at T_1, isothermally expand the vapor to zero pressure, heat the ideal vapor to T_2, and isothermally compress to saturation conditions. Since the initial and final states are the same in both cases, the enthalpy changes of the two operations must be equal:

$$\lambda_1 + (H_1^* - H_{s_{g_1}}) + C_{p_g}^* (T_2 - T_1) - (H_2^* - H_{s_{g_2}}) = \lambda_2 + C_{sl}(T_2 - T_1) \quad (21)$$

Rearranging and applying to an infinitesimal temperature change, dT,

$$(C_{sl} - C_{p_g}^*)\, dT = -d\lambda - d(H^* - H_{s_g})$$

$$C_{sl} - C_{p_g}^* = -\frac{d\lambda}{dT} - \frac{d(H^* - H_{s_g})}{dT} \quad (22)$$

Since the term $d(H^* - H_{s_g})$ involves both a temperature and a pressure change, it must be expressed in terms of partial differentials:

$$\frac{d(H^* - H_{s_g})}{dT} = \left[\frac{\partial(H^* - H_{s_g})}{\partial T}\right]_p + \left[\frac{\partial(H^* - H_{s_g})}{\partial p}\right]_T \frac{dp_s}{dT} \quad (23)$$

All the terms on the right-hand side of Equation 24 may be obtained from generalizations, presumably applicable to all substances. Thus, differentiating Equation 20,

$$\frac{d\lambda}{dT_r} = \frac{-0.361RB}{(1 - T_{rB})^{0.38}} \left(\frac{T_B}{T_B - 43}\right)^2 \frac{1}{(1 - T_r)^{0.62}} \quad (25)$$

A generalized relation between $(H^* - H_s)$ and reduced temperature and pressure was introduced by Watson and Nelson (*23*) and improved by several others (*8, 10, 24, 26*). Graphical differentiation of this relation with respect to reduced temperature at constant pressure permits evaluation of the second term of Equation 24. The first part of the third term similarly may be evaluated by differentiation with respect to reduced pressure at constant temperature. The last part of the third term is evaluated by Equation 17.

For differentiation, a pressure-enthalpy correction chart for the gaseous state was prepared, taking into account the improved data calculated by Edmister (*8*) and York and Weber (*26*) and extended to the low reduced temperature range by the Joule-Thomson data on water (*11*). This chart was graphically differentiated with respect to temperature and pressure, and the data obtained are summarized in Figures 6 and 7 and in Tables XII and XIII. Because of the uncertainty of the basic enthalpy correction chart at conditions in the saturated region, particularly at low temperatures, the curves of Figures 6 and 7 were adjusted by cross plotting to obtain consistent relations which, when incorporated in Equation 24, gave the best average agreement with the ex-

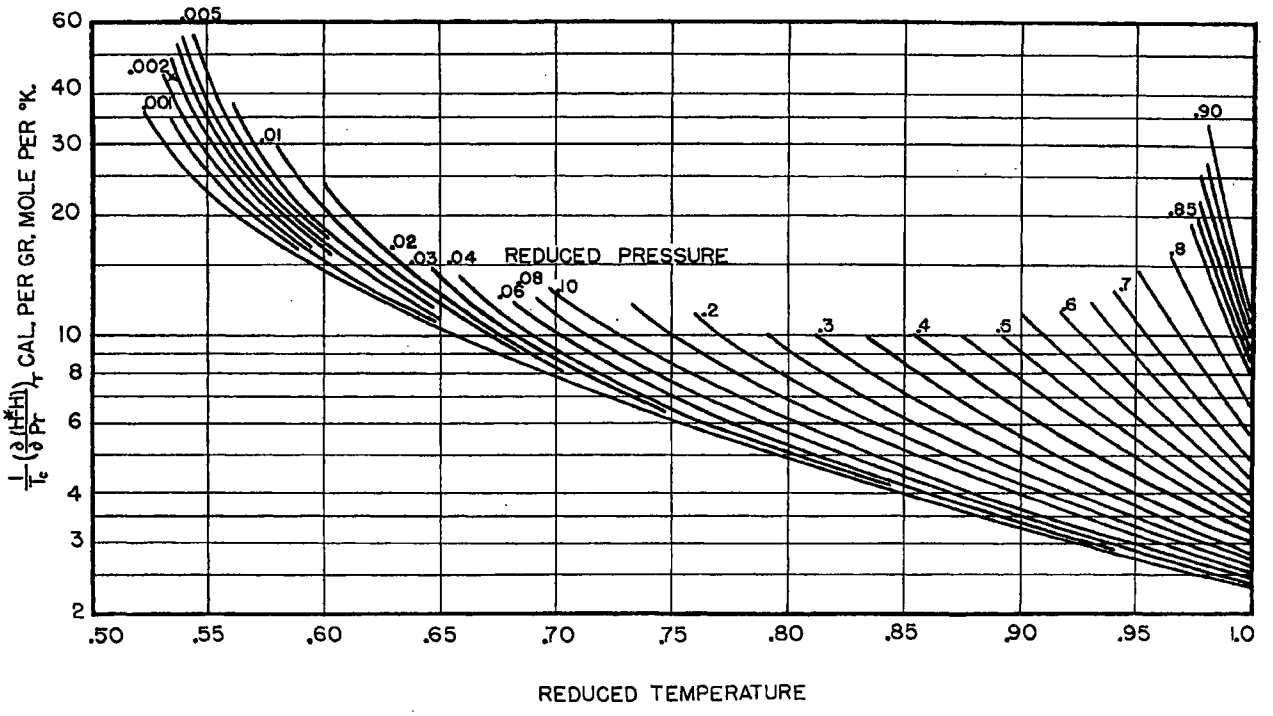

Figure 7. Differential Pressure Correction to Enthalpy of Gases

Substituting Equation 23 in 22 and writing in terms of reduced conditions,

$$C_{sl} - C_{p_g}^* = -\left(\frac{d\lambda}{dT_r}\right)\frac{1}{T_c} - \left[\frac{\partial(H^* - H_s)}{\partial T_r}\right]_p \frac{1}{T_c} - \left[\frac{\partial(H^* - H_s)}{\partial p_r}\right]_T \frac{1}{P_c}\frac{dp_s}{dT} \quad (24)$$

Table XI. Heats of Vaporization

Temperature, ° C.	λ, cal./gram mole Calcd.	λ, cal./gram mole Exptl.	Temperature, ° C.	λ, cal./gram mole Calcd.	λ, cal./gram mole Exptl.
		WATER (*12*)			
83	9,680	9,890	277	6,380	6,720
115	9,250	9,530	307	5,460	5,740
147.5	8,800	9,110	322	5,020	5,240
180.5	8,300	8,660	335	4,500	4,670
210.5	7,740	8,140	348.5	3,850	3,980
245	7,100	7,470	364	2,960	3,040
			373.3	1,020	1,060
		AMMONIA (*81*)			
−49.9	5,870	5,770	91.8	3,310	(3,180)
− 9.5	5,340	5,260	100	3,045	(3,050)
+31.0	4,690	4,640	108.1	2,730	(2,700)
71.6	3,870	(3,780)	116.2	2,340	(2,250)
			124.3	1,800	(1,640)
		BENZENE (*11*)			
0	8,250	8,350	180	5,700	5,790
60	7,680	7,600	220	4,780	4,850
100	7,000	7,060	260	3,420	3,420
140	6,400	6,440	280	2,160	2,140
		ETHYL ALCOHOL (*11*)			
0	10,450	10,110	160	6,950	7,150
40	9,760	9,900	200	5,650	5,280
80	8,970	9,350	220	4,260	3,960
120	8,090	8,350	240	1,990	1,760
		BUTANE (*19*)			
24.9	5,140	5,050	110.9	3,380	3,170
67.9	4,400	4,310			
		PROPANE (*17*)			
20.8	3,680	3,460	88.1	1,785	1,490
54.8	2,960	2,780	98.1	916	610
73.8	2,410	2,210			
		SULFUR DIOXIDE (*11*)			
−10	5,930	6,090	40	5,180	4,950
+20	5,490	5,400	60	4,810	4,500

perimental values of $(C_{sl} - C_v^*)$ for water and ammonia. In all of this work Equations 16 and 18 were used for the calculation of vapor pressures, and it is recommended that this procedure be followed in using Figures 6 and 7.

Figure 7 is not in good agreement with $(\partial H/\partial P)_T$ data calculated by Kennedy, Sage, and Lacey (*13*) from their Joule-Thomson measurements on *n*-butane and *n*-pentane. Edmister (*8*) pointed out that the data of these investigators did not conform with his generalized relations. Similarly, Watson and Smith (*24*) found that a generalized plot of Joule-Thomson coefficients showed large differences from the experimental data. These discrepancies indicate that differentiation of the generalized enthalpy-pressure relation tends to magnify its inherent errors. It is probable that the absolute values of the functions plotted in Figures 6 and 7 may differ from experimental values for some substances by as much as 50 per cent. However, it is hoped that these errors will tend to compensate one another when the two charts are used together in conjunction with Equation 24 and Equations 16 and 18 for calculating pressures.

Heat capacity data in general are so unreliable that it is difficult to find good comparable values on both the liquid and gaseous state with which to test Equation 24. Table XIV compares values calculated from the equation with experimental data for water, ammonia, pentane, butane, and propane. The experimental values for the hydrocarbons were taken from the general correlation of Holcomb and Brown (*9*) at temperatures below 70° F. These are actually heat capacities at constant pressure, but at reduced temperatures below 0.8 the difference from the heat capacity of the saturated liquid becomes small. At higher temperatures the data of Sage and co-workers from the indicated sources were selected. These investigators made actual measurements of the heat capacities of the saturated liquid.

The agreement in Table XIV is reasonably good except in the case of butane at the higher temperatures. Although these few comparisons do not confirm the reliability of Equation 24, it is encouraging that agreement is obtained on both nonpolar and highly polar compounds of both low and high boiling points. Figures 6 and 7 are not recommended for reduced temperatures above 0.96 or below 0.55. At reduced temperatures below 0.55 the difference between the heat capacity of the liquid and the ideal gas appears to approach independence of temperature, and it is believed that this assumption is preferable to attempting to extend Figure 7.

In the recommended temperature range it seems probable that the calculated heat capacity differences should not be in error by more than 25 per cent. Although much better accuracy is to be desired, such errors are not too serious, particularly when one is working with materials of high molal heat capacities for which the difference in heat capacities is

Table XII. Values of $-\frac{1}{T_c}\left(\frac{\partial(H^* - H)}{\partial T_R}\right)_P$ in Small Calories per Gram Mole per ° K.

P_r	$T_r = 0.55$	$T_r = 0.6$	$T_r = 0.7$	$T_r = 0.8$	$T_r = 0.9$	$T_r = 0.95$	$T_r = 1.0$
0.001	0.140	...	...	...	....	....	....
0.002	0.275	0.181	...	...	....	....	....
0.003	0.415	0.270	0.121		....	....	....
0.006	0.88	0.55	0.242	0.126	....	....	....
0.01	...	0.95	0.40	0.210	0.128	...	...
0.02	...	...	0.80	0.42	0.254	0.195	0.158
0.03	...	...	1.23	0.63	0.38	0.29	0.186
0.06	...	...	2.82	1.33	0.77	0.59	0.47
0.1	...	...	...	2.46	1.34	1.0	0.79
0.2	...	...	...	7.0	3.12	2.20	1.63
0.4	...	...	...	...	9.5	5.7	4.0
0.5	...	...	...	...	18.5	8.6	5.7
0.7	...	...	...	...	....	27	11.4
0.9	...	...	...	...	....	....	33

Table XIII. Values of $\frac{1}{T_c}\left(\frac{\partial(H^* - H)}{\partial P_r}\right)_T$ in Small Calories per Gram Mole per ° K.

P_r	$T_r = 0.55$	$T_r = 0.6$	$T_r = 0.7$	$T_r = 0.8$	$T_r = 0.9$	$T_r = 0.95$	$T_r = 0.98$	$T_r = 1.0$
0.001	25.2	14.6	7.8	4.88	3.29	2.73	2.48	2.32
0.002	32.0	15.8	7.9	4.88	3.29	2.73	2.48	2.32
0.005	46	17.5	8.0	4.88	3.29	2.73	2.48	2.32
0.01	..	20.8	8.1	4.88	3.29	2.73	2.48	2.32
0.02	..	24.0	8.2	4.88	3.29	2.73	2.48	2.32
0.03	..	..	8.5	5.0	3.35	2.73	2.48	2.32
0.06	..	..	10.1	5.25	3.4	2.80	2.50	2.34
0.10	..	..	12.8	6.05	3.65	3.00	2.64	2.44
0.2	..	..	..	7.8	4.20	3.29	2.88	2.63
0.3	..	..	..	11.7	5.0	3.70	3.15	2.84
0.5	..	..	..	....	9.0	5.45	4.15	3.5
0.6	..	..	..	....	..	7.3	5.05	4.0
0.7	..	..	..	....	..	10.9	6.6	4.8
0.8	..	..	..	....	..	...	10.7	6.6
0.85	..	..	..	....	..	...	15.0	8.1
0.90	..	..	..	....	..	...	34.0	11.2

Table XIV. Difference between Heat Capacities of Saturated Liquid and Its Ideal Gas

		$(C_{sl} - C^*_{pg})$, cal./g. mole/° K.				$(C_{sl} - C^*_{pg})$, cal./g. mole/° K.	
T_r	T° C.	Calcd.	Exptl.	T_r	T° C.	Calcd.	Exptl.
			WATER (*12*)				
0.55	83	11.0	10.0	0.85	277	14.4	13.6
0.60	115	11.5	10.1	0.90	307	17.0	16.4
0.65	147.5	11.5	10.3	0.92	322.5	18.6	18.0
0.70	180.5	11.8	10.7	0.94	335	20.7	20.7
0.75	210.5	11.9	11.2	0.96	348.5	28.0	25.1
0.80	245	12.3	11.6				
			AMMONIA (*21*)				
0.55	−49.9	9.8	9.8	0.85	71.6	12.9	12.6
0.60	−29.8	9.9	1.0	0.90	91.8	15.1	14.7
0.65	− 9.5	9.8	10.2	0.92	100.0	17.1	16.2
0.70	+10.7	10.4	10.5	0.94	108.1	16.9	17.8
0.75	31.0	10.7	10.9	0.96	116.2	19.9	20.9
0.80	51.3	11.4	11.5				
			n-PENTANE (*9*)				
0.55	−14.6	9.9	10.0	0.7	55.9	11.4	11.9
0.6	+ 8.9	10.1	10.4	0.8	103.9	11.6	13.6
			n-BUTANE (*9, 15, 20*)				
0.55	−39.1	8.7	7.6	0.8	67.9	10.3	14.4
0.6	−17.1	8.8	8.7	0.9	110.9	12.9	17.6
0.7	+24.9	9.4	10.9				
			PROPANE (*9, 15, 20*)				
0.55	−67.7	5.2	6.1	0.8	25.6	8.2	9.3
0.6	−49.1	5.8	6.4	0.9	63.0	13.5	13.4
0.7	−11.7	6.3	8.2				

small in comparison to the heat capacity of the vapor. At present no better general method for estimating these properties is available.

DIFFERENCE BETWEEN HEAT CAPACITY AT CONSTANT PRESSURE AND HEAT CAPACITY OF SATURATED LIQUID

The heat capacity of a saturated liquid C_{sl} expresses the change in enthalpy accompanying a simultaneous increase in both temperature and pressure:

$$C_{sl} = \left(\frac{\partial H}{\partial T}\right)_P + \left(\frac{\partial H}{\partial p}\right)_T \frac{dp_s}{dT} \qquad (26)$$

In terms of reduced conditions,

$$(C_{pl} - C_{sl})_{TP} = -\left(\frac{\partial H}{\partial p_r}\right)_T \frac{1}{P_c}\left(\frac{dp_s}{dT}\right) \qquad (27)$$

Values of $\frac{1}{P_c}\left(\frac{\partial H}{\partial p_r}\right)$ may be obtained from Figure 2, and dp_s/dT is calculated from Equation 17, permitting complete evaluation of Equation 27.

Table XV. Difference between Heat Capacity at Constant Pressure and Heat Capacity of Saturated Liquid (Water, *12*)

		$(C_p - C_s)$, cal./g. mole/° K.	
T° C.	T_r	Calcd.	Exptl.
204.4	0.738	−0.08	−0.09
287.8	0.867	+0.33	+0.54
315.6	0.910	+0.92	+1.11
326.7	0.927	+1.75	+2.16
337.8	0.943	+3.0	+3.64

Table XV compares results calculated from Equation 27 with the accepted values for water. The agreement is not particularly good, but the quantity sought is not large except at conditions near the critical. Furthermore, it is believed that maximum errors are probably encountered when Figure 2 is applied to water because of the unusually low reduced pressures corresponding to a given reduced temperature at saturation. As a result, saturation values for water fall on the extrapolated portion of Figure 2 at pressures below the range of the hydrocarbon data from which it was derived. Better accuracy should be obtained from Equation 27 when applied to other materials of lower critical pressures.

ACKNOWLEDGMENT

This investigation was carried out with the financial support of the Wisconsin Alumni Research Foundation, under the sponsorship of the University Research Committee. The helpful criticism and suggestions of O. A. Hougen are gratefully acknowledged.

NOMENCLATURE

A, B = constants in Calingaert-Davis vapor pressure equation
C = heat capacity
C^* = heat capacity of ideal gas
d = liquid density
H = enthalpy
H^* = enthalpy of ideal gas
J = mechanical equivalent of heat
M = molecular weight
p = pressure
P = pressure
R = gas law constant
S = entropy
T = absolute temperature
v = molal volume
V = volume of n moles
z = compressibility factor (gaseous)
λ = molal heat of vaporization
ρ = liquid density, mass per unit volume
ψ = $\frac{J\rho_l}{P_c\omega_l}(H_{cp} - H)_T$
ω = liquid expansion factor

Subscripts
B = normal boiling point
c = critical value
cp = critical pressure
g = gaseous state
l = liquid state
r = reduced value
s = saturated liquid or vapor

LITERATURE CITED

(1) Bennewitz and Rossner, *Z. physik. Chem.*, 39B, 126 (1938).
(2) Brown, G. G., Souders, M., and Smith, R. L., IND. ENG. CHEM., 24, 513 (1932).
(3) Calingaert, G., and Davis, D. S., *Ibid.*, 17, 1287 (1925).
(4) Cope, J. Q., Lewis, W. K., and Weber, H. C., *Ibid.*, 23, 887 (1931).
(5) Cox, E. R., *Ibid.*, 15, 592 (1923).
(6) Dobratz, C. J., *Ibid.*, 33, 759 (1941).
(7) Dodge, B. F., *Ibid.*, 24, 1353 (1932).
(8) Edmister, W. C., *Ibid.*, 30, 352 (1938).
(9) Holcomb, D. E., and Brown, G. G., *Ibid.*, 34, 590 (1942).
(10) Hougen and Watson, "Industrial Chemical Calculations", 2nd ed., New York, John Wiley & Sons, 1936.
(11) International Critical Tables, New York, McGraw-Hill Book Co., 1926.
(12) Keenan and Keyes, "Thermodynamic Properties of Steam", New York, John Wiley & Sons, 1936.
(13) Kennedy, E. R., Sage, B. H., and Lacey, W. N., IND. ENG. CHEM., 28, 718 (1936).
(14) Meissner, H. P., *Ibid.*, 33, 1440 (1941).
(15) Sage, B. H., and Lacey, W. N., *Ibid.*, 27, 1484 (1935).
(16) *Ibid.*, 34, 730 (1942).
(17) Sage, B. H., Lacey, W. N., and Schaafsma, J. G., *Ibid.*, 26, 1218 (1934).
(18) *Ibid.*, 27, 48 (1935).
(19) Sage, B. H., Webster, D. C., and Lacey, W. N., *Ibid.*, 29, 1188 (1937).
(20) *Ibid.*, 29, 1309 (1937).
(21) U. S. Bur. of Standards, *Circ.* 142 (1923).
(22) Watson, K. M., IND. ENG. CHEM., 23, 360 (1931).
(23) Watson, K. M., and Nelson, E. F., *Ibid.*, 25, 880 (1933).
(24) Watson, K. M., and Smith, R. L., *Natl. Petroleum News*, July, 1936.
(25) York, R., IND. ENG. CHEM., 34, 535 (1942).
(26) York, R., and Weber, H. C., *Ibid.*, 32, 388 (1940).

WVMP SAR Reference 3-27

CRC Handbook of Chemistry and Physics, 75th. ed., CRC Press, Boca Raton, Florida, 1994.

Pages 6-10 to 6-11.

PROPERTIES OF WATER IN THE RANGE 0 — 100 °C

This table summarizes the best available values of the density, specific heat capacity at constant pressure (C_p), vapor pressure, viscosity, thermal conductivity, dielectric constant, and surface tension for liquid water in the range 0 — 100 °C. All values (except vapor pressure) refer to a pressure of 100 kPa (1 bar). The temperature scale is IPTS-68.

t °C	Density g/cm³	C_p J/g K	Vap. pres. kPa	Visc. μPa s	Ther. cond. mW/K m	Diel. const.	Surf. ten. mN/m
0	0.99984	4.2176	0.6113	1793	561.0	87.90	75.64
10	0.99970	4.1921	1.2281	1307	580.0	83.96	74.23
20	0.99821	4.1818	2.3388	1002	598.4	80.20	72.75
30	0.99565	4.1784	4.2455	797.7	615.4	76.60	71.20
40	0.99222	4.1785	7.3814	653.2	630.5	73.17	69.60
50	0.98803	4.1806	12.344	547.0	643.5	69.88	67.94
60	0.98320	4.1843	19.932	466.5	654.3	66.73	66.24
70	0.97778	4.1895	31.176	404.0	663.1	63.73	64.47
80	0.97182	4.1963	47.373	354.4	670.0	60.86	62.67
90	0.96535	4.2050	70.117	314.5	675.3	58.12	60.82
100	0.95840	4.2159	101.325	281.8	679.1	55.51	58.91
Ref.	1—3	2	1, 3	3	3	4	5

REFERENCES

1. L. Harr, J. S. Gallagher, and G. S. Kell, *NBS/NRC Steam Tables*, Hemisphere Publishing Corp., 1984.
2. K. N. Marsh, Ed., *Recommended Reference Materials for the Realization of Physicochemical Properties*, Blackwell Scientific Publications, Oxford, 1987.
3. J. V. Sengers and J. T. R. Watson, Improved international formulations for the viscosity and thermal conductivity of water substance, *J. Phys. Chem. Ref. Data*, 15, 1291, 1986.
4. D. G. Archer and P. Wang, The dielectric constant of water and debye-huckel limiting law slopes, *J. Phys. Chem. Ref. Data*, 19, 371, 1990.
5. N. B. Vargaftik, et al., International tables of the surface tension of water, *J. Phys. Chem. Ref. Data*, 12, 817, 1983.

ENTHALPY OF VAPORIZATION OF WATER

The enthalpy (heat) of vaporization of water is tabulated as a function of temperature on the IPTS-68 scale.

REFERENCE

Marsh, K. N., Ed., *Recommended Reference Materials for the Realization of Physicochemical Properties*, Blackwell, Oxford, 1987.

t °C	$\Delta_{vap}H$ kJ/mol	t °C	$\Delta_{vap}H$ kJ/mol
0	45.054	200	34.962
25	43.990	220	33.468
40	43.350	240	31.809
60	42.482	260	29.930
80	41.585	280	27.795
100	40.657	300	25.300
120	39.684	320	22.297
140	38.643	340	18.502
160	37.518	360	12.966
180	36.304	374	2.066

FIXED POINT PROPERTIES OF H_2O AND D_2O

	Unit	H_2O	D_2O
Molar mass	g/mol	18.01528	20.02748
Melting point (101.325 kPa)	°C	0.00	3.82
Boiling point (101.325 kPa)	°C	100.00	101.42
Triple point temperature	°C	0.01	3.82
Triple point pressure	Pa	611.73	661
Triple point density (l)	g/cm^3	0.99978	1.1055
Triple point density (g)	mg/L	4.885	5.75
Critical temperature	°C	373.99	370.74
Critical pressure	MPa	22.064	21.671
Critical density	g/cm^3	0.322	0.356
Critical specific volume	cm^3/g	3.11	2.81
Maximum density (saturated liquid)	g/cm^3	0.99995	1.1053
Temperature of maximum density	°C	4.0	11.2

REFERENCES

L. Haar, J. S. Gallagher, and G. S. Kell, *NBS/NRC Steam Tables*, Hemisphere Publishing Corp., 1984.

J. M. H. Levelt Sengers, J. Straub, K. Watanabe, and P. G. Hill, Assessment of critical parameter values for H_2O and D_2O, *J. Phys. Chem. Ref. Data*, 14, 193, 1985.

J. Kestin, et. al., Thermophysical properties of fluid D_2O, *J. Phys. Chem. Ref. Data*, 13, 601, 1984.

J. Kestin, et. al., Thermophysical properties of fluid H_2O, *J. Phys. Chem. Ref. Data*, 13, 175, 1984.

P. G. Hill, R. D. C. MacMillan, and V. Lee, A fundamental equation of state for heavy water, *J. Phys. Chem. Ref. Data*, 11, 1, 1982.

THERMAL CONDUCTIVITY OF SATURATED H_2O AND D_2O

This table gives the thermal conductivity λ for water (H_2O or D_2O) in equilibrium with its vapor. Values for the liquid (λ_l) and vapor (λ_v) are listed, as well as the vapor pressure.

REFERENCES

1. J. V. Sengers and J. T. R. Watson, Improved international formulations for the viscosity and thermal conductivity of water substance, *J. Phys. Chem. Ref. Data*, 15, 1291, 1986.

2. N. Matsunaga and A. Nagashima, Transport properties of liquid and gaseous D_2O over a wide range of temperature and pressure, *J. Phys. Chem. Ref. Data*, 12, 933, 1983.

	H_2O			D_2O	
t/°C	P/kPa	λ_l/(mW/K m)	λ_v/(mW/K m)	P/kPa	λ_l/(mW/K m)	λ_v/(mW/K m)
0	0.6	561.0	16.49			
10	1.2	580.0	17.21	1.0	575	17.0
20	2.3	598.4	17.95	2.0	589	17.8
30	4.2	615.4	18.70	3.7	600	18.5
40	7.4	630.5	19.48	6.5	610	19.3
50	12.3	643.5	20.28	11.1	618	20.2
60	19.9	654.3	21.10	18.2	625	21.0
70	31.2	663.1	21.96	28.8	629	21.9
80	47.4	670.0	22.86	44.2	633	22.8
90	70.1	675.3	23.80	66.1	635	23.8
100	101.3	679.1	24.79	96.2	636	24.8
150	476	682.1	30.77	465	625	30.8
200	1555	663.4	39.10	1546	592	39.0
250	3978	621.4	51.18	3995	541	52.0
300	8593	547.7	71.78	8688	473	75.2
350	16530	447.6	134.59	16820	391	143.0

WVMP SAR Reference 3-28

COMSOL Multiphysics Version 4.3 Software Test Documentation, B-STP-A-00027, Revision 0, Kesterson, M.R., Savannah River National Laboratory, Aiken, South Carolina, December 3, 2012.

(Redacted version)

COMSOL Multiphysics

Versions 4.3

Software Test Documentation

B-STP-A-00027

Revision 0

December 3, 2012

Comsol Multiphysics

Software Revision Number: 4.3

Revision History Log

Revision #	Date	Description of Revision
0	10/29/12	Initial Issue

Approvals:

[redacted]

M.R. Kesterson, Author/Design Agency — Date
Applied Computati nal Engineering and Statistics

[redacted]

D.A. urel o, Independent Reviewer (IR-2) — Date
Applied Computational
Engineering and Statistics

[redacted]

W.A. Drown, Cognizant Quality Function — Date
Quality Engineering

[redacted]

S.J. Hensel, Design Authority — Date
Manager, Computational Engineering and Sciences

Table of Contents

1.0 SCOPE

The software COMSOL Multiphysics is a general purpose engineering analysis program. The COMSOL software is divided into submodules that can be employed based on the type of problem being solved. For the purposes of this test plan, the Heat Transfer module is utilized to enable the modeling of heat transfer via conduction, convection, and radiation.

The Software Test Plan (STP) delineated in this document will cover the software testing, software acceptance, and software baseline of the COMSOL software.

2.0 SOFTWARE AND PRODUCT IDENTIFICATION

Project Name:	Not applicable
Software Product Name:	COMSOL Multiphysics
Operating Division:	Savannah River National Laboratory
Facility:	Applied Computational Engineering and Statistics
Location of Target System:	703-41A
Software Lead Engineer:	Matt Kesterson 703-41A, Room 255 (803) 725-5975

3.0 REFERENCE DOCUMENTS

3.1 B-SQP-A-00057, Rev. 0, "Software Quality Assurance Plan for COMSOL Multiphysics", January 2012.

3.2 IEEE Std. 829-1998, IEEE Standard for Software Test Documentation.

3.3 SRT-EMS-940084, "Heat Transfer Software Test Plan", February 1995, Attachement 9.1

4.0 RESOURCES

4.1 Test Lead Engineer

COMSOL – Matt Kesterson

4.2 Special Equipment

SRNL computer Lenovo Thinkstation 6493-AL7.

4.3 System Configuration

RedHat Enterprise Linux version 5.

5.0 TESTING ACTIVITIES

5.1 Software Operating Environment

COMSOL will operate under the RedHat Linux Operating Environment.

5.2 Existing Test Plans

None

5.3 Test Problems

For computer software, one acceptable method of testing is technical evaluation by tests which demonstrate its capability to produce valid results for the test cases. The test plan for validating the software requirements requires matching the requirements with the test problems, making sure that the test problem is well defined, building the model using the software, inputting required data such as, material properties, loading conditions, boundary conditions, setting the model for run, and finally comparing the results. One test problem can validate more than one requirement in a test run. Fifteen problems have been selected to test the code analysis options that are frequently used in analyses at SRS. These test problems are described in Attachment 9.1. These problems have been used in the past for the dedication of this type of software. For each problem, written and graphical descriptions are provided to define the problem. The option tested is identified and the expected solution is given along with the methodology used in arriving at the solution. The expected solution is obtained from an analytical solution, experimental results, or results from other industry standard software codes.

Attachment 9.1 consists of a set of problems for which solutions have been published, or for which solutions are derived using standard analytical methods, or solution comparison with other software codes, or recommended benchmark problems. The problems were selected with the intent of testing a wide range of: 1) element types, and 2) analysis procedures. 2-D, 3-D, and axisymmetric problems with radiation boundary conditions, Dirichlet (Temperature =constant), and Neumann (heat flux dT/dx = constant) boundary conditions have been solved. These test cases provide an excellent baseline for the analysis and development work which is performed in the SRNL at the SRS.

Note regarding units: When modeling heat transfer due to radiation, an absolute temperature system must be used. COMSOL does not currently have syntax for the Rankine system, the degrees F is used with input temperatures increased by 459.67, and output temperatures reduced by 459.67 (or else reported as Rankine temperatures).

5.4 Acceptance Criteria

The accuracy of solution should be within 0.5% for typical benchmark problems, and within 5% for non-standard problems in comparison with solutions from "industry accepted" codes or experiments.

5.5 Test Logs/Reports

The Test Engineer will create a test logbook for recording any errors or deficiencies encountered during testing, if necessary. The test cases and printed input/output files from the software shall also serve as test documentation. All result directories shall be preserved to verify the input parameters. Input/output files for the various test cases are listed in Attachment 9.4.

5.6 Special Plant/System Configuration

The computer system is a Lenovo Thinkstation 6493-AL7 with the RedHat Linux Enterprise Edition, version 5.

5.7 Training Requirements

The Test Engineer shall be trained in the use of the software. The Owner shall document the training and the background experience of the Test Engineer.

Testing Complete:

[redacted]

Owner, S.J. Hensel Date

[redacted]

Test Engineer, M.R. Kesterson Date

5.8 Schedule

Not Applicable.

5.9 Limiting Conditions

Not Applicable

5.10 Initial Conditions

Software shall be installed such that the program can run locally on the target machine. Material databases shall be installed along with the source file installation.

5.11 Error/Deficiencies Handling

If errors or deficiencies during testing are found, the Test Engineer shall take the following steps:

- immediately stop the testing
- contact the software Owner for error/deficiency resolution
- software Owner shall review the requirements, test method, or Test Engineer's steps to determine the source of error
- The software Owner may revise the requirement, revise the test method or revise the Test Engineer's steps to resolve the error/deficiency.

5.12 Regression Testing

If a requirement or test case is rewritten, all previously testing requirements shall be retested to ensure no adverse effects.

5.13 Recovery Plan

Not applicable.

6.0 ACCEPTANCE

Test results review and approval:

[redacted]

M.R. Kesterson, Design Agency Date

[redacted]

D.A. Tamburello, Date
Independent Reviewer (IR-2)

Owner Acceptance of Software:

[redacted]

S.J. Hensel, Owner Date

7.0 BASELINE ESTABLISHED

Test Lead Engineer:

[redacted]

M.R. Kesterson Date

Design Agency:

[redacted]

M.R. Kesterson Date

Design Authority:

[redacted]

S.J. Hensel Date

8.0 SUMMARY AND CONCLUSIONS

The COMSOL software is classified, tested, and maintained in accordance with the requirements set forth in QAP 20-1 of Manual 1Q. The test problems modeled and run on this software give results that meet the stated acceptance criteria. It is concluded that the COMSOL software will perform its intended safety function.

9.0 ATTACHMENTS

9.1 SRT-EMS-940084, Heat Transfer Software Test Plan, February 1995.
9.2 Test Results and Tester Comments.
9.3 Computer Files

ATTACHMENT 9.1
Heat Transfer Software Test Plan

Table of Contents

PROBLEM 1 :

Infinitely Long Hollow Cylinder with Applied Heat Flux

OPTION(S) TESTED:

Conduction with heat flux (Steady-state, British units)

DESCRIPTION:

A heat flux (q") is applied at the right wall (r_2) and temperature (T_o) is held constant at the left wall (r_1). Steady-state temperatures are calculated assuming an axisymmetric geometry.

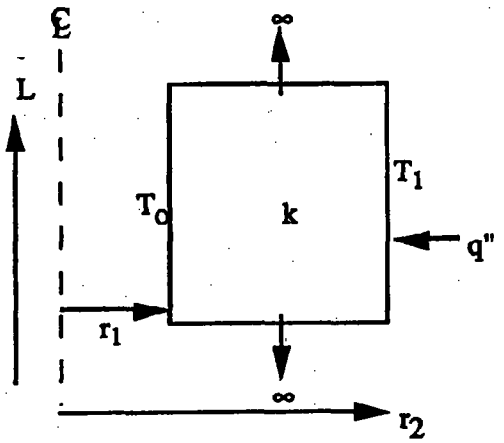

Parameters:

q" = 20 Btu/hr-ft^2	r_2= 3 ft.
T_o = 100° F	k = 1 Btu/hr-ft-°F
r_1 = 2 ft.	L = length (infinite)

EXPECTED SOLUTION:

The temperature at the right boundary (r_2) can be found from the expression:

$$q = \frac{2\pi Lk(T_1 - T_o)}{\ln(r_2/r_1)}$$

Rearranging,

$$T_1 = T_0 + \frac{\ln(r_2/r_1)q}{2\pi kL}$$

By definition the heat rate (q) in Btu/hr can be written as

$$q = 2\pi r_2 L q''.$$

Substituting into the previous equation yields

$$T_1 = T_0 + \frac{\ln(r_2/r_1)2\pi r_2 L q''}{2\pi k L}$$

Simplifying and substituting values gives

$$T_1 = T_0 + \frac{\ln(r_2/r_1) r_2 q''}{k}$$

$$T_1 = 100 + \frac{\ln(3/2)(3)(20)}{1}$$

$$T_1 = 100 + 24.328$$

$$T_1 = 124.328$$

The temperature at the right wall (r_2) is found analytically to be 124.328°F.

REFERENCE: Kreith, Frank, and Black, William Z. Basic Heat Transfer, Harper & Row, New York, 1980, pg 55.

PROBLEM 2 :

Infinitely Long Cylinder with Internal Heat Generation and Convection

OPTION(S) TESTED:

Internal heat generation and convection (Steady-state, British units)

DESCRIPTION:

Heat is generated internally (q''') throughout the solid and is conducted to the right wall at temperature T_s where it is transported by convection to the environment at temperature T_∞. The convective heat transfer coefficient is constant. Steady-state temperatures at the centerline (T(0))are calculated assuming an axisymmetric geometry.

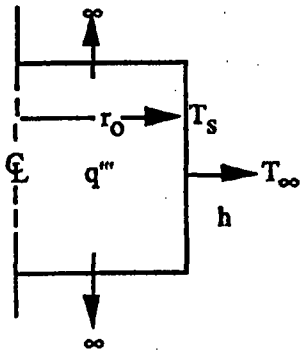

Parameters:

$q''' = 50$ Btu/hr-ft^3
$h = 1$ Btu/hr-ft-°F
$T_\infty = 100$ °F
$r_o = 1$ ft.
$k = 1$ Btu/hr-ft-°F

EXPECTED SOLUTION:

The temperature at the outside surface (r_o) can be found from Newton's law of cooling

$$q = hA(T_s - T_\infty)$$

where A is the surface area of the outside of the cylinder:

$$A = 2\pi r_o L.$$

The heat rate (q) in Btu/hr is found from the cylinder volume and volumetric heat generation (q'''):

$$q = q'''(\pi r_o^{\,2} L)$$

Rearranging Newton's law of cooling and substituting the volumetric heat source gives

$$T_s = T_\infty + \frac{q'''r_o}{2h}$$

$$T_s = 100 + \frac{50(1)}{2(1)}$$

$$T_s = 125$$

The centerline temperature (T(0)) can be found from:

$$T(r) = \frac{q'''r_o^2}{4k}\left(1 - \frac{r^2}{r_o^2}\right) + T_s$$

Substituting at r = 0

$$T(0) = \frac{50(1)}{4(1)} + 125$$

$$T(0) = 12.5 + 125$$

$$T(0) = 137.5$$

The temperature at the centerline(T(0)) is found analytically to be 137.5 °F.

REFERENCE:

Kreith, Frank, and Black, William Z. Basic Heat Transfer, Harper & Row, New York, 1980, pg 72.

PROBLEM 3 :

1D Slab with Internal Heat Generation

OPTION(S) TESTED:

Temperature dependent conductivity (Steady-state, British units)

DESCRIPTION:

Heat is generated internally (q''') in a slab with thickness 2L. The heat is conducted through the solid slab to a fixed wall temperature of T_o. The conductivity is linearly dependent on temperature. Steady-state temperatures at the centerline (x=0) are calculated assuming a slab geometry.

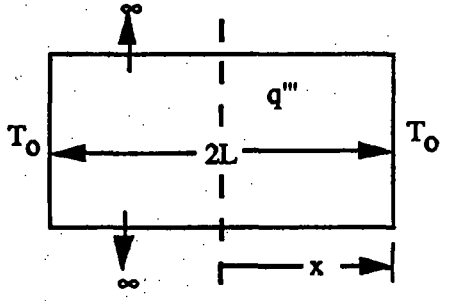

Parameters:	$T_o = 100°$ F	L = 1 ft
	$q''' = 500$ Btu/hr-ft^3	$k = k_0(1 + bT)$
	$k_0 = 1$ Btu/hr-ft-°F	$b = 0.1°$ F^{-1}

EXPECTED SOLUTION:

The thermal conductivity is expressed as $k = k_0(1 + bT)$.

The temperature at x=0 can be found from the expression:

$$\frac{(T(x) - T_0) + \frac{b}{2}(T^2(x) - T_0^2)}{q''' L^2/2k_0} = 1 - (x/L)^2$$

Substituting for $x = 0$ yields

$$\frac{(T(0) - T_0) + \frac{b}{2}(T^2(0) - T_0^2)}{q''' L^2/2k} = 1$$

$$T(0) - T_0 + \frac{b}{2}(T^2(0) - T_0^2) = \frac{q'''L^2}{2k}$$

$$T(0) - 100 + 0.05T^2(0) - 500 = 250$$

$$T(0) = \frac{-1 \pm \sqrt{1 + 4(0.05)(850)}}{0.1} = \frac{-1 \pm \sqrt{171}}{0.1} = 120.767, -140.770$$

Since −140.770 is a physically meaningless root for this problem, T(0) = 120.767.

The temperature at the centerline (x=0) is found analytically to be 120.767 °F.

REFERENCE: Arpaci, Vedat S. Conduction Heat Transfer, Addison-Wesley Publishing Company, Reading, MA., 1966, pg 131.

PROBLEM 4 :

Transient Conduction in a Semi-infinite Solid

OPTION(S) TESTED:

Transient solution (Transient, British units)

DESCRIPTION:

A heat flux (q") is conducted into a semi-infinite solid having an initial temperature (T_0) of 100°F. The temperature at the surface x=0 is calculated in 0.5 hr intervals from 0 to 2 hours.

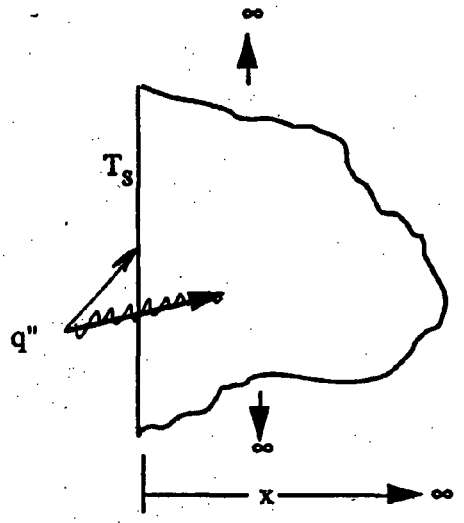

Parameters:

k = 1 Btu/ft-hr-°F **T_0 = 100°F**
c_p = 1 Btu/lbm-°F **q" = 10 Btu/hr-ft^2**
ρ = 1 lbm/ft^3

EXPECTED SOLUTION:

The transient temperature at the left boundary can be found from the expression:

$$T_s = T_0 + \frac{2q''\left(\frac{\alpha t}{\pi}\right)^{1/2}}{k}$$

Substituting values gives

$$T_s = T_0 + 20\sqrt{t/\pi}$$

Note: In the diagram, the heat flux is on the edge of the slab. The arrow pointing to the center was an error in the original document and marked out by hand on the original.

The temperatures at the surface in 0.5 hour intervals are found analytically:

time (minutes)	Temperature (°F) at x=0
0	100.000
0.5	107.979
1.0	111.284
1.5	113.820
2.0	115.958

REFERENCE:

Incropera, Frank P., and DeWitt, David.P. Fundamentals of Heat Transfer, John Wiley & Sons, New York, 1981. pg 205.

PROBLEM 5 :

Concentric Cylinders Modeled as 2-D Plates with Radiation

OPTION(S) TESTED:

Radiation (Transient, British units)

DESCRIPTION:

Radiative heat transfer occurs between concentric regions 2 and 4 (region 3 is void). All surface emmittances and absorptivites are 1. Region 2 radiates to region 4 and region 4 radiates to the ambient. Region 1 is a heat source of 3702.6 Btu/hr-ft.^{3}. The temperatures at locations T3, T8, and T4 are calculated for times of 0, 30, and 90 minutes.

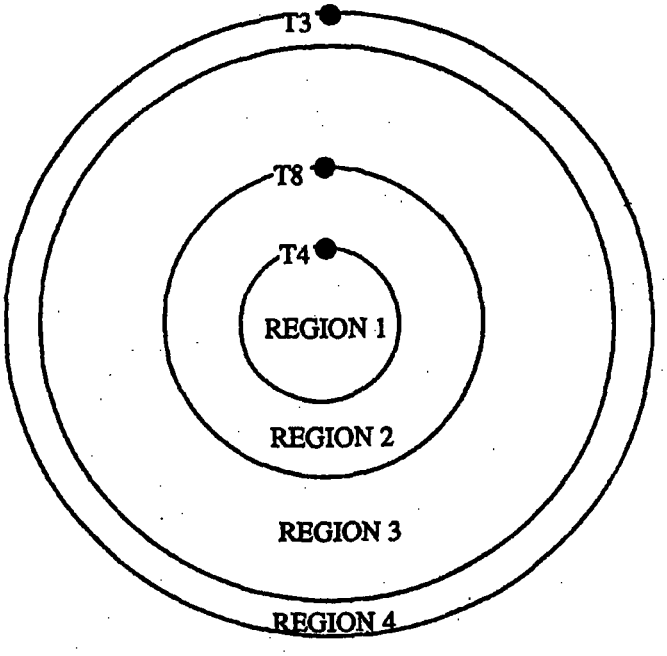

REGION	~~O.D.~~ RADIUS (inches)
1	~~6.9~~ 6.5
2	15.25
3	21.25
4	21.5

Material	Conductivity (Btu/hr-ft-°F)	Specific Heat (Btu/lb$_m$)	Density (lb$_m$/ft^3)
REGION 1	139.7	0.214	169
REGION 2	26	0.113	489
REGION 4	26	0.113	489

Table 1: Material Properties

Note: In the diagram, the radius of region 1 was incorrect in the original print of the test case and was corrected by hand before the original document submission

Time (minutes)	Ambient Temperature (°F)
0	130°F
0 - 30	1475°F
30 - 90	130°F

Table 2: Ambient Temperature

EXPECTED SOLUTION:

The temperatures at locations T3, T8, and T4 are shown below for times of 0, 30, and 90 minutes.

Time (minutes)	Temperatures (°F)		
	T3	T8	T4
0	278.6	399.2	417.5
30	1272.2	708.8	505.4
90	397.4	568.4	595.4

REFERENCE:

Glass, Robert E., Sample Problem Manual For Benchmarking of Cask Analysis Codes (SAND88-0190 TTC-0780 UC-71), Sandia National Laboratories, Albuquerue, NM 87185, February 1988.

PROBLEM 6 :

Freezing of a Square Solid - The Two Dimensional Stefan Problem

OPTION(S) TESTED:

Phase change (Transient, SI units)

DESCRIPTION:

This problem is the two-dimensional Stefan problem: a square block of material is initially liquid, just above the freezing temperature. The temperature of its outside perimeter is reduced suddenly by -45°, so that the block starts to freeze from the outside towards the core. The latent heat of freezing (70.26 J/kg) occurs between the solidus and liquidus temperatures of -0.25° C and -0.15° C, respectively. The initial temperature of the material is 0° C.

The block is a square with a side length of 8 meters. Symmetry allows the mesh to be generated on only one quarter of the model. A graphical ABAQUS solution is presented for the first 5 seconds of the transient at the points 'A' and 'B' which are shown in the figure below. The ABAQUS element used is type DC2D4 (four-node, bilinear quadrilateral).

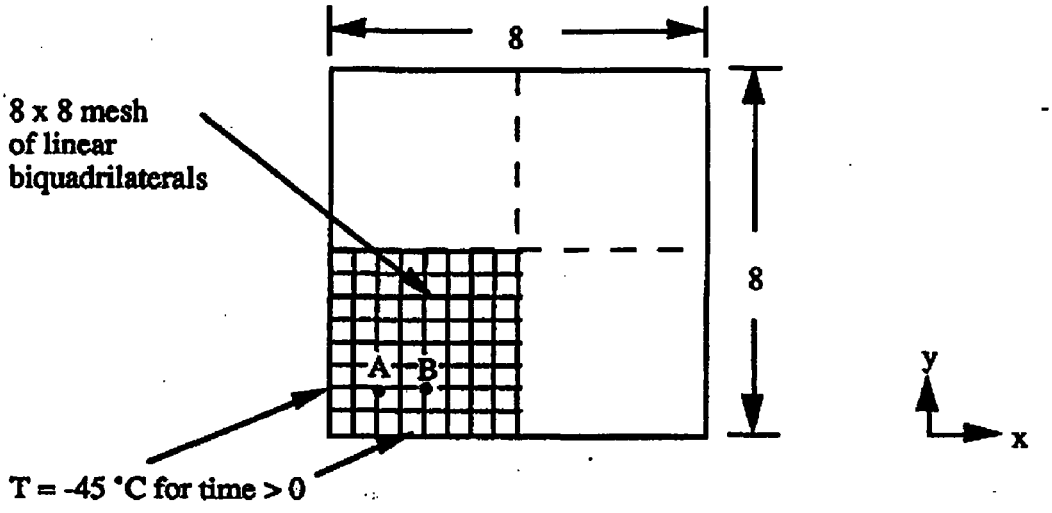

Parameters: $k = 1.08$ W/m-°C $\quad c_p = 1.0$ J/kg
$\rho = 1.0$ kg/m^3

EXPECTED SOLUTION:

Plots of the temperatures computed by COMSOL Multiphysics should be similar to those computed by ABAQUS.

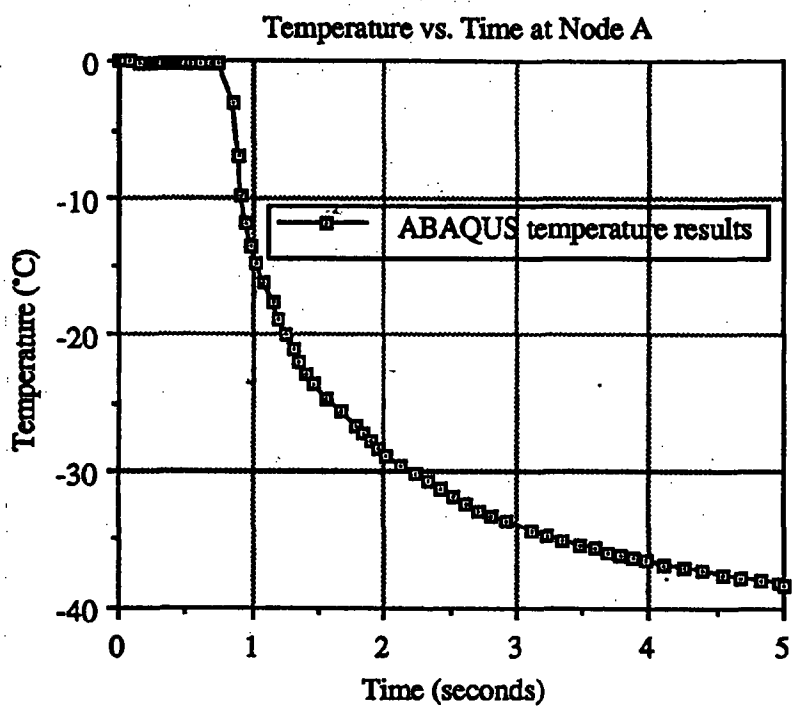
Temperature vs. Time at Node A
0
-10
-20
-30
-40
Temperature (°C)
ABAQUS temperature results
0
1
2
3
4
5
Time (seconds)

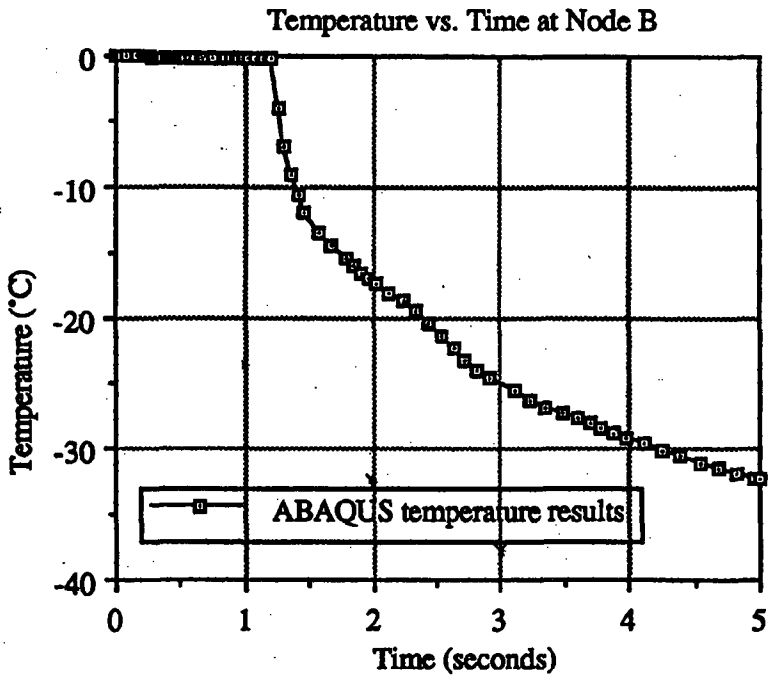
Temperature vs. Time at Node B
0
-10
-20
-30
-40
Temperature (°C)
ABAQUS temperature results
0
1
2
3
4
5
Time (seconds)

PROBLEM 7 :

Insulated Slab with Radiation

OPTION(S) TESTED:

Conduction and radiation (Steady-state, SI units)

DESCRIPTION:

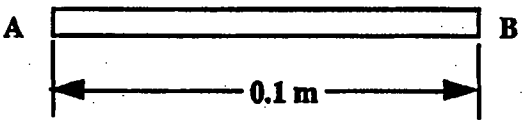

Parameters: $T_a = 1000$ K $\varepsilon_b = 0.98$
$T_{ambient} = 300$ K $k = 55.6$ W/m-° C

This problem is found in ABAQUS V5.2 Verification Manual, page 6.2.2. The ABAQUS element type tested is DC2D8 (8 noded quadrilateral elements). The model used a uniform mesh with 10 elements along the length.

Geometry consists of a rectangular region with zero heat flux along the top and bottom boundary, and fixed temperature (T_a) at the left end. Heat is conducted through the solid to the right end at temperature (T_b) which radiates to an environment at 300 K. The right end has an emissivity (ε_b). There is no internal heat generation.

This is a test recommended by the National Agency for Finite Element Methods and Standards (U.K.): Test T2 from NAFEMS publication TNSB, Rev. 3, "The Standard NAFEMS Benchmarks," October 1990. The temperature results are compared for point B.

EXPECTED SOLUTION:

The temperature at point B is computed by ABAQUS to be 653.80 °C.

PROBLEM 8 :

Insulated Slab with Variable Temperature Boundary Condition

OPTION(S) TESTED:

Transient analysis using a variable temperature boundary condition (Transient, SI units)

DESCRIPTION:

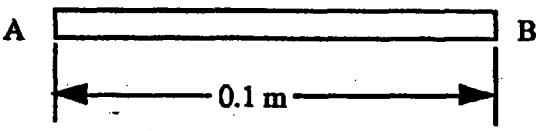

Parameters:

$T_a = 0°$ C
$T_b = 100\sin(\pi t/40)°$ C where t is in seconds
$\rho = 7200$ kg/m^3
$k = 35.0$ W/m-°C
$c_p = 440.5$ J/kg°C

This problem is found in ABAQUS V5.2 Verification Manual, pg 6.2.3. The ABAQUS element type tested is DC1D3 (1-D with 3 nodes per bar element).

Geometry consists of a rectangular region with zero heat flux along the top and bottom boundary, and fixed temperature (T_a) at the left end and with a varying temperature (T_b) at the right end. There is no internal heat generation.

This is a test recommended by the National Agency for Finite Element Methods and Standards (U.K.): Test T3 from NAFEMS publication TNSB, Rev. 3, "The Standard NAFEMS Benchmarks," October 1990. The temperature results are compared for .

EXPECTED SOLUTION:

The target solution is 36.60° C at x = 0.08 m and 32 secs .

PROBLEM 9 :

2-D Slab with Convection

OPTION(S) TESTED:

2-D with convection (Steady-state, SI units)

DESCRIPTION:

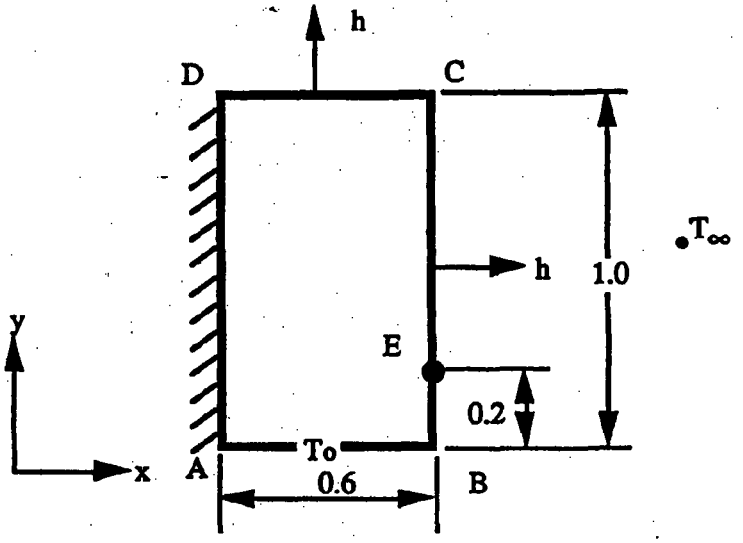

Parameters: $h = 750\ W/m^{2\circ}\ C$; $T_o = 100^\circ\ C$; $k = 52\ W/m^\circ\ C$, $T_\infty = 0^\circ\ C$

This problem is found in ABAQUS V5.2 Verification Manual, page 6.2.4. The ABAQUS element type tested is DC3D8 (3-D with 8 nodes per hexagonal element). The mesh is uniform and the width (Δx) and height (Δy) for each element is 0.1 m. There are four elements through the thickness (Δz) for the ABAQUS model.

Geometry consists of a rectangular region with zero heat flux along the left boundary, and convection to the ambient at T_∞ along right and top boundaries. The bottom is held at a constant temperature (T_o). There is no internal heat generation.

This is a test recommended by the National Agency for Finite Element Methods and Standards (U.K.): Test T4 from NAFEMS publication TNSB, Rev. 3, "The Standard NAFEMS Benchmarks," October 1990.

EXPECTED SOLUTION:

The temperature at point E as computed by ABAQUS is 18.26 °C.

PROBLEM 10 :

1M X 1M Square Aluminum Plate

OPTION(S) TESTED:

Nodal point heat source (Steady-state, SI units)

DESCRIPTION:

A square aluminum plate has a left boundary fixed at 100.0 K and a right boundary with a constant heat flux of 1000.0 W/m^2. At the bottom heat is lost to the environment at 300K through convection with a coefficient of 13.4 W/m^2-K. The top boundary is insulated. At the center of the plate (0.5, 0.5) is a nodal point heat source of 1000W. The plate is uniformly meshed (4x4) with sixteen 4-noded quadrilaterals. P3/THERMAL results are compared to ABAQUS results at the specified coordinates.

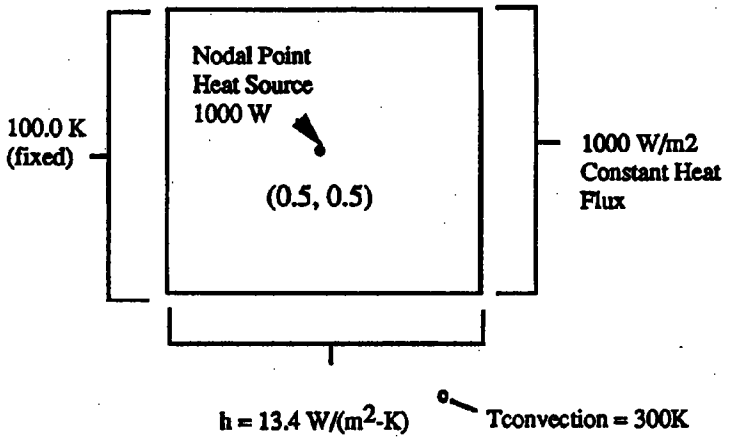

Parameters: $k_{aluminum}$ = 293.076 W/mK

EXPECTED SOLUTION:

The temperatures computed by ABAQUS at three coordinates are shown below:

Coordinates	Temperature (K)
(1, 1)	108.0906
(0.5, 0.5)	107.1976
(1, 0)	112.1438

PROBLEM 11 :

"Stiff" Thermal Problem with the Direct Solver

OPTION(S) TESTED:

Numerical convergence (Steady-state, SI units)

DESCRIPTION:

This problem has been designed to illustrate the thermally "stiff" problem. A material with a lower thermal conductivity and width of 0.5 m is sandwiched between two materials with a higher conductivity and width of 1 m. Temperature and heat flux boundary conditions are imposed on the surfaces as illustrated. QTRAN has Iterative (SOL = 0) and Direct (SOL=2) solution options. For "stiff" thermal problems iterative solvers tend to converge very slowly while direct solvers work very efficiently. This problem is solved using the direct solver. Temperature results are compared to ABAQUS V5.2 temperature results at the coordinates x = 1.0 and y = 9.0.

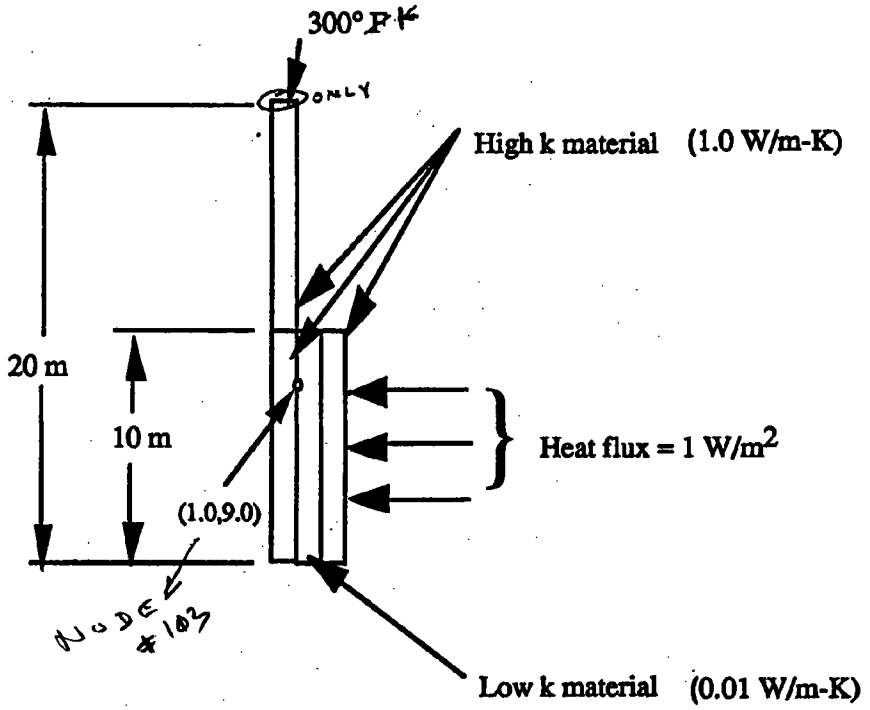

EXPECTED SOLUTION:

The temperature at coordinates (1.0,9.0) is computed by ABAQUS to be 409.690502 K.

PROBLEM 12 :

Infinitely Long Hollow Cylinder with Multiple Materials

OPTION(S) TESTED:

Conduction through multiple materials (Steady-state, British units)

DESCRIPTION:

An infinitely long hollow cylinder is composed of 9 concentric cylinders of various materials, some of which have temperature dependent thermal conductivities. There are constant temperature boundary conditions at the inner cylinder wall of 339° F and between the stainless steel/fiberglass interface of 190° F. The objective is find the temperature at the fiberfrax/stainless steel interface.

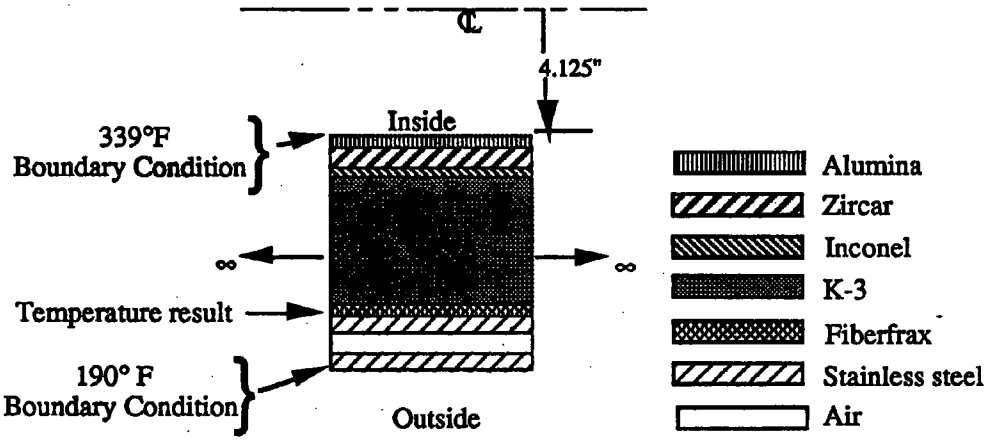

Parameters: $T_i = 339°$ F $\quad T_o = 190°$ F
$r_o = 14.275$ $\quad r_i = 4.125$
L = length (infinite)

Material	outer radius (r_o) (inches)	inner radius (r_i) (inches)	Conductivity (k) (Btu/hr-ft-°F)
Alumina	4.455	4.125	13.1 @ 339° F
Zircar	5.195	4.455	0.054 @ 305° F
Inconel	5.5	5.195	8.16 @ 271° F
K-3	11.25	5.5	2.5 @ 268° F
Fiberfrax	12.0	11.25	0.055 @ 251° F
Stainless steel	13.4	12.0	9.54 @ 237° F
Air	13.9	13.4	0.0184 @ 214° F
Stainless steel	14.275	13.9	9.23 @190° F

The rate of heat transfer by conduction across the materials (q) can be determined from

$$q = \frac{2\pi kL(T_i - T_o)}{\ln(r_o/r_i)} = \frac{(T_i - T_o)}{R_t}$$

The rate of heat transfer by conduction across the materials (q) can be determined from

$$q = \frac{2\pi kL(T_i - T_o)}{\ln(r_o/r_i)} = \frac{(T_i - T_o)}{R_t}$$

The total thermal resistance (R_t) is found by the summation of individual resistances:

$$R_t = \Sigma \frac{\ln(r_o/r_i)}{2\pi kL}$$

Substituting values between the 339° F boundary condition (T_i) and 190° F boundary condition (T_o) yields $R_t = 1.0064$. When $T_i = 339°$ F and $T_o = 190°$ F, q = 148.0451 Btu/hr.

The total thermal resistance (R_t) between the 190° F boundary condition and the stainless steel/fiberglass interface is calculated to be 0.3192. Substituting $R_t = 0.3192$, q = 148.0451, and $T_o = 190°$ F into the equation for heat transfer by conduction gives $T_i = 237.25°$ F.

EXPECTED SOLUTION:

The temperature at the stainless steel/fiberfrax interface is analytically found to be 237° F.

REFERENCE: Kreith, Frank, and Black, William Z. Basic Heat Transfer, Harper & Row, New York, 1980, pp 55, 56.

PROBLEM 13 :

2-D Plate with Two Isothermal Boundaries

OPTION(S) TESTED:

Spatially dependent temperature boundary condition (Steady-state, SI units)

DESCRIPTION:

A 2-D plate has a constant temperature of 0 K at the left and right boundaries. A spatially dependent temperature boundary condition is imposed at the top and bottom of the plate as shown below:

$$T(x, y) = x \qquad 0 \le x \le 1$$
$$T(x, y) = 2 - x \qquad 1 < x \le 2.$$

Temperatures are calculated analytically at three randomly selected nodal locations: (1.45, 1.1), (0.85, 1.5), and (0.15, 0.7).

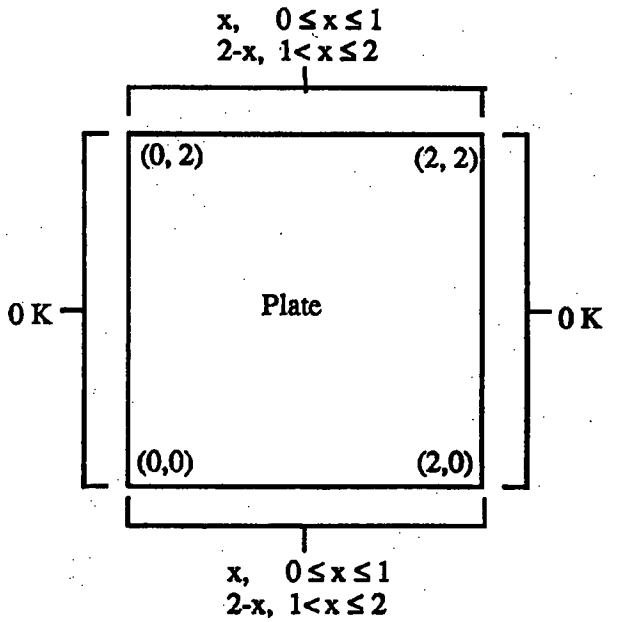

Parameters:

a = 2 m (plate length) b = 2 m (plate width)

EXPECTED SOLUTION:

The temperature at any (x,y) coordinate within the domain can be found from

$$T(x,y) = \frac{8}{\pi^2}\sum_{n=1}^{\infty}\frac{\sin(n\pi/2)}{n^2}\left\{\frac{\sinh\left(\frac{n\pi}{a}\right)y + \sinh\left[\frac{n\pi}{a}(b-y)\right]}{\sinh\left(\frac{n\pi}{a}\right)b}\right\}\sin\left(\frac{n\pi}{a}\right)x$$

The solution is found from the following FORTRAN program and output after substituting values for the plate length and width and summing the first 35 terms. Temperatures are calculated at the three arbitrarily selected points within the domain: (1.45, 1.1), (0.85, 1.5), and (0.15, 0.7).

PROGRAM

```
                program sum
c
      print*, 'Enter x : '
      read (*,*) x
      print*, 'Enter y : '
      read (*,*) y
c
      tsum = 0.0
      pi = 3.14159265
      do 10 n = 1, 35
       at = n*pi/2.0
       gin = (sinh(at*y) + sinh(at*(2-y)))/sinh(n*pi)
       sum = sin(at)/n**2 * gin * sin(at*x)
       tsum = tsum + sum
 10   continue
c
      write (*, *) 'sum = ', 8.0*tsum/pi**2
c
      stop
      end
```

OUTPUT

```
 f77 sum.f
% a.out
 Enter x :
1.45
 Enter y :
1.1
 sum =  0.2477080
% a.out
 Enter x :
0.85
 Enter y :
1.5
 sum =  0.4228634
% a.out
 Enter x :
0.15
 Enter y :
0.7
 sum =  8.1770860E-02
```

The temperatures calculated at the three points are shown below :

Node	Coordinates	Temperature (K)
472	(1.45, 1.1)	0.2477080
1479	(0.85, 1.5)	0.422863
1145	(0.15, 0.7)	0.081771

REFERENCE:
Powers, David L. Boundary Value Problems, Clarkson College of Technology, Academic Press, Inc., 1979. pp 182, 183.

PROBLEM 14 :

Radiation Exchange between Two Infinitely Long Cylinders and Space

OPTION(S) TESTED:

Radiation view factor calculations (Steady-state, SI units)

DESCRIPTION:

To test performance of P3/THERMAL's integrated viewfactor/radiation resistor generation program, a benchmark analysis was chosen that has an exact solution. This thermal radiation benchmark consists of two parallel cylinders, each 1-meter in radius, with the centerlines separated by 2.25 meters. A uniform heat flux of 1000 W/m^2 is applied on the outer surfaces. The cylinder material is assumed to be a near perfect conductor (thermal conductivity of 7920 W/m-K) to make the radial temperature gradient small so that the analytical solution can be easily shown. The surface emissivity is 1.0. The space temperature (T_∞) is taken as absolute zero. The relatively close proximity of the cylinders makes this benchmark a significant challenge to a radiation view factor code. This benchmark demonstrates P3/THERMAL's view factor program accuracy for a complicated view factor problem as well as the capability of the solver to model the radiation network.

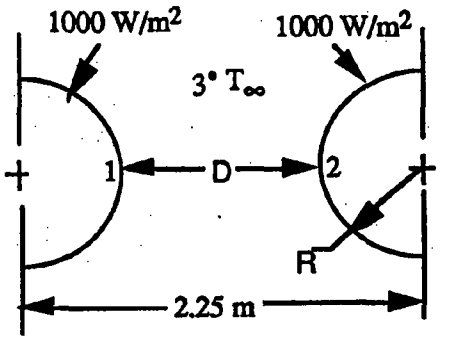

Parameters: D = 0.25 m R = 1 m
q" = 1000 W/m^2 $\sigma = 5.7(10)^{-8}$ W/m^2-K^4

EXPECTED SOLUTION:

The net heat flux between surface 1 and the environment is

$$q''_{1\text{-}3} = \sigma F_{1\text{-}3}(T_1^4 - T_3^4)$$

The viewfactors (F) for this arrangement can be expressed as

$$F_{1\text{-}2} + F_{1\text{-}3} = 1.0.$$

with

with

$$F_{1-2} = \frac{2}{\pi}\left[(X^2 - 1)^{1/2} + \frac{\pi}{2} - \cos^{-1}\left(\frac{1}{X}\right) - X \right]$$

$$\text{where } X = 1 + \frac{D}{2R}$$

Evaluating, $F_{1-2} = 0.30895$ and $E_{1-3} = 0.69105$.

Substituting these values into the expression for the net heat flux q''_{1-3} yields $T_1 = 399.700$ K.

The temperature of the cylinder surface is analytically found to be 399.700 K.

REFERENCES:

Siegel, Robert and Howell, John. Thermal Radiation Heat Transfer, 2nd. ed., Hemisphere Publishing Co., 1981. pg 205.

PROBLEM 15 :

3-D Brick with Heat Flux, Convection, and Temperature Boundary Conditions

OPTION(S) TESTED:

3-D conduction (Steady-state, SI units)

DESCRIPTION:

A brick has a width of 1.0 m (Δz), length of 2.0 m (Δx), and height of 1.0 m (Δy). A heat flux (q''_f) of 245 W/m^2 is applied at the plane $z = 1$. Convection (q''_c) with a convective heat transfer coefficient of 180 W/m^{2}K occurs to an environment at 250 K at the plane $x = 2$. The boundary at $y = 0$ is held at a constant temperature of 300 K. The remaining boundaries are insulated. The thermal conductivity of the brick is 40 W/mK.

The brick is uniformly meshed with 250 8-noded hexahedrons, each having an element edge length of 0.2 m. Temperatures computed by ABAQUS are shown at three arbitrarily selected nodal locations within the brick.

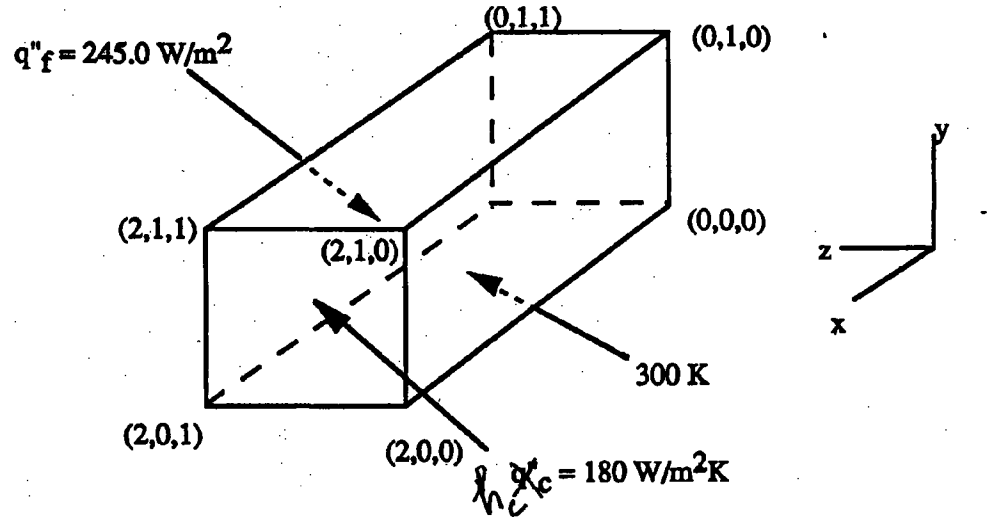

EXPECTED SOLUTION:

The temperatures at three nodes are found by ABAQUS as shown below:

Node	Coordinates (x,y,z)	Temperature (K)
305	(1.4, 0.6, 0.8)	287.566078
227	(1.2, 0.4, 0.6)	293.430702
82	(0.8, 0.2, 0.2)	298.230642

ATTACHMENT 9.2 – TEST RESULTS

The following results compare the COMSOL solutions to the theoretical or other solutions at the specified critical points. The test cases (Problem #s) identified in Attachment 9.1 were run on Redhat Linux Enterprise Edition version 5 and therefore satisfy the RSS #1 [B-SQP-A-00057, Attachment A]. Computer input and output files are listed in Attachment 9.4.

Test Problem 1: Infinitely Long Hollow Cylinder with Applied Heat Flux

Results: The temperature at the right boundary (r_2)

COMSOL 4.3 (°F)	Analytical (°F)	Error (%)
124.33	124.328	<0.01

The temperature contours are shown in Figure 1.

Tester's Comments: This problem satisfies the RSS # 3.2a, 3.2b, 3.2d, 3.3, 3.4b, 3.4e, and 3.6. Software calculated result meets the acceptance criteria.

Test Problem 2: Infinitely Long Hollow Cylinder with Internal Heat Generation and Convection

Results: The temperature at the centerline (r_o)

COMSOL 4.3 (°F)	Analytical (°F)	Error (%)
137.5	137.5	<0.01

The temperature contours are shown in Figure 2.

Tester's Comments: This problem satisfies the RSS # 3.2a, 3.2b, 3.2d, 3.3, 3.4a, 3.4b, 3.4g, and 3.6. Software calculated result meets the acceptance criteria.

Test Problem 3: 1-D Slab with Internal Heat Generation

Results: The temperature at centerline (x=0):

COMSOL 4.3 (°F)	Analytical (°F)	Error (%)
120.77	120.767	<0.01

The temperature contours are shown in Figure 3.

Tester's Comments: This problem satisfies the RSS # 3.2a, 3.2b, 3.2d, 3.3, 3.4b, 3.4e, 3.4g, and 3.6. Software calculated result meets the acceptance criteria.

Test Problem 4: Transient Conduction in a Semi-infinite solid

Results: The temperatures at x = 0, at 30 minute interval:

Time (Hours)	COMSOL 4.3 (°F)	Analytical (°F)	Error (%)
0	100.000	100.000	<0.01
0.5	107.978	107.977	<0.01
1.0	111.283	111.283	<0.01
1.5	113.812	113.821	<0.01
2.0	115.958	115.959	<0.01

The temperature contours are shown in Figure 4.

Tester's Comments: This problem satisfies the RSS # 3.2a, 3.2b, 3.2d, 3.2f, 3.2g, 3.3, 3.4b, 3.4e, and 3.6. Software calculated results meet the acceptance criteria.

Test Problem 5: Concentric Cylinders Modeled as 2-D Plates with Radiation

Results: The temperatures at T3, T4, and T8 are:

Time (min)	COMSOL 4.3 (°F)			**Reference (°F)**			4.3 Error (%)		
	T3	**T8**	**T4**	**T3**	**T8**	**T4**	**T3**	**T8**	**T4**
0	278.4	400.0	417.8	278.6	399.2	417.5	0.07%	0.20%	0.07%
30	1273.2	710.2	505.5	1272.2	708.8	505.4	0.08%	0.20%	0.02%
90	398.7	569.5	596.2	397.4	568.4	595.4	0.33%	0.19%	0.13%

The temperature contours are shown in Figure 5.

Tester's Comments: This problem satisfies the RSS # 3.2a, 3.2b, 3.2d, 3.2e, 3.2f, 3.3, 3.4b, 3.4f, 3.4g, and 3.6. Software calculated results meet the acceptance criteria.

Problem 6: Freezing of a Square Solid – The 2-D Stefan Problem

Results: The temperatures at Points A and B are given in Figure 6:

Tester's Comments: This problem satisfies the RSS # 3.2a, 3.2b, 3.2c, 3.2d, 3.f, 3.3, 3.4b, 3.4e, 3.5, and 3.6. Temperatures calculated by COMSOL are in good agreement with ABAQUS results. COMSOL does not have specific inputs for latent heat due to phase change, but COSOL does give the user great flexibility by allowing the user to input equations describing the systems phase change. Based on these observations, the results obtained using COMSOL are in good agreement with the ABAQUS results.

Problem 7: Insulated Slab with radiation

Results: The temperature at point B is:

COMSOL 4.3 (°C)	ABAQUS (°C)	Error (%)
653.85	653.80	<0.01

The temperature contours are shown in Figure 7.

Tester's Comments: This problem satisfies the RSS # 3.2a, 3.2b, 3.2d, 3.2e, 3.2f, 3.3, 3.4b, 3.4f, and 3.6. Software calculated result meets the acceptance criteria.

Problem 8: Insulated Slab with Variable Temperature Boundary Condition.

Results: The temperature at point B (x = 0.08 m and 32 secs) is:

COMSOL 4.3 (°C)	ABAQUS (°C)	Error (%)
36.60	36.60	<0.01

The temperature contours are shown in Figure 8.

Tester's Comments: This problem satisfies the RSS # 3.2a, 3.2b, 3.2d, 3.2f, 3.3, 3.4b, 3.4c, 3.4e, and 3.6. Software calculated result meets the acceptance criteria.

Problem 9: 2-D Slab with Convection

Results: The temperature at point E is:

COMSOL 4.3 (°C)	ABAQUS (°C)	Error (%)
18.25	18.26	<0.05

The temperature contours are shown in Figure 9.

Tester's Comments: This problem satisfies the RSS # 3.2a, 3.2b, 3.2d, 3.2f, 3.3, 3.4a, 3.4b, 3.4e, and 3.6. Software calculated result meets the acceptance criteria.

Problem 10: 1M X 1M Square Aluminum Plate

Results: The temperatures at three nodes are:

Node	Coordinates	COMSOL 4.3 (°K)	ABAQUS (K)	Error (%)
5	(1, 1)	108.1249	108.0906	0.032
3	(0.5, 0.5)	107.83248	107.1976	0.529
4	(1, 0)	112.14712	112.1438	<0.01

The temperature contours are shown in Figure 10.

Tester's Comments: This problem satisfies the RSS # 3.2a, 3.2b, 3.2d, 3.2f, 3.3, 3.4a, 3.4b, 3.4e, 3.4g, and 3.6. Software calculated results meet the acceptance criteria.

Problem 11: "Stiff" Thermal Problem with Direct Solver

Results: The temperature at coordinate (1.0, 9.0) is:

COMSOL 4.3 (°K)	ABAQUS (°K)	Error (%)
409.69505	409.690502	<0.01

The temperature contours are shown in Figure 11.

Tester's Comments: This problem satisfies the RSS # 3.2a, 3.2b, 3.2d, 3.2f, 3.3, 3.4b, 3.4e, and3.6. Software calculated result meets the acceptance criteria.

Problem 12: Infinitely Long Hollow Cylinder with Multiple Materials

Results: The temperature at the Fiberfrax/stainless steel interface is:

COMSOL 4.3 (°F)	Analytical (°F)	Error (%)
237.25	237.25	<0.01

The temperature contours are shown in Figure 12.

Tester's Comments: This problem satisfies the RSS # 3.2a, 3.2b, 3.2d, 3.2f, 3.3, 3.4b, 3.4e, and 3.6. Software calculated result meets the acceptance criteria.

Problem 13: 2-D Plate with Two Isotherm Boundaries

Results: The temperatures at the selected nodal points are:

Node	Coordinates	COMSOL 4.3 (°K)	Analytical (K)	Error (%)
932	(1.45, 1.1)	0.24815	0.2477080	0.18
1248	(0.85, 1.5)	0.42375	0.422863	0.21
578	(0.15, 0.7)	0.08189	0.081973	0.10

The temperature contours are shown in Figure 13.

Tester's Comments: This problem satisfies the RSS # 3.2a, 3.2b, 3.2d, 3.2f, 3.3, 3.4b, 3.4d, 3.4e, and 3.6. Software calculated results meet the acceptance criteria.

Problem 14: Radiation Exchange between Two Infinitely Long Cylinders and Space
Results: The temperature at the cylindrical surface is:

COMSOL 4.3 (°K)	Analytical (°K)	4.3 Error (%)
399.65	399.700	0.01

The temperature contours are shown in Figure 14.

Tester's Comments: This problem satisfies the RSS # 3.2a, 3.2b, 3.2d, 3.2e, 3.2f, 3.3, 3.4b, 3.4e, 3.4f, and 3.6. Software calculated result meets the acceptance criteria.

Problem 15: 3-D Brick with Heat Flux, Convection, and Temperature Boundary Conditions

Results: The temperature at the cylindrical surface is:

Node	Coordinates	COMSOL 4.3 (°K)	ABAQUS (°K)	4.3 Error (%)
623	(1.4, 0.6, 0.8)	287.34454	287.566078	0.08
1061	(1.2, 0.4, 0.6)	293.24771	293.430702	0.06
1939	(0.8, 0.2, 0.2)	298.17468	298.230642	0.02

The temperature contours are shown in Figure 15.

Tester's Comments: This problem satisfies the RSS # 3.2a, 3.2b, 3.2d, 3.2e, 3.2f, 3.3, 3.4a, 3.4b, 3.4e, and 3.6. Software calculated results meet the acceptance criteria.

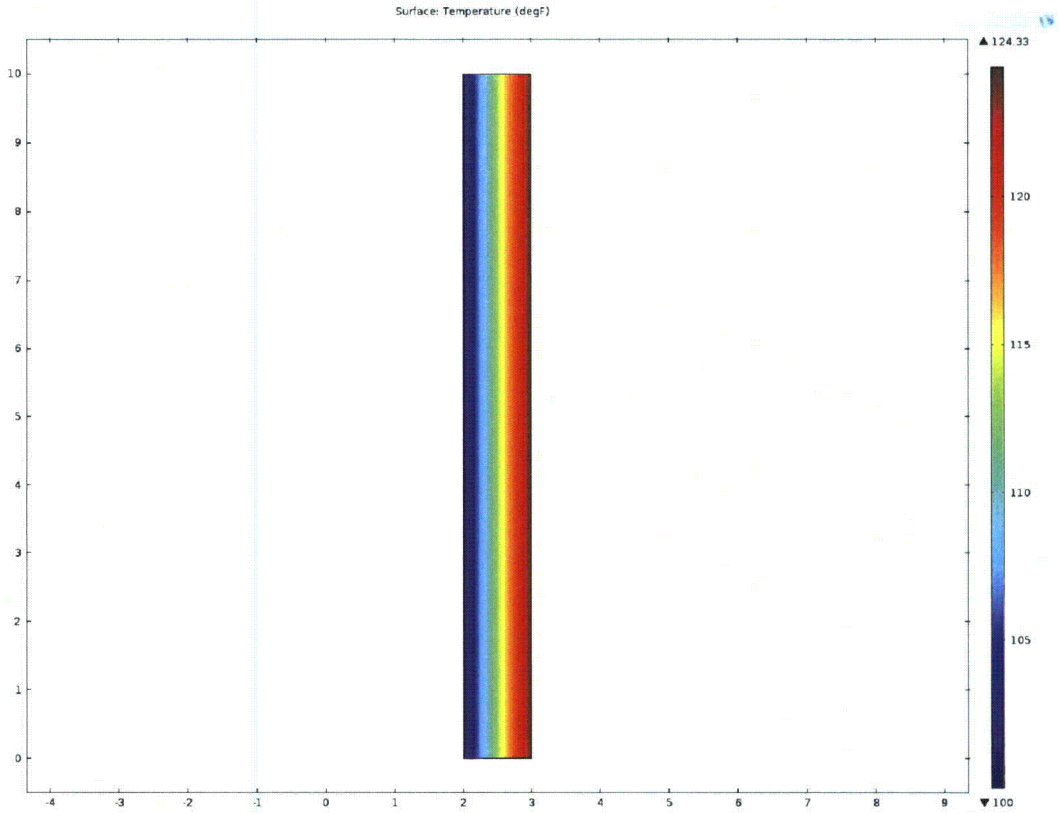

Figure 1 – Temperature Contours for Test Problem No. 1

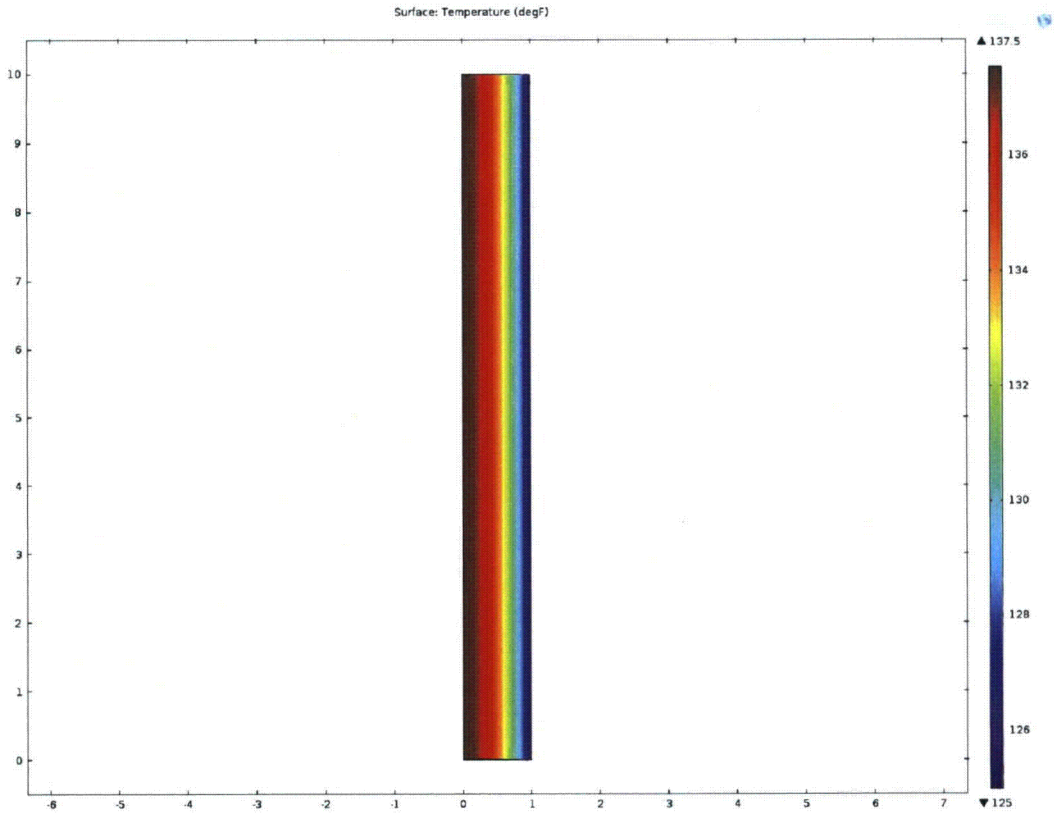

Figure 2 – Temperature Contours for Test Problem No. 2

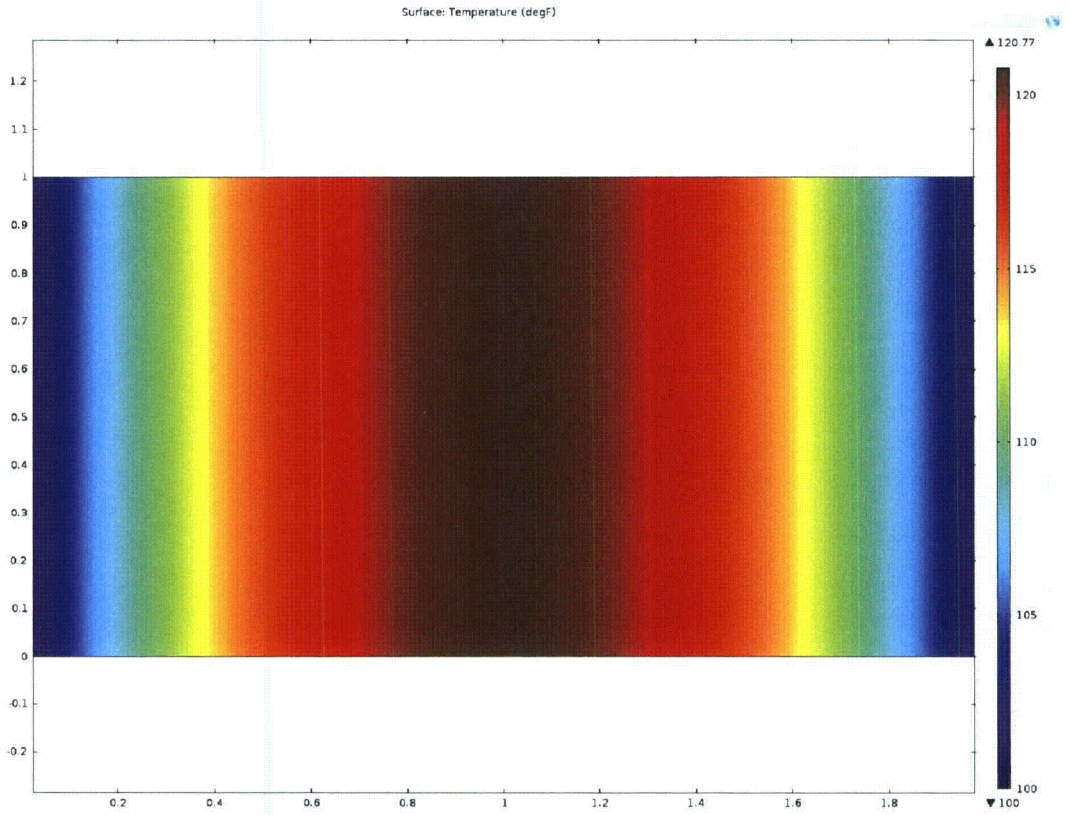

Figure 3 – Temperature Contours for Test Problem No. 3

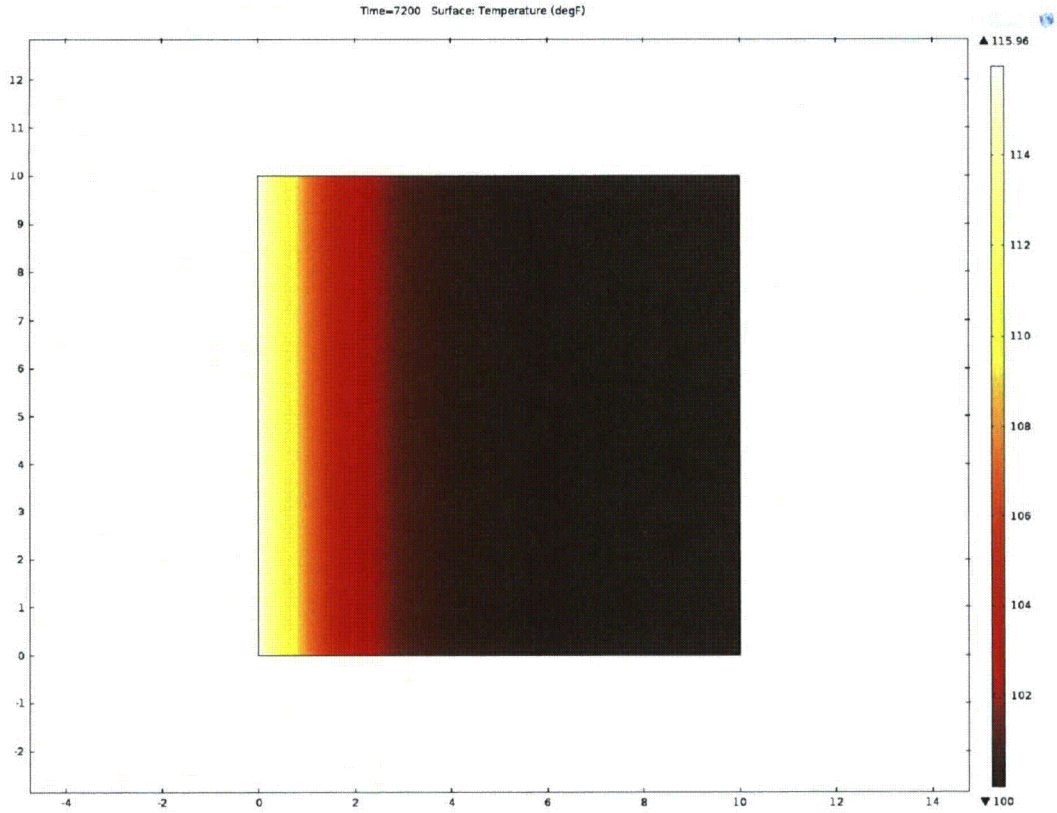

Figure 4 – Temperature Contours for Test Problem No. 4

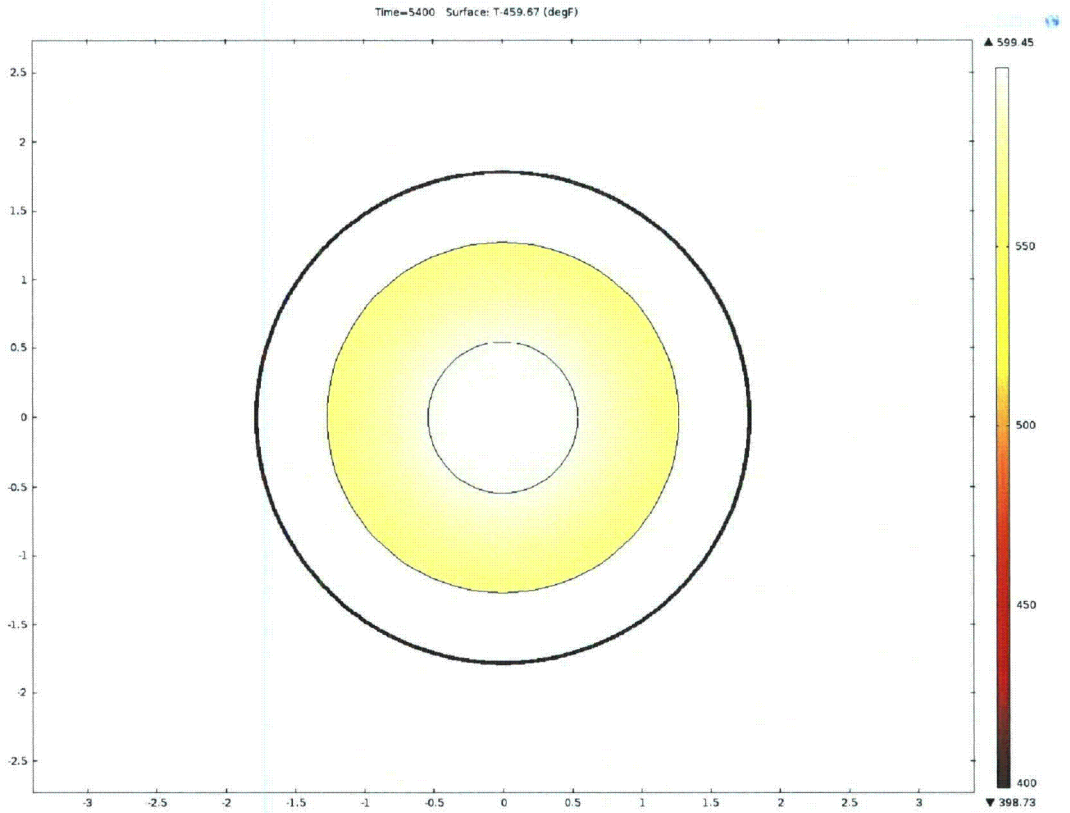

Figure 5 – Temperature Contours for Test Problem No. 5

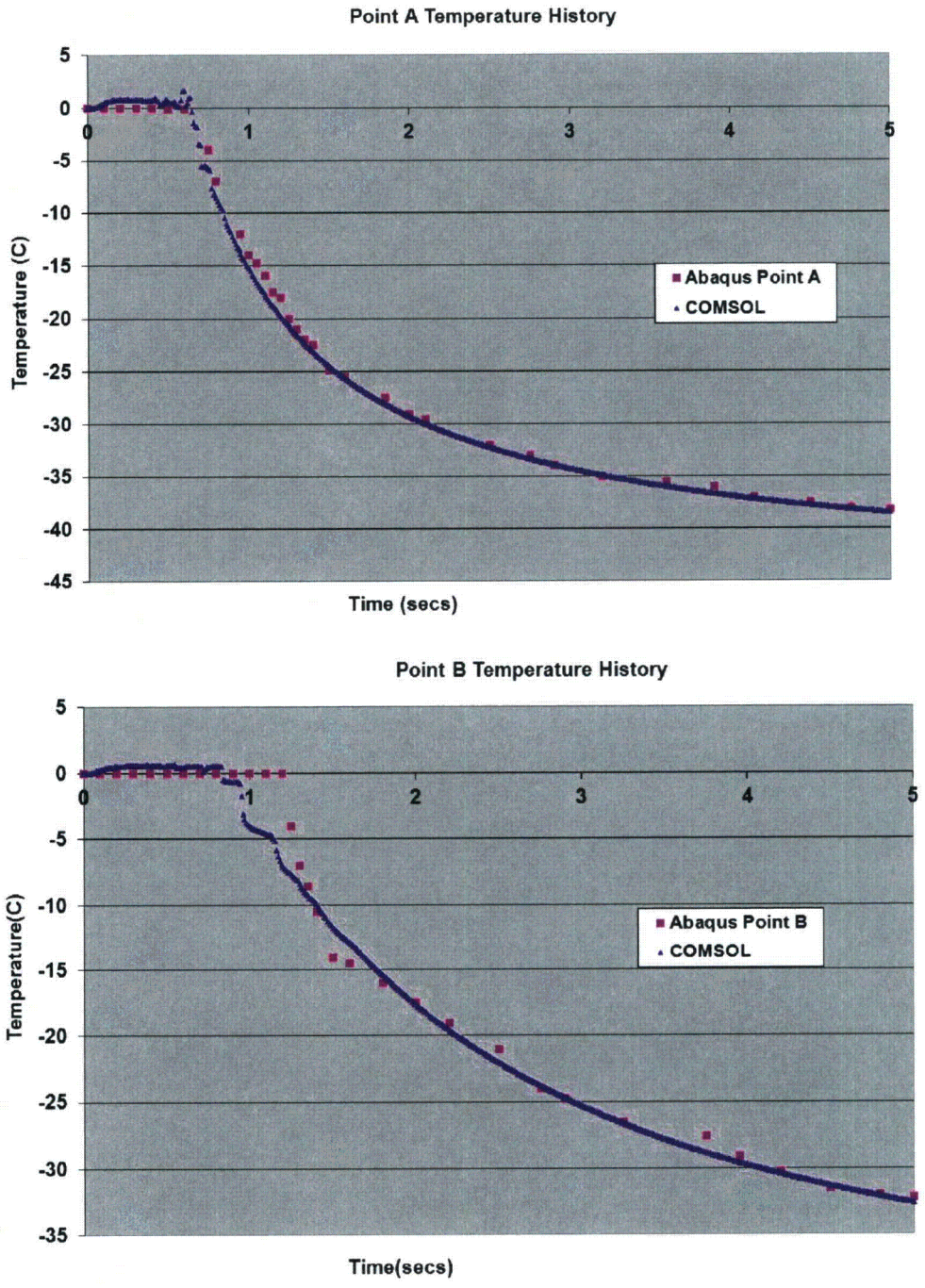

Figure 6 - Temperature Plots for Test Problem No. 6

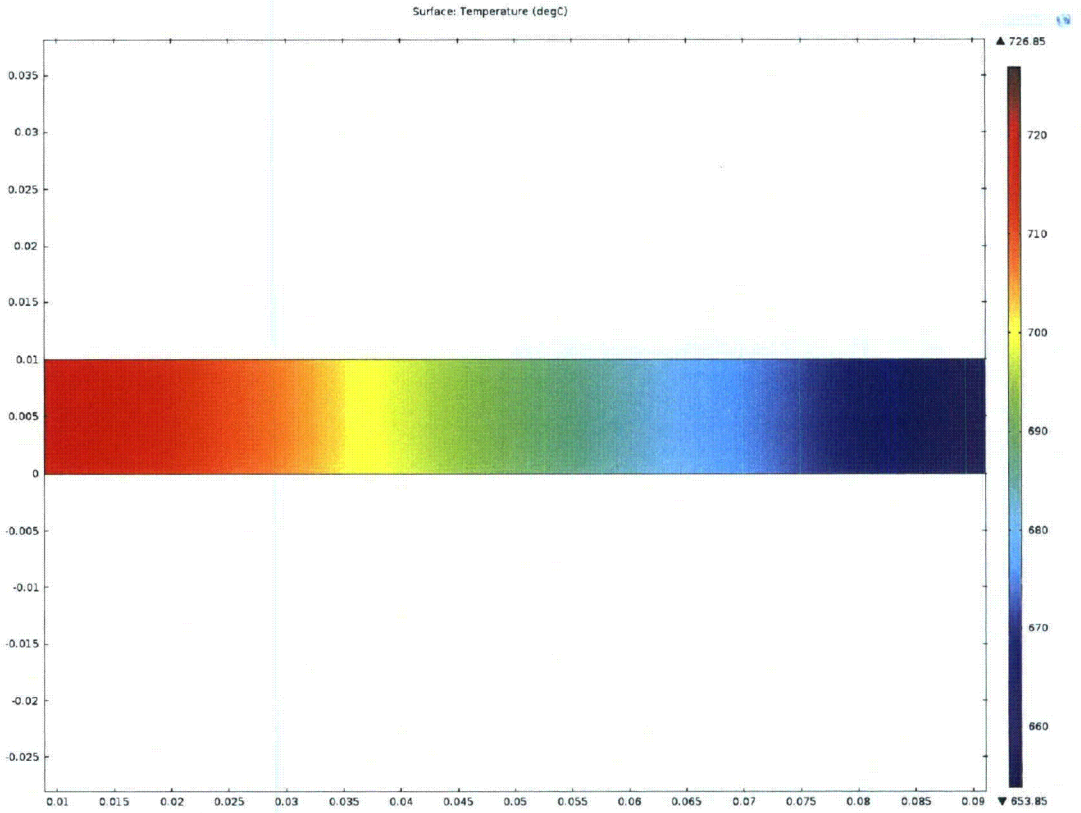

Figure 7– Temperature Contours for Test Problem No. 7

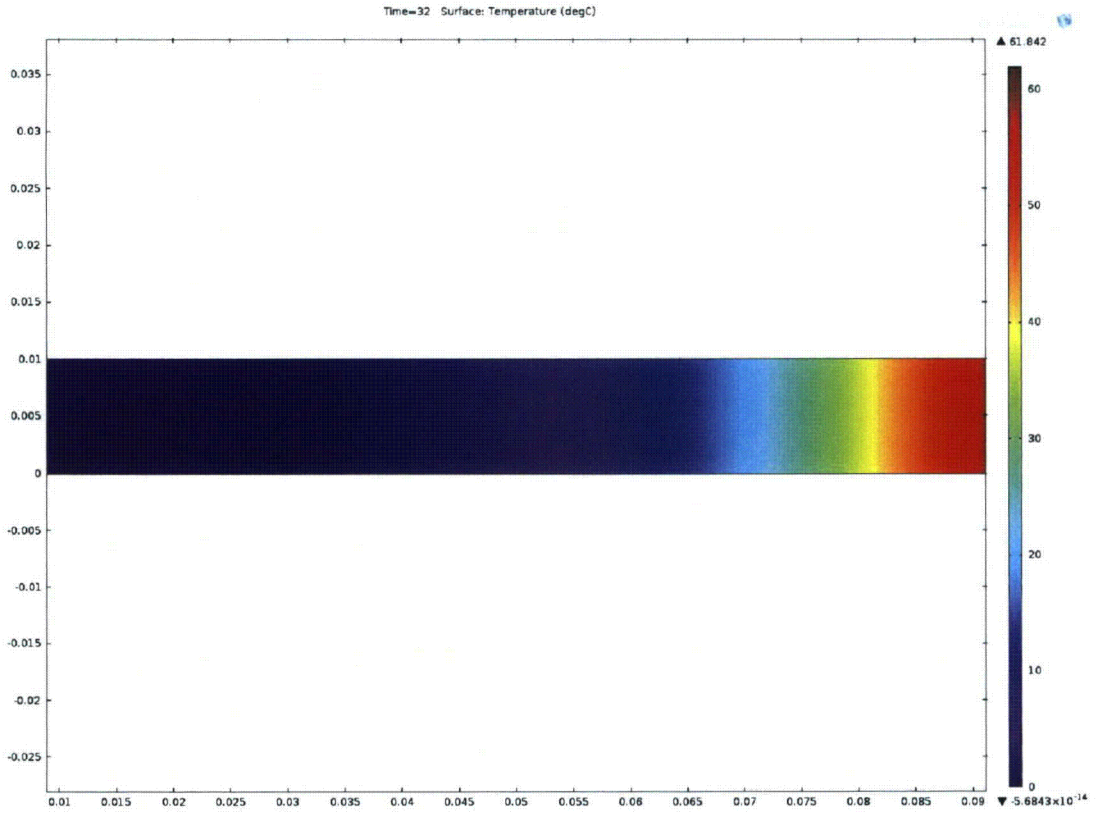

Figure 8– Temperature Contours for Test Problem No. 8

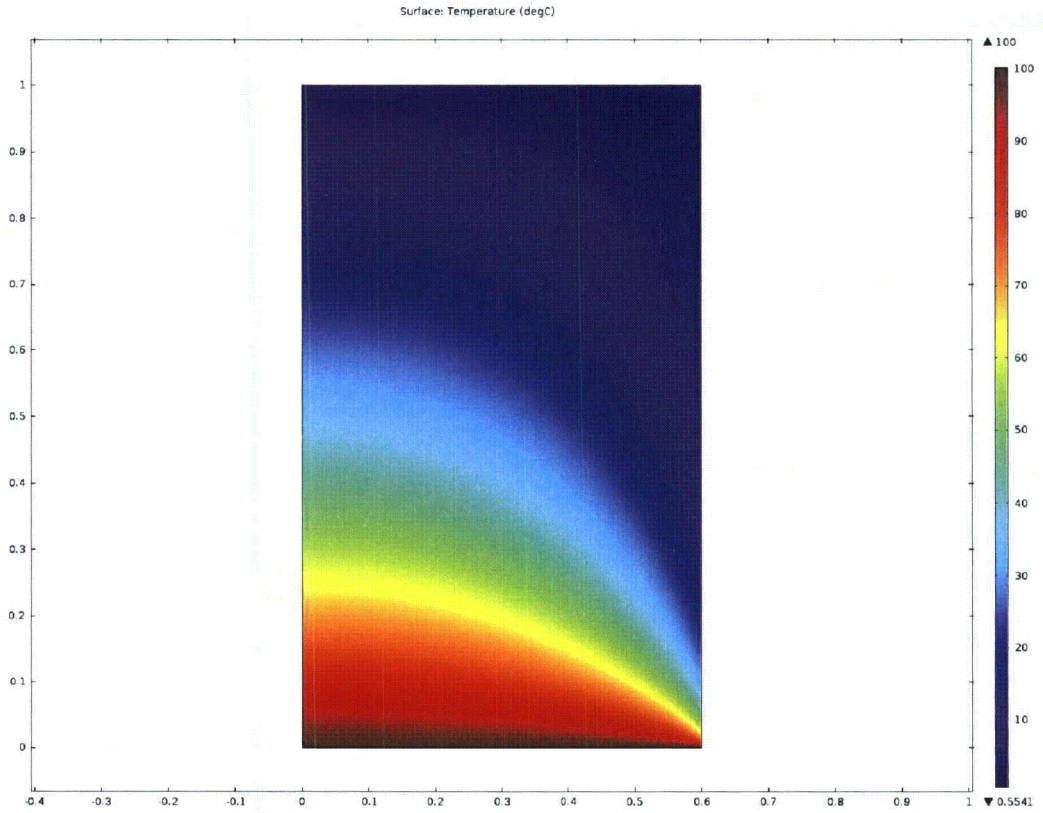

Figure 9– Temperature Contours for Test Problem No. 9

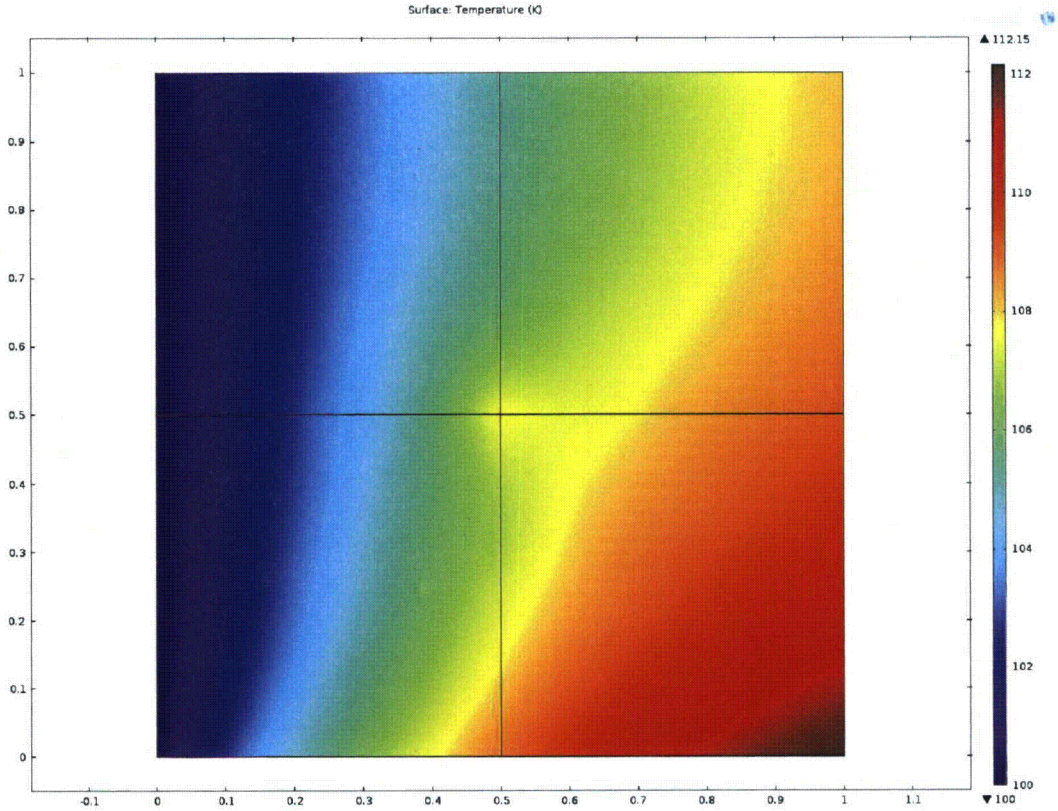

Figure 10– Temperature Contours for Test Problem No. 10

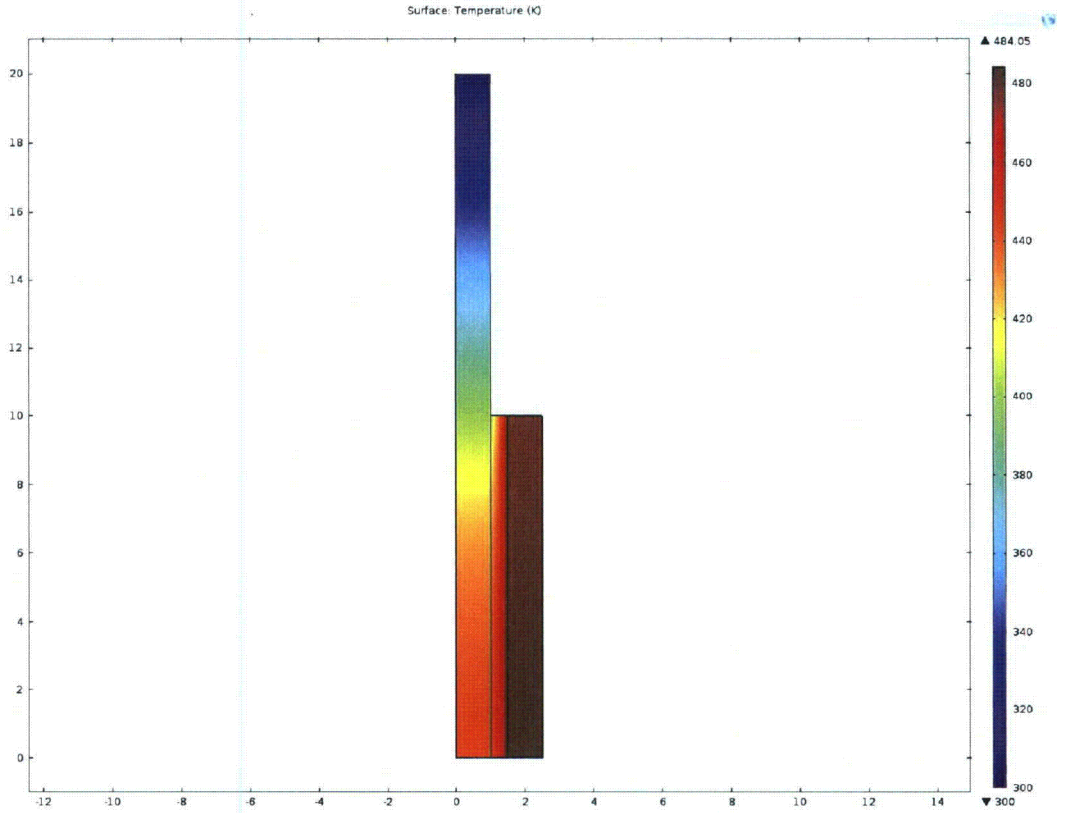

Figure 11– Temperature Contours for Test Problem No. 11

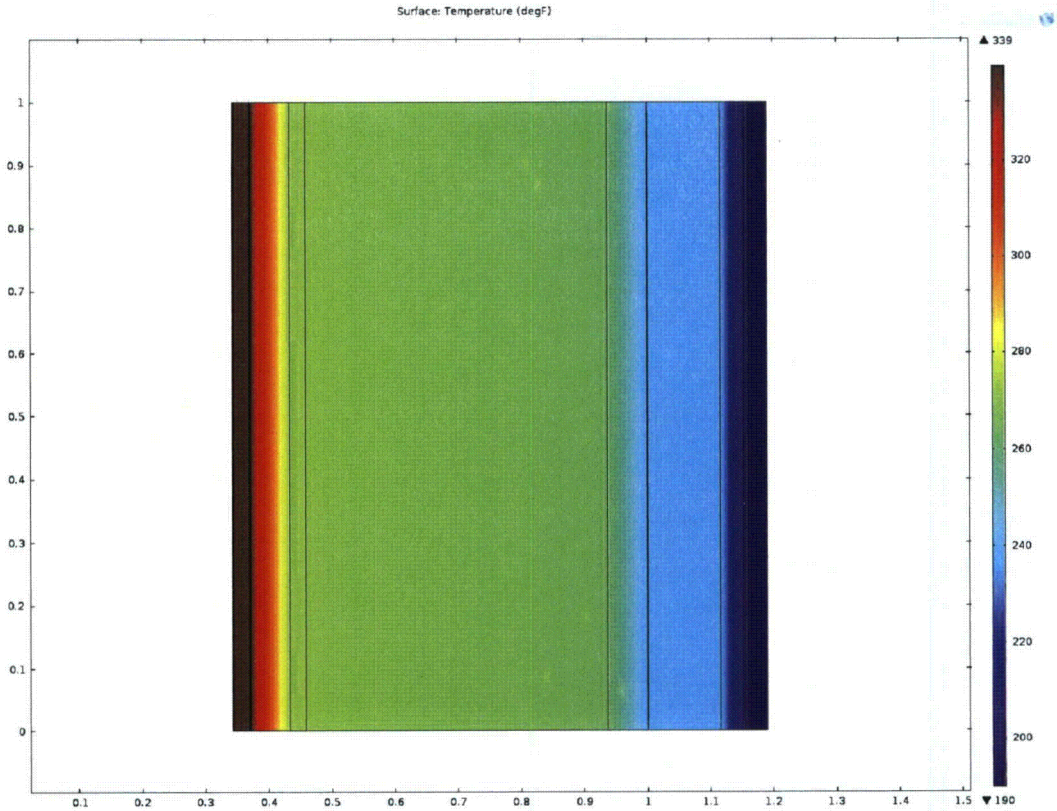

Figure 12– Temperature Contours for Test Problem No. 12

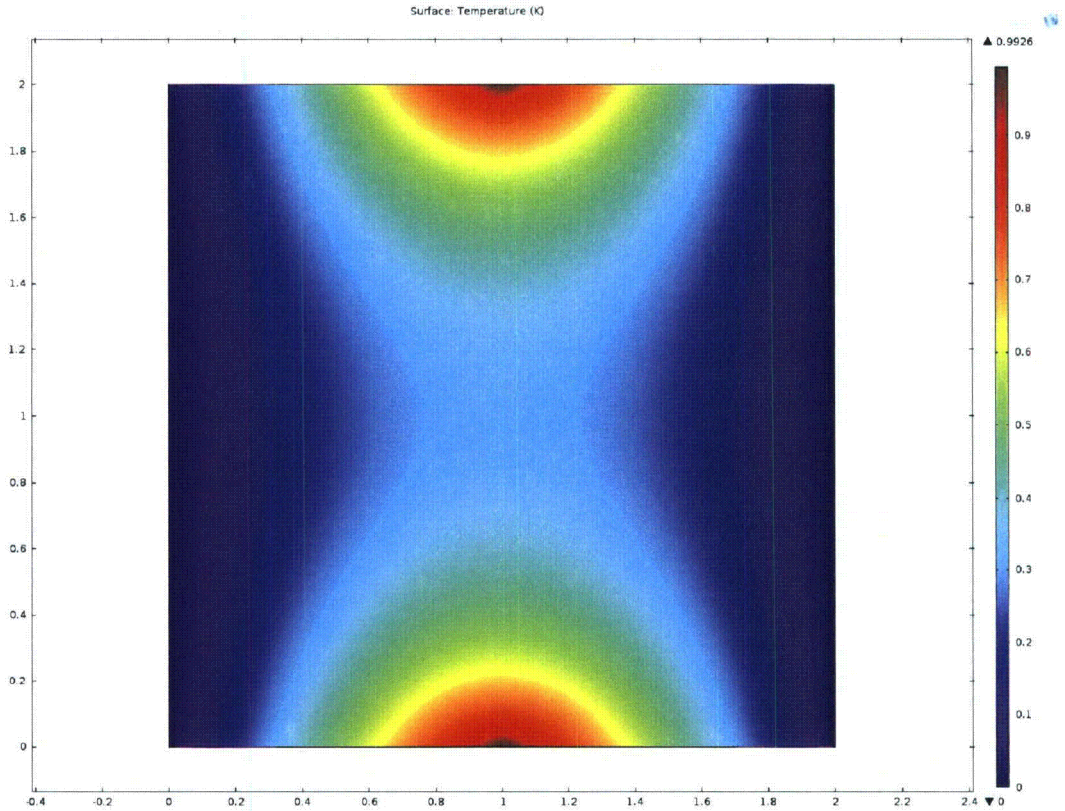

Figure 13– Temperature Contours for Test Problem No. 13

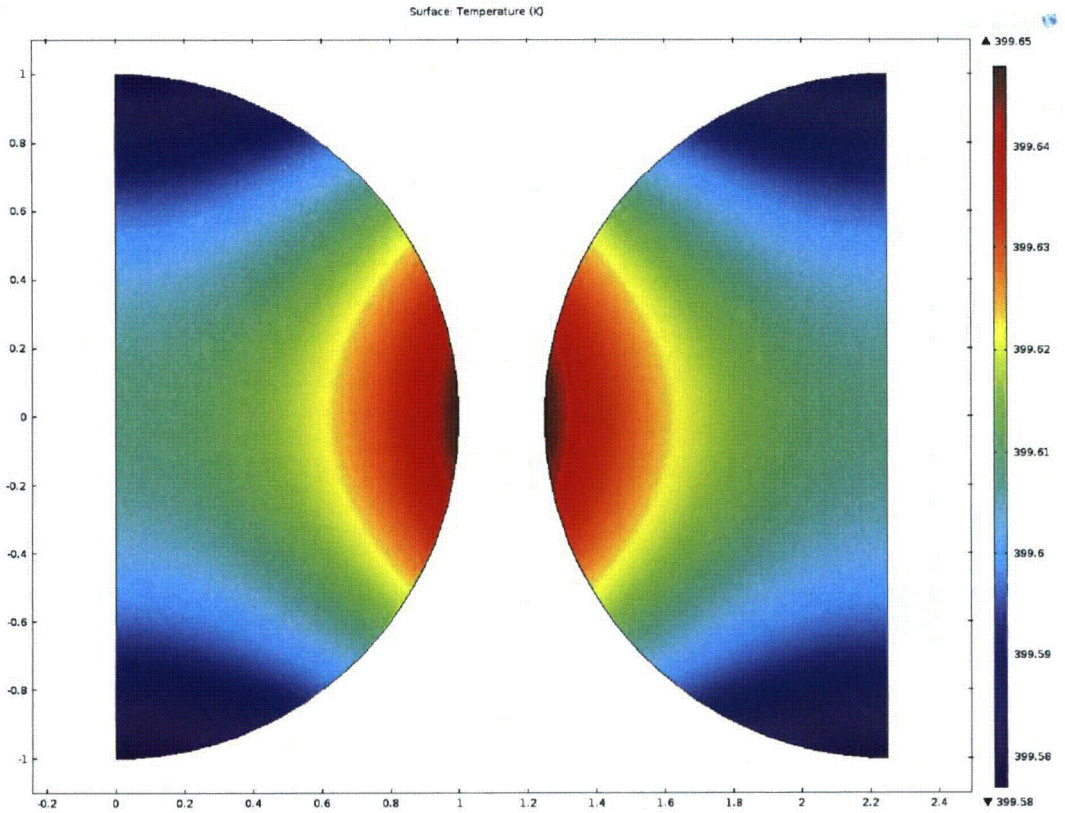

Figure 14– Temperature Contours for Test Problem No. 14

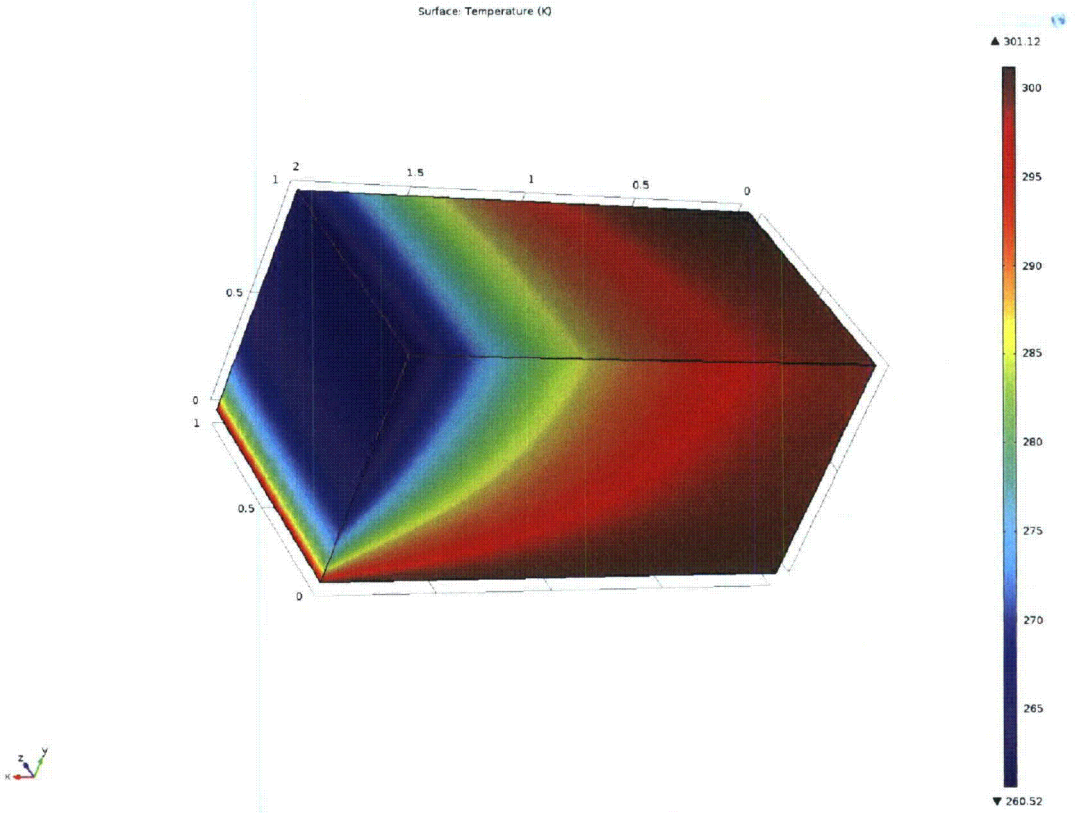

Figure 15– Temperature Contours for Test Problem No. 15

Attachment 9.3 - Computer Files

All folders are located in:

/hpc/archive/ems/qa/comsol/Comsol43

Test Case	Model File	Date/Time Stamp	SubFolder
1	Testcase1.mph	10/42012 11:49AM	TestCase1
2	Testcase2.mph	10/4/2012 11:52 AM	TestCase2
3	Testcase3.mph	10/4/2012 11:53 AM	TestCase3
4	Testcase4.mph	10/4/2012 12:01 PM	TestCase4
5	Testcase5.mph	10/4/2012 1:09 PM	TestCase5
6	Testcase6.mph	10/15/2012 6:52 AM	TestCase6
7	Testcase7.mph	10/15/2012 7:11 AM	TestCase7
8	Testcase8.mph	10/15/2012 7:15 AM	TestCase8
9	Testcase9.mph	10/15/2012 7:29 AM	TestCase9
10	Testcase10.mph	10/15/2012 8:09 AM	TestCase10
11	Testcase11.mph	10/15/2012 8:13 AM	TestCase11
12	Testcase12.mph	10/25/2012 2:49 PM	TestCase12
13	Testcase13.mph	10/25/2012 2:25 PM	TestCase13
14	Testcase14.mph	10/25/2012 2:36 PM	TestCase14
15	Testcase15.mph	10/25/2012 2:42 PM	TestCase15

WVMP SAR Reference 3-29

"NCT and HAC Thermal Analysis for the MC5PV," M-CLC-A-00448, Revision 1, Kesterson M.R., Savannah River National Laboratory, Aiken, South Carolina, July 25, 2013.

Redacted Version

OS[illegible] 45-24 (Rev 1[illegible]-6-201[illegible])

[illegible]r[illegible]. Re[illegible], 2[illegible]

Calc lat'on Cov r Sheet

Calcul 'on Number
M-CLC-A-00448
Functional Classifica 'on
SC

Calculation Type
◉ Type 1 ○ Type 2

Type 1 Calculation Status
○ Preliminary ◉ Confirmed

Computer Program Number
COMSOL Multiphysics ☐ N/A

Version/Release Number
COMSOL 4.3a

Purpose and Objective
This calculation evaluates the thermal performance of the Bulk Tritium Shipping Package (BTSP) for the Normal Conditions of Transport (NCT) and Hypothetical Accident conditions (HAC) containin an Mound Configuration 5 Process Vessel package (MC5PV). M imum temperatures of various components are calculated and compared against their design limits.

[redacted]

Summary of Conclusion

. The NCT and HAC analyses show that the maximum co pon nt temp ra ur s are b low their design limits.

2. Th analy es show that the B SP Mou d Config tion 5 roce V sel package meets th thermal design r quirements given i 10 CF Part 71.

[illegible]

[illegible] Date

[redacted]

[illegible] ure Date

NA

Design Authority (Print Name)
[illegible]unton

[redacted]

Revisions

Revision	Description
0	Original Issue
1	Updated tables 6, 7, and 8 to reflect current HAC temperature limits.

Table of Contents

Nomenclature and Units

h = Convection Heat Transfer Coefficient (Btu/hr-ft^2-°F)
k = Thermal Conductivity (Btu/hr-ft-°F)
ρ = Density (lb/ft^3)
C_p = Specific Heat (Btu/lb-°F)
L = Characteristic Length (ft)
T = Temperature (°F)

Acronyms and Abbreviations

CCSS	Configuration Control Support Structure
CCV	Contamination Control Vessel
CoC	Certificate of Compliance
CV	Containment Vessel
DOT	Department of Transportation
BTSP	Bulk Tritium Shipping Package
HAC	Hypothetical Accident Conditions
HAC/Solar	Hypothetical Accident Conditions (Steady State) with Insolation
HSV	Hydride Storage Vessel
HTV	Hydride Transport Vessel
MC5PV	Mound Configuration 5 Process Vessel
NCT	Normal Conditions of Transport
NCT/Solar	Normal Conditions of Transport with Insolation
NCT/Shade	Normal Conditions of Transport without Insolation
PV	Product Vessel
SARP	Safety Analysis Report for Packaging
SRNL	Savannah River National Laboratory
SS	Stainless Steel

1.0 INTRODUCTION

This document describes the thermal performance of the Bulk Tritium Shipping Package (BTSP) for the Normal Conditions of Transport (NCT) and the Hypothetical Accident Conditions (HAC) containing the Mound Configuration 5 Process Vessel (MC5PV) package. The BTSP has been previously evaluated for multiple product vessel (PV) configurations [1]. Figure 1 shows a schematic of the BTSP package with a generic PV content. This calculation evaluates the MC5PV within the BTSP. The MC5PV was previously authorized for shipment in the AL-M1 Nuclear Packaging (DOE CoC No. USA/9507/BLF)[2]. The general configuration of the MC5PV in a BTSP is shown in Figure 1 and a photo of the MC5PV are shown in Figure 2.

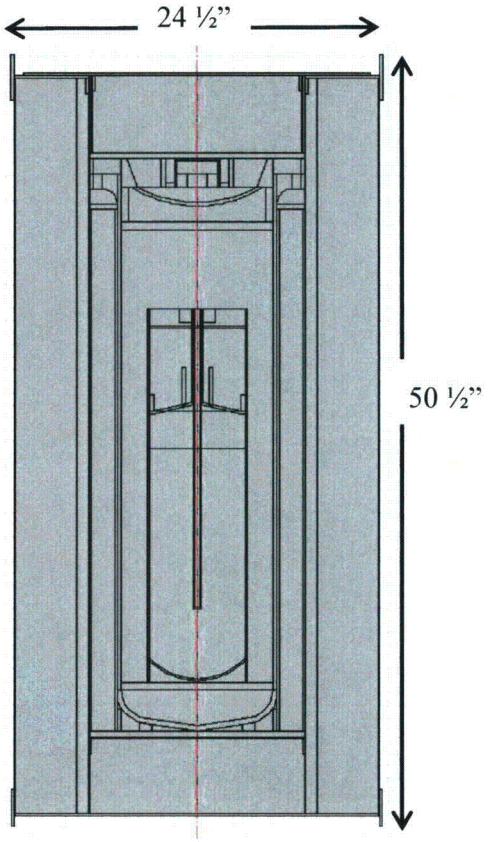

Figure 1 Schematic and dimensions of the BTSP package containing the CV.

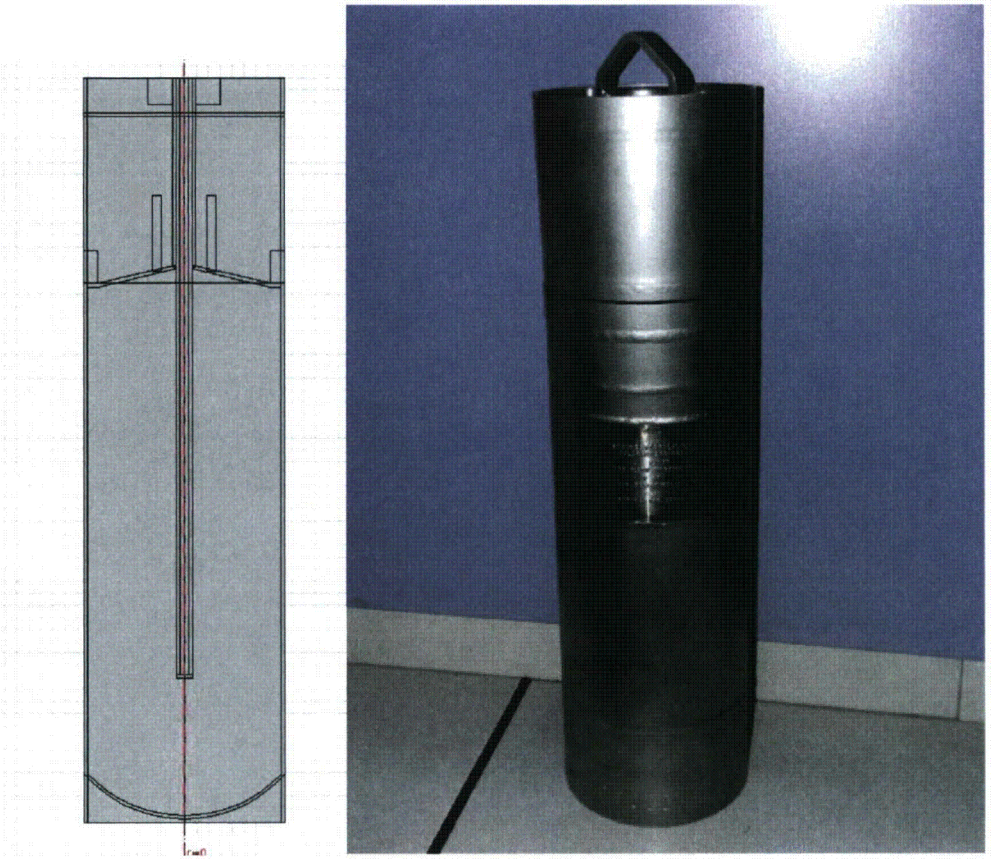

Figure 2 Sketch and Photo of the MC5PV Product Vessel

Technical specifications for the BTSP packaging components are provided on the BTSP engineering drawings[3]. Package design specifications relevant to the thermal analysis are summarized below.

2.0 INPUTS AND ASSUMPTIONS

2.1 Package Construction

Drum and Lid Assembly

The BTSP drum assembly consists of a 16 gauge Type 304L stainless steel (SS) drum shell with top and bottom bands welded to SS top and bottom plates and a 16 gage SS liner. A CV support shelf is welded to the bottom of the liner assembly. The drum top plate is fitted for a bolted-flange closure and is closed by a lid assembly. The closure lid incorporates a cylinder of Thermal Ceramics Vermiculite TR-19™ Block insulation. The drum assembly bottom is welded closed with a SS plate after the volume is fitted with a cylinder of the TR-19™ block insulation. The assembly construction details are defined on Drawings R-R4-G-00040, R-R3-G-00049 and R-R3-G-00051.[3]

Compressed Fiberfrax®, Last-A-Foam® and Vermiculite TR-19

Three layers of Fiberfrax® insulation blanket with density 7-10 lb/ft^3 are wrapped around outside of the drum liner. The drum fabrication process has liquid General Plastics Manufacturing Company Last-A-Foam® FR-3710[4] polyurethane foam being poured into the annular region between the insulation blanket and the drum wall. The Last-A-Foam® expands and becomes rigid as it cures, with a bulk density of 10 lb/ft^3. The expanding foam compresses the 1.5 inch layer of Fiberfrax® to approximately ¾ inch. Because the thickness of the Fiberfrax® is approximately halved, its density is assumed to double. This assumption is based on the compression of Fiberfrax® in the 9977 package that has similar construction [5]. Details are shown in Drawing R-R2-G-00051.[3] The Vermiculite TR-19 is block insulation with a bulk density of 23 lb/ft^3. The TR-19 blocks are located both above and below the CV and in contact with the drum lid and base.

Containment Vessel (CV)

The BTSP CV is a SS pressure vessel designed, analyzed and fabricated in accordance with Section III, Subsection NB of the ASME Code, with design conditions of 500 psig at 400°F. The CV is fabricated from Type 304L SS seamless pipe having a minimum 0.250 inch wall thickness terminated by a machined base welded at one end (R-R3-G-00013) with a flange welded to the other.

The CV body is closed by a 304/304L SS lid secured by bolts. The CV leaktight containment seal, per ANSI N14.5, is made by an inner Inconel Alloy 718 C-ring while an outer elastomeric O-ring provides the capability of post-load verification of the seal.[6] The CV Lid has a 1-inch valve assembly protected by a valve cap attached with cap screws. Valve assembly and the C-rings[6] that fit into these grooves complete the leaktight closure assembly. The construction details are given in Drawings R-R1-G-00024, R-R3-G-00013, R-R4-G-00037, and R-R4-G-00038.[3]

Honeycomb Cylinder

The honeycomb cylinder is fabricated using 5052 aluminum and is covered both inside and outside with a layer of resin impregnated fiberglass cloth to give it a smooth and abrasion resistance surface. The construction details are given in drawing R-R2-G-00054.[3] Figure 3 shows the end view of the honeycomb cylinder and the CV assembly with the insulating pad placed on the honeycomb cylinder.

Aluminum Foam Spacers

Two aluminum foam spacers, placed inside the top and bottom the CV, provide impact protection. The construction details are given in drawing R-R4-G-00039.[3]

Silicone Pad

A silicone rubber pad, reinforced with fiberglass, is placed at the bottom of the drum liner as a flexible wear surface for the CV. The details are given in the drawing R-R2-G-00070.[3]

Insulating Pad

An insulating pad placed on the CV closure lid (see Figure 3) provides added thermal protection

to the CV seals. The pad is made of KAO-Tex Superwool insulation made by Thermal Ceramics. The design details are given in the drawing R-R2-G-00069.[3] The pads thermal properties are assumed to be the same as the Fiberfrax® insulation blanket due to their similarity in materials and construction.

Fiberglass Coated Honeycomb Cylinder

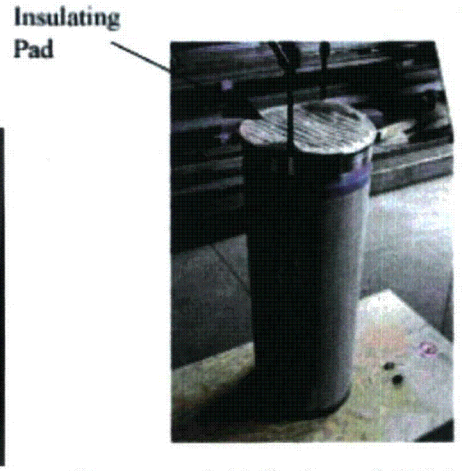

Honeycomb Cylinder and CV Assembly

Figure 3 Aluminum Honeycomb Cylinder and CV Assembly

2.2 Thermal Properties

Insulation Materials

The thermal conductivity *k* of the polyurethane foam is an important property for the NCT analyses. The foam vendor gives the thermal conductivity values at room temperature only. The values at higher temperatures were calculated previously[1] and are reported in **Table 1**. The density and specific heat values of the foam are modeled as constant values. The modified Sandia equation was validated for the 9977 package model [5].

The thermal conductivity of the compressed Fiberfrax® insulation blanket surrounding the liner is based on testing at SRNL.[8] Thermal properties of the compressed blanket are listed in **Table 1**. Vermiculite TR-19 Block insulation thermal properties are listed in Table 1.

Honeycomb Cylinder & Aluminum Foam Spacers

The honeycomb cylinder is procured based on a minimum strength and the foil thickness and cell size may vary to meet that requirement. The thermal properties of the aluminum honeycomb used in the analyses are based on testing and calculations. The radial plane *k* values are based on thermal conductivity tests[8] on aluminum 5052 honeycomb samples having appropriate cell size and foil thickness and a density of 12 lb/ft^3. The aluminum foam spacers are small compared to the honeycomb cylinder and are assumed to have the same thermal properties. The properties are modeled as constants and are listed in Table 2.

Other Materials

The properties of stainless steel and aluminum are listed in Table 2. Thermal properties of the silicone pad are approximated with grey silicone rubber [9]. The values are listed in Table 2.

Contents

The MC5PV contains a sorbent material with adsorbed tritiated water. The sorbent material can be a 4A, 5A, or 13X molecular sieve. The heat capacity of the various molecular sieves is constant and the density varies by 2% for the beaded material. The 5A molecular sieve density is an average of the other types of sieves. Therefore, for the purpose of this calculation, the thermal properties 5A molecular sieve used[10]. The heat generation of the contents is assumed to be the content maximum of 3.3 Watts [2]. A sensitivity analysis for the thermal properties of the contents is described in section 4.4.2.

In addition to the molecular sieve material, the contents can contain up to 2kg of water [2]. Water has a higher thermal conductivity than the molecular sieve materials and will therefore yield lower content temperatures for the steady state evaluations. The addition of water content will also add additional heat capacity to the content region, thereby also lowering the maximum temperatures attained in the transient case.

Gases

Tritium gas is assumed to fill the empty spaces inside the MC5PV. The space between the CV and the MC5PV is evacuated and filled with helium during the CV loading. The helium gas pressure is 1 to 5 psi [11] above the atmospheric pressure to ensure inert environment in the CV during transport. Air is assumed to fill any gaps between the CV and the silicon pad or honeycomb cylinder. Thermal properties of the tritium, helium and the air are given in Table 2.

Table 1 Thermal Properties of Insulating Materials

Material	Thermal Conductivity k, (Btu/hr-ft-°F)	Density ρ, (lb/ft^3)	Specific Heat Cp, (Btu/lb-°F)
Fiberfrax (compressed) Insulation Blanket (Values are based on tests at SRNL) [8] (Same for Insulating Pad)	2.14E-02 @ 70.0°F 2.25E-02 @ 122.0°F 2.43E-02 @ 185.0°F	20	0.27
Vermiculite TR-19 Block Insulation[12]	6.33E-02 @ 400.0°F 6.67E-02 @ 600.0°F 7.00E-02 @ 800.0°F 7.33E-02 @ 1000.0°F 7.75E-02 @ 1200.0°F 8.17E-02 @ 1400.0°F	23	0.20
Polyurethane Foam Insulation FR-3710 (During NCT and pre-fire)[7]	2.325E-02 @ 68.0°F 2.690E-02 @ 140.7°F 3.285E-02 @ 248.4°F 3.906E-02 @ 348.6°F	10	0.353

Table 2 Thermal Properties of Other Materials

Material	Thermal Conductivity k, (Btu/hr-ft-°F)	Density ρ, (lb/ft^3)	Specific Heat Cp, (Btu/lb-°F)
Honeycomb Cylinder (Radial plane) (Aluminum 5052)[8]	0.196	15.22 [a]	0.22
Honeycomb Cylinder (Axial plane) (Aluminum 5052)[8]	0.0982	15.22 [a]	0.22
Aluminum Foam Spacers (Radial) – Assumed same as honeycomb cylinder	0.196	16.9 [a]	0.22
Aluminum Foam Spacers (Axial) - Assumed same as honeycomb cylinder	0.0982	16.9 [a]	0.22
Aluminum (Type 6061 T-6)[13]	90.0	169.3	0.216
304L Stainless Steel[14]	7.74108 @ 32.0°F 9.43444 @ 212.0°F 12.5793 @ 932.0°F 14.9983 @ 1292.0°F	494.429	1.200E-01 @ 32.0°F 1.350E-01 @ 752.0°F
Tritium Gas (Hydrogen property values are used)[9]	0.105@80°F 0.119@170°F 0.132@260°F 0.145@350°F 0.169@530°F	5.11E-03@80°F 4.38E-03@170°F 3.83E-03@260°F 3.41E-03@350°F 2.79E-03@530°F	3.419@80°F 3.448@170°F 3.461@260°F 3.463@350°F 3.471@530°F
Helium[14]	8.177E-02 @ 32°F 8.685E-02 @ 77°F 9.096E-02 @ 120°F 9.846E-02 @ 212°F 1.226E-01@ 392°F 1.684E-01 @ 932°F 2.552E-01 @ 2192°F	0.01105	0.124
Air[14]	1.516E-02@80°F 1.735E-02@170°F 1.944E-02@260°F 2.142E-02@350°F 4.178E-02@1520°F	0.0735	0.240@80°F 0.237@212°F 0.265@1070°F 0.277@1520°F
Molecular Sieve 5A (Contents)[10]	0.48	44	0.19
Silicone Pad[9]	0.18	91.73	0.35
Aluminum shells[15]	0.185	28	0.22

Note: The numbers in brackets are the references at the end of the calculation.
[a] Based on bulk assembly

Surface Emissivities

Experience with the analyses for drum type packages (9975, 9977 and 9978) has shown that changes in the internal surface emissivities result in a relatively small change (< 5°F) in the predicted temperatures. The emissivity values for the various surfaces are listed in Table 3. These were used previously in certified drum type packages[1] and have shown acceptable agreement with test results. The emissivity values for honeycomb cylinder, silicone pad and insulating pad are obtained from the sources cited.

Table 3 Surface Emissivities

Surface		Emissivity
Component	**Material**	
CV	304L Stainless Steel	0.30
Drum Liner	304L Stainless Steel	0.30
Bottom of Lid	304L Stainless Steel	0.30
CCSS	Aluminum	0.20
Honeycomb Cylinder[1]	Aluminum/Fiberglass	0.75
Exterior of Drum (NCT & pre-fire)	304L Stainless Steel	0.21
Exterior of Drum (during HAC post-fire)	304L Stainless Steel	0.80
Silicone Pad (grey soft rubber)[2]	Silicone Rubber Pad	0.86
Insulating Pad (Kao-Tex with cover)[2]	Fiberglass Cloth Cover	0.77

[1] www.infraed-thermography.com/material-1.htm

[2] www.ib.cnea.gov.ar/~experim2/Cosas/omega/emisivity.htm

The surface emissivity values in Table 3 are for the gray and diffuse surfaces. The CV is a machined stainless steel component with clean surfaces. These surfaces are not polished. The drum surface is assumed as received (medium finish). For the NCT analyses, the drum surface thermal emissivity value (0.21) and solar absorptivity (0.498 or $\approx$ 0.50) are based on the detailed analysis for different types of drum surfaces.[22] The drum surface emissivity value during HAC post-fire phase is the minimum value (0.8) specified in the 10CFR 71.73. The corresponding solar absorptivity of the drum surface which is oxidized and is of dark gray color is assumed to be 0.9. A lower drum surface emissivity value results in higher component temperatures during post-fire cooling.

2.3 Geometry Modeling Assumptions

2.3.1 Drum and Lid Assembly

The dimensional details of the various components are given in drawings in Reference 3. The dimensions used in making the models are the nominal values and no attempt is made to incorporate tolerances in the dimensions. Nuts, bolts and welds are not included in the model because their impact on the temperature distribution is negligible. Since the gaps between components are small, it is assumed that the various components inside the drum remain concentric. A minor shifting of the components has only secondary effects on the package temperature field. The resulting thermal models are axisymmetric and are depicted in various figures only as half model.

2.3.2 Other Components

The gas valve assembly is located off-center in the CV Lid design but is modeled in the center. Valving and tubing connected on to the MC5PV are not amenable to accurately model in an axisymmetric model. Therefore, the MC5PV geometry is modified to include a ring at the top of the vessel representing the mass of the valving and tubing.

3.0 ANALYTICAL METHODS AND COMPUTATIONS

The mathematical equations describing the thermal models are solved by numerical methods. The general purpose conduction-radiation computer code COMSOL Multiphysics® was used to perform the computations.[16] This computer code meets site nuclear safety QA requirements.[17] Work was performed in accordance with the WSRC E7 manual.[18]

3.1 NCT Thermal Models

The NCT models for the NCT/Shade and NCT/Solar were developed using the COMSOL Multiphysics software. Boundary conditions, described in section 3.2, meet the intent of those specified for NCT in 10CFR71.71.[19] In the thermal analysis, the limiting components are the containment vessel, its C-ring seals, and the polyurethane foam insulation. Temperature limits for components of the BTSP for the NCT are tabulated, along with predicted maximum temperatures, for the MC5PV model in Tables 4 and 5. The BTSP model for NCT analyses includes interior metal surfaces, namely the drum shell and its liner, CV surfaces, and the metal surfaces between the drum lid, drum liner and the upper part of the CV lid.

Three modes of heat transfer - namely conduction, convection, and radiation - are considered in the analysis. Natural convection is evaluated on the outer drum surface but is ignored inside the CV cavity and in small gaps. This simplification is conservative since it yields higher local temperatures. Radiation is considered in all gas filled areas of the model. The pressures of gases in internal cavities are assumed to be one atmosphere.

The modeled MC5PV package contains maximum of 5.6 kg of molecular sieve material [2] with adsorbed tritiated water. The thermal properties of a loaded molecular sieve are not directly known. Therefore, a sensitivity analysis was performed, section 4.4.2, to determine the effect on the package temperature of a dry mixture and a mixture that is principally all water. For these

calculations the thermal properties of a 5A molecular sieve[10] were used. The maximum heat generation of the contents is assumed to be 3.3 Watts. Figure 4 shows the color representation of the materials with the MC5PV as the source model. The fill height of the molecular sieve was determined by the mass, density of the molecular sieve and the internal dimensions of the AL-M1 container. Having a lower mass or higher density molecular sieve will yield lower sieve volumes and if the decay heat remains constant, slightly higher (by 6°F) content temperatures will be seen. Section 4.4.2 discusses the effect of the molecular sieve density on the thermal analysis.

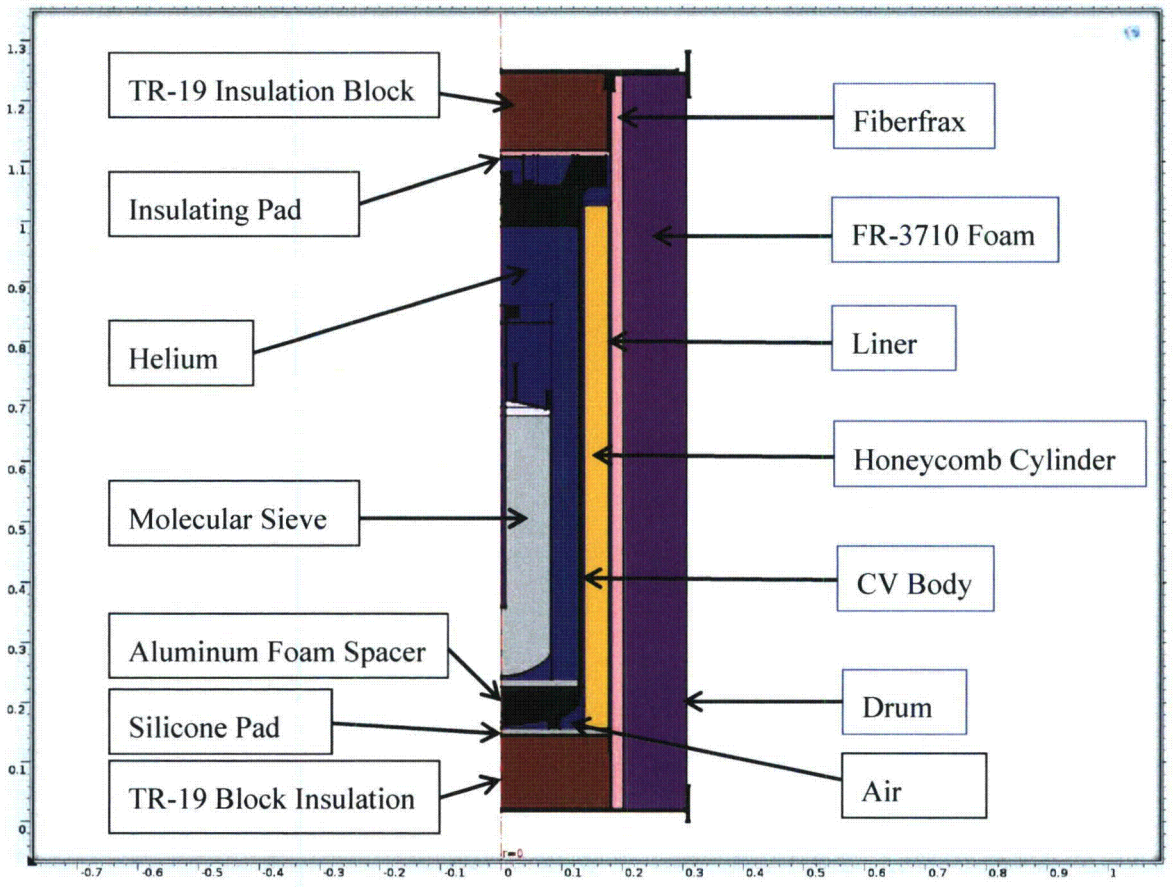

Figure 4 - Material Representation for BTSP with MC5PV.

3.2 Boundary Conditions

The boundary conditions used in the analytical models include the ambient temperature, solar heating, and convection and radiation heat exchange from the drum surfaces. Solar heating used in the NCT/Solar analyses is applied as heat flux to the drum's outer surface. 10CFR 71.71 prescribes a total insolation energy of 800 cal/cm^2 over a period of 12 hours on a horizontal surface and 400 cal/cm^2 over a period of 12 hours on the vertical surface, alternating 12 hours on and 12 hours off. The corresponding time averaged heat fluxes are 245.77 Btu/ft^2-hr on the top

of the package and 122.88 Btu/ft^2-hr on the side of the package. The applied solar fluxes using absorptivity of 0.50 are 122.88 Btu/ft^2-hr on the top of the package and 61.44 Btu/ft^2-hr on the side of the package. As listed in Table 3, the emissivity value for the outer surface of the drum is 0.21 for the pre-fire condition and 0.8 for the post-fire condition. Other specific parameters and related assumptions are summarized in the description of the NCT/Solar model below.

Description of the NCT/Solar Model

All NCT/Solar calculations were performed under the following conditions:

1. The drum is in an upright position and the contents are assumed to remain concentric during transport.
2. The drum bottom surface is adiabatic.
3. There is radiative heat transfer from the sides and top of the drum to the ambient.
4. There is natural convection heat transfer from the sides and top of the drum to the ambient.
5. The ambient temperature is 100°F.
6. Insolation is applied as solar heat flux. The applied solar fluxes are 122.88 Btu/ft^2-hr on the top of the package and 61.44 Btu/ft^2-hr on the side of the package. These heat fluxes are applied continuously rather than as a step function with a period of 12 hours.
7. The polyurethane foam thermal conductivity is the calculated value obtained from Reference [5]. The thermal conductivity values are validated by the environmental thermal test described in Reference [1].
8. The thermal properties for 50% compressed Fiberfrax® are used for the insulating blanket surrounding the drum liner.
9. The Content decay heat is 3.3 Watts.

The model for the NCT/Shade was the same as that for the NCT/Solar except that the insolation heat flux was omitted.

Description of the NCT/Shade Model

1. The drum is in an upright position.
2. The drum bottom surface is adiabatic.
3. There is radiation heat transfer from the sides and top of the drum to the ambient.
4. There is natural convection heat transfer from the drum sides and top to the ambient.
5. The ambient temperature is 100°F in shade
6. The polyurethane foam thermal conductivity is the calculated value obtained from Reference [5].Unburned foam properties are applied to the foam in the drum.
7. The Content decay heat is 3.3 Watts.

3.3 HAC Thermal Models

The HAC/solar analysis refers to the steady state analysis with a 100 °F ambient temperature and insolation during the post-fire phase where the drum surface optical properties reflect the dark gray surface appearance of the fire affected drum surface. For the HAC/solar analysis, the solar absorptivity is assumed 0.9 and the emissivity as 0.8. Lower emissivity gives higher steady state temperatures for this analysis. The analysis results are given in Section 4.0.

Description of the HAC/Solar Fire Model

1. The drum is in an upright position with contents.
2. The drum bottom surface is adiabatic.
3. There is radiation heat transfer from the sides and top of the drum to the ambient.
4. There is natural convection heat transfer from the drum sides and top to the ambient.
5. The ambient temperature is 1475°F.
6. Insolation is applied as solar heat flux assuming solar absorptivity of 0.9 for the drum surface during post-fire cooling. The applied solar fluxes are 221.18 Btu/ft^2-hr on the top of the package and 110.59 Btu/ft^2-hr on the side of the package. These heat fluxes are applied continuously rather than as a step function with a period of 12 hours.
7. Thermal properties for air are used in place of the polyurethane foam. This is due to charring of the foam during the fire phase.
8. The Content decay heat is 3.3 Watts.

Description of the HAC/Solar Model

1. The drum is in an upright position with contents.
2. The drum bottom surface is adiabatic.
3. There is radiation heat transfer from the sides and top of the drum to the ambient.
4. There is natural convection heat transfer from the drum sides and top to the ambient.
5. The ambient temperature is 100°F.
6. Insolation is applied as solar heat flux assuming solar absorptivity of 0.9 for the drum surface during post-fire cooling. The applied solar fluxes are 221.18 Btu/ft^2-hr on the top of the package and 110.59 Btu/ft^2-hr on the side of the package. These heat fluxes are applied continuously rather than as a step function with a period of 12 hours.
7. Pristine foam (10 lb/ft^3) thermal properties are applied to the char cavity in the drum. This is a highly conservative assumption for the transient post-fire model, due to the pristine foam having a higher density and heat capacity compared to air. The package will retain heat for a longer period of time and yield higher maximum temperature for the transient case.
8. The Content decay heat is 3.3 Watts.

4.0 RESULTS

4.1 NCT/Shade Model Results

The MC5PV NCT/Shade model examined a temperature profile for a 3.3 Watt heat source. The maximum predicted temperatures of the limiting components are listed in Table 4. Figure 5 is the package temperature contour.

Table 4 NCT/Shade Maximum Component Temperatures (°F)

Component	BSTP/MC5PV Model (°F)	Temperature Limit (°F)
CV Wall	112	400
CV C-ring	105	1200
Cap C-Ring	106	1200
Bellows Valve	106	400
Honeycomb Cylinder	111	350
MC5PV Contents	154	NA
Drum Surface	101	NA
Last-A-Foam® FR-3710	107	300
Gas in CV (Volume Average)	111	NA
Gas in MC5PV (Volume Average)	117	NA

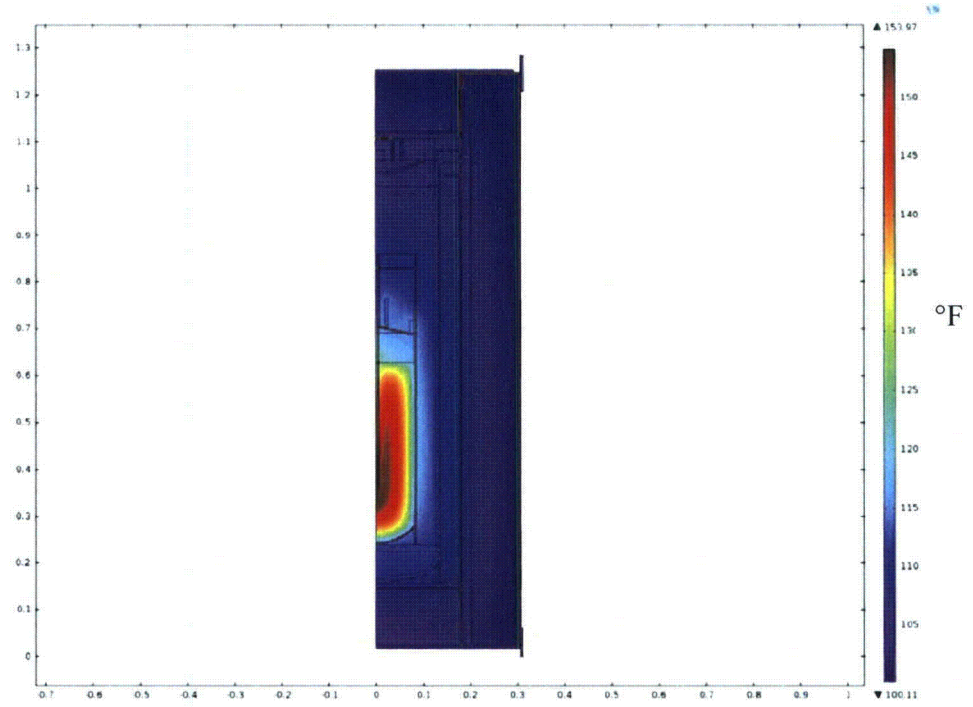

Figure 5 MC5PV Prefire Temperature Profiles for NCT/Shade

4.2 NCT/Solar Model Results

The MC5PV NCT/Solar model determined a temperature profile for a 3.3 Watt heat source. The maximum predicted temperatures of the limiting components are listed in Table 5. The package temperature contour is Figure 6.

Table 5– NCT/Solar Maximum Component Temperatures (°F)

Component	BTSP/MC5PV Model (°F)	Temperature Limit (°F)
CV Wall	158	400
CV C-ring	157	1200
Cap C-ring	158	1200
Bellows Valve	158	400
Honeycomb Cylinder	157	350
Contents	185	NA
Drum Surface	164	NA
Last-A-Foam® FR-3710	159	300
Gas in CV (Volume Average)	159	NA
Gas in MC5PV (Volume Average)	163	NA

4.2.1 Volume Average Gas Temperature

Volume average gas temperature is required for calculating the maximum normal operating pressure (MNOP) inside the CV. Average gas temperature was calculated by volume averaging of nodal temperatures in the CV cavity. The average gas temperature for the MC5PV NCT/Solar configuration is 163°F.

4.2.2 Volume Average Foam Temperature

The volume average foam temperature for the MC5PV configuration is 147°F. The volume average foam temperature data is required in assessing the structural performance of the BTSP during NCT.

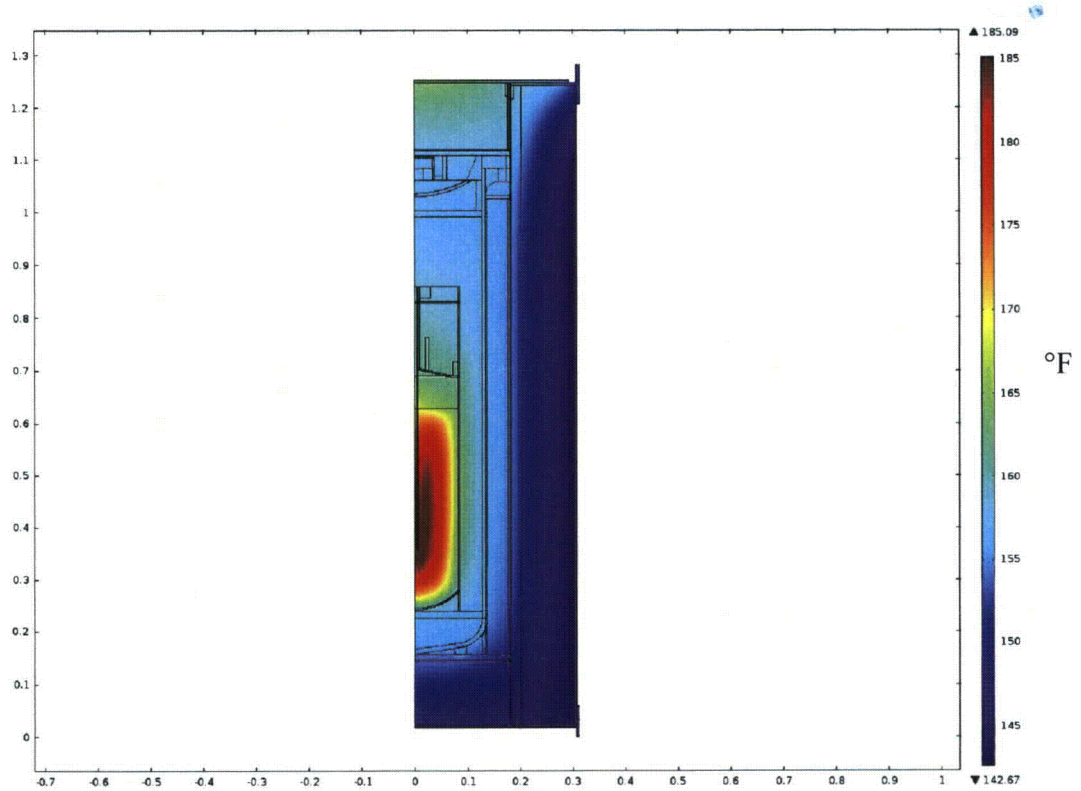

Figure 6 MC5PV Model Temperature Profiles for NCT/Solar

4.3 Results for the HAC/Solar Model

The HAC/Solar Fire model is used to calculate component temperatures during the fire event and refers to the thermal model with insolation effect during post-fire phase. Table 6 lists the maximum component temperatures of the MC5PV model during the fire phase while Table 7 lists the maximum component temperatures during the cooldown phase.

Table 6– HAC/Solar Maximum Component Temperatures During Fire

Component	BTSP/MC5PV Model (°F)	Temperature Limit (°F)
CV Wall	161	500
CV C-ring	161	1200
Cap C-ring	158	1200
Bellows Valve	158	400
Honeycomb Cylinder	180	NA
Contents	185	NA
Drum Surface	1474	NA
Last-A-Foam® FR-3710	1471	NA
Gas in CV (Volume Average)	159	NA
Gas in MC5PV (Volume Average)	163	NA

Table 7– HAC/Solar Maximum Component Post-Fire Temperatures

Component	BTSP/MC5PV Model (°F)	Temperature Limit (°F)
CV Wall	238	500
CV C-ring	236	1200
Cap C-ring	236	1200
Bellows Valve	236	400
Honeycomb Cylinder	273	NA
Contents	284	NA
Drum Surface	1474	NA
Last-A-Foam® FR-3710	1471	NA
Gas in CV (Volume Average)	236	NA
Gas in MC5PV (Volume Average)	218	NA

The post-fire temperatures are calculated using the HAC/Solar model. The only difference in this thermal model is the replacement of foam/char with air in the foam cavity. The steady state temperatures are given in Table 8.

Table 8 HAC/Solar Steady State Component Post Fire Temperatures

Component	BTSP/MC5PV Model (°F)	Temperature Limit (°F)
CV Wall	161	500
CV C-ring	160	1200
Cap C-ring	161	1200
Bellows Valve	161	400
Honeycomb Cylinder	160	NA
Contents	187	NA
Drum Surface	171	NA
Last-A-Foam® FR-3710 (replaced as Air post fire)	164	NA
Gas in CV (Volume Average)	161	NA
Gas in MC5PV (Volume Average)	166	NA

As shown in Table 7, the component temperatures are well below their design limits. Figure 7 is the temperature profiles for the MC5PVconfiguration during the HAC/Solar event.

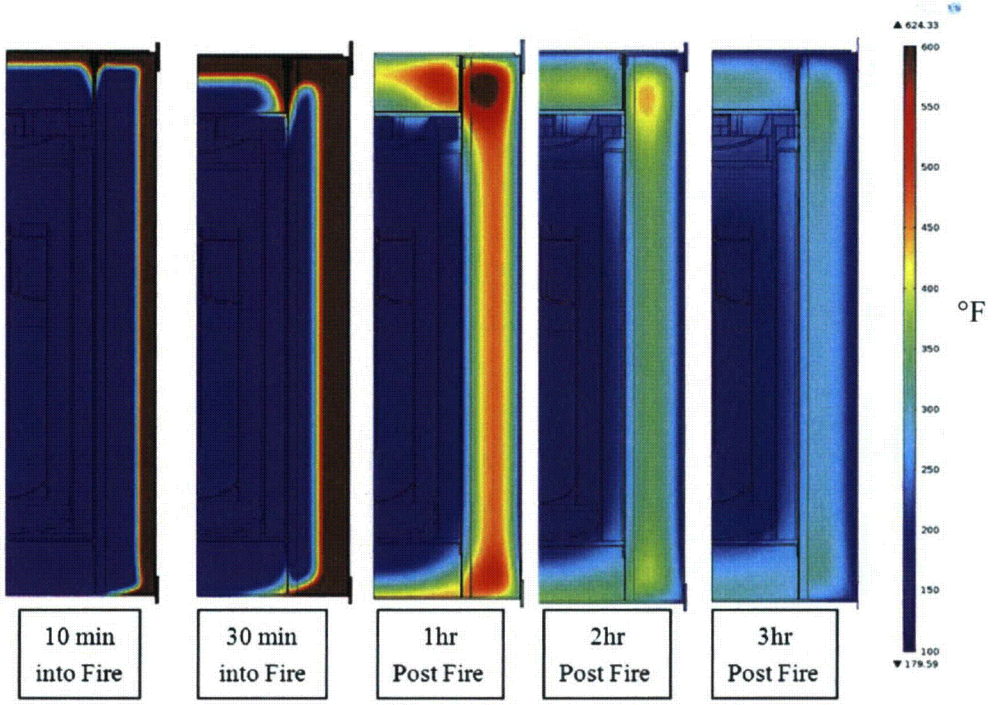

Figure 7 - HAC/Solar Temperature Profiles (peak temperatures are 30 minutes into fire). 1 hr post fire is at 1.5 hr simulation time.

Note: Temperature scale was set to a maximum of 600°F for comparison of plots. Any dark red color represents a value of 600°F or higher.

4.4 Uncertainty/Sensitivity Analyses

Uncertainties in thermal properties and other important parameters are minimized by making sure that their threshold values are used to yield conservative results. Uncertainties are addressed by performing simple sensitivity analyses. Sensitivity analyses were performed for finite element mesh size and thermal properties.

4.4.1 Mesh Size Sensitivity

A mesh sensitivity analysis was performed to ensure that the various thermal models had sufficient number of elements to give stable results. The number of elements was increased from 192,880 to 516,528 elements in the NCT/Solar. The maximum contents temperature with the increased number of elements was found to be less than 0.1% lower compared to the smaller number of elements. The model with the lower number of elements was used in the analyses.

4.4.2 Thermal Properties

FR-3710 foam free rise density of 10 lb/ft^3 and the corresponding thermal conductivity (k) values are used in the thermal analyses. However, the actual packed density of the FR-3710 foam in the prototype packages was found to be approximately 12.4 lb/ft^3 [21]. Since k of the foam increases with the density, the actual k would be higher.[4] For the NCT steady state analysis, higher k results in lower CV temperatures and therefore actual foam k does not impact the NCT analysis results. For the HAC analyses, higher density foam has lower thermal diffusivity than the lower density foam[4] and hence lower CV temperatures during HAC fire event.

The model was evaluated replacing the thermal properties of the 5A molecular sieve with water. Water having a higher thermal conductivity yielded steady state temperatures for the contents that were 20°F lower than when evaluated with the 5A molecular sieve material. For the transient case, water also has a higher heat capacity and therefore yields contents temperatures 80°F lower during the HAC fire.

The density of the molecular sieve material was varied to determine the effect on the steady state temperature of the package. A lower density was not simulated since a lower density will yield a larger molecular sieve volume. Using the same decay heat of 3.3 Watts over a larger volume will distribute the heat load and result in a lower maximum content temperature. A density that is 50% higher (66 lb/ft^3) yields a steady state maximum temperature 6°F higher for the contents.

5.0 CONCLUSIONS

1. The NCT and HAC analyses show that the maximum component temperatures are below their design limits.
2. The analyses show that the BTSP Mound Configuration 5 Process Vessel package meets the thermal design requirements given in 10 CFR Part 71.

6.0 REFERENCES

1. M-CLC-A-00340 Rev.1, BTSP Thermal Testing and Model Validation for Normal Conditions of Transport (NCT), Savannah River Nuclear Solutions, Aiken, SC (2010).
2. Safety Analysis Report for Packaging (SARP): Model AL-M1 Nuclear Packaging (DOE C of C No. USA/9507/BLF), MOUND, Miamisburg, OH, November 24, 1987.
3. Drawings:
   - R-R1-G-00022 – Packaging Assembly
   - R-R1-G-00023 – Drum Plug and Lid Assembly
   - R-R1-G-00024 – CV Assembly
   - R-R2-G-00048 – Drum Plug Sub Assembly
   - R-R2-G-00054 – Honeycomb Cylinder
   - R-R3-G-00013 – CV Weldment
   - R-R3-G-00049 – Drum Lid Weldment
   - R-R3-G-00051 – Drum and Liner Weldment
   - R-R4-G-00035 – CV Flange
   - R-R4-G-00036 – CV Base
   - R-R4-G-00037 – CV Lid
   - R-R4-G-00038 – CV Protection Cap
   - R-R4-G-00039 – CV Upper & Lower Spacers
   - R-R4-G-00040 – Drum and Liner Details
   - R-R2-G-00069 – Insulating Pad
   - R-R2-G-00070 – Silicone Pad
4. Design Guide for Use of Last-A-Foam FR-3700 for Crash and Fire Protection of Nuclear Material Shipping Containers (including data from cited references in this guide), General Plastics Manufacturing Company, Tacoma WA.
5. Safety Analysis Report for Packaging, Model 9977 B(M)f-96, S-SARP-G-00001, Rev. 2, Savannah River National Laboratory, 2007
6. • Parker O-ring Handbook, ORD-5700, Parker Hannifin Corp., Cleveland, OH (2007).
   • Seals for Extreme Environment, Parker-Hannifin Advanced Products Co., North Haven, CT.
7. E.G. Wenski, Properties of 30 lb/ft^3 Rigid Polyurethane Foams, SAND97-0120 (Appendix D), (March 1997).
8. W. L. Daugherty, Thermal Conductivity Data for Candidate Materials, SRNL-MST-2007-00127, (June 2008).
9. DC Products, www.dcproducts.com.au/RTV_Silicone_Solutions/Tech_Data_Sheets/RTV88-tds.pdf, May 2013
10. • Sigma Aldrich, www.sigmaaldrich.com/chemistry/chemical-synthesis/learning-center/technical-bulletins/al-1430/molecular-sieves.html, May 2013
    • Pnj Resources, LLC, www.pnjresources.com/Molecular%20Sieves.html, May 2013
11. Safety Analysis Report for Packaging, Bulk Tritium Shipping Package -1 (BTSP-1), S-SARP-G-00004, Rev. 4, Savannah River National Laboratory, (2012).
12. Morgan Thermal Ceramics http://www.morganthermalceramics.com/files/datasheets/4tr19tr19hstr201014-100.pdf, May 2013

13. ASME Boiler and Pressure Vessel Code, Section II, Part D, American Society of Mechanical Engineers, New York, NY (2004).
14. MSC.PATRAN THERMAL 2008 r1, Online Manual, MSC Software Company, Santa Ana, Ca (2008)
15. R. C. Dykhuizen and A. R. york, Packing Materials for Heat Producing Payloads, RAMTRANS, Vol. 3, No. 2/3, p. 135-139, Nuclear Technology Publishing (1992)
16. Comsol Multiphysics version 4.3a, COMSOL, Inc., Burlingame, Massachusetts (2012).
17. (1) G-SQP-A-00057 Rev. 0, Software Quality Assurance Plan for COMSOL Multiphysics (2012).
    (2) B-STP-A-00027 Rev. 0, COMSOL Multiphysics Version 4.3 Software Test Documentation, (2012).
18. Conduct of Engineering, Manual E-7, Engineering Calculations, Savannah River Nuclear Solutions, Savannah River Site, Aiken, SC.
19. Packaging and Transportation of Radioactive materials, Code of Federal Regulations, Title 10, Part 71, Washington, DC (2006).
20. Heat Transfer, by D. R. Pitts and L. E. Sissom, Schaum's Outline Series, McGraw-Hill Book Co. (1977).
21. M-CLC-A-00305 Rev.4, NCT and HAC Thermal Analysis for the BTSP, Savannah River Nuclear Solutions, Aiken, SC (2011).
22. M-TRT-A-00026, Solar Absorbance and Emittance of Stainless Steel at 400K, Savannah River Nuclear Solutions, Aiken, SC (2014)

WVMP SAR Reference 3-30

Fundamentals of Heat and Mass Transfer, 5th ed.,
Incropera, F.P., and D. P. DeWitt, John Wiley & Sons, Inc.,
Hoboken, New Jersey (2002).

Chapter 9, pages 605, 610.

where the Rayleigh number,

$$Ra_L = Gr_L Pr = \frac{g\beta(T_s - T_\infty)L^3}{\nu\alpha} \tag{9.25}$$

is based on the characteristic length L of the geometry. Typically, $n = \frac{1}{4}$ and $\frac{1}{3}$ for laminar and turbulent flows, respectively. For turbulent flow it then follows that $\bar{h}_L$ is independent of L. Note that all properties are evaluated at the film temperature, $T_f \equiv (T_s + T_\infty)/2$.

9.6.1 The Vertical Plate

Expressions of the form given by Equation 9.24 have been developed for the vertical plate [5–7]. For laminar flow ($10^4 \lesssim Ra_L \lesssim 10^9$), $C = 0.59$ and $n = 1/4$, and for turbulent flow ($10^9 \lesssim Ra_L \lesssim 10^{13}$), $C = 0.10$ and $n = 1/3$. A correlation that may be applied over the *entire* range of Ra_L has been recommended by Churchill and Chu [8] and is of the form

$$\overline{Nu}_L = \left\{0.825 + \frac{0.387\,Ra_L^{1/6}}{[1 + (0.492/Pr)^{9/16}]^{8/27}}\right\}^2 \tag{9.26}$$

Although Equation 9.26 is suitable for most engineering calculations, slightly better accuracy may be obtained for laminar flow by using [8]

$$\overline{Nu}_L = 0.68 + \frac{0.670\,Ra_L^{1/4}}{[1 + (0.492/Pr)^{9/16}]^{4/9}} \qquad Ra_L \lesssim 10^9 \tag{9.27}$$

When the Rayleigh number is moderately large, the second term on the right-hand side of Equations 9.26 and 9.27 dominates, and the correlations are the same form as Equation 9.24, except that the constant, C, is replaced by a function of Pr. Equation 9.27 is then in excellent quantitative agreement with the analytical solution given by Equations 9.21 and 9.20. In contrast, when the Rayleigh number is small, the first term on the right-hand side of Equations 9.26 and 9.27 dominates, and the equations yield the same behavior since $0.825^2 \approx 0.68$. The presence of leading constants in Equations 9.26 and 9.27 accounts for the fact that, for small Rayleigh number, the boundary layer assumptions become invalid and conduction parallel to the plate is important.

It is important to recognize that the foregoing results have been obtained for an isothermal plate (constant T_s). If the surface condition is, instead, one of uniform heat flux (constant q_s''), the temperature difference $(T_s - T_\infty)$ will vary with x, increasing from the leading edge. An approximate procedure for determining this variation may be based on results [8, 9] showing that $\overline{Nu}_L$ correlations obtained for the isothermal plate may still be used to an excellent approximation, if $\overline{Nu}_L$ and Ra_L are defined in terms of the temperature difference at the midpoint of the plate, $\Delta T_{L/2} = T_s(L/2) - T$. Hence, with $\bar{h} \equiv q_s''/\Delta T_{L/2}$, a correlation such as Equation 9.27 could be used to determine $\Delta T_{L/2}$ (for example, using a trial-and-error technique), and hence the midpoint surface temperature $T(L/2)$. If it is assumed that $Nu \propto Ra_x^{1/4}$ over the entire plate, it follows that

$$\frac{q_s'' x}{k\Delta T} \propto \Delta T^{1/4} x^{3/4}$$

or

$$\Delta T \propto x^{1/5}$$

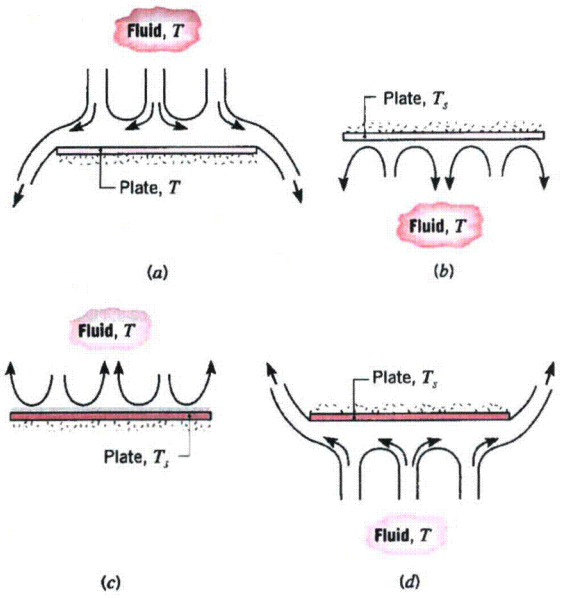

FIGURE 9.7 Buoyancy-driven flows on horizontal cold ($T_s < T_\infty$) and hot ($T_s > T_\infty$) plates: (*a*) Top surface of cold plate. (*b*) Bottom surface of cold plate. (*c*) Top surface of hot plate. (*d*) Bottom surface of hot plate.

where A_s and P are the plate surface area (one side) and perimeter, respectively. Using this characteristic length, the recommended correlations for the average Nusselt number are

Upper Surface of Hot Plate or Lower Surface of Cold Plate [19]:

$$\overline{Nu}_L = 0.54\, Ra_L^{1/4} \quad (10^4 \lesssim Ra_L < 10^7,\ Pr \gtrsim 0.7) \tag{9.30}$$

$$\overline{Nu}_L = 0.15\, Ra_L^{1/3} \quad (10^7 \lesssim Ra_L < 10^{11},\ \text{all } Pr) \tag{9.31}$$

Lower Surface of Hot Plate or Upper Surface of Cold Plate [20]:

$$\overline{Nu}_L = 0.52\, Ra_L^{1/5} \quad (10^4 \lesssim Ra_L \lesssim 10^9,\ Pr \gtrsim 0.7) \tag{9.32}$$

Additional correlations can be found in [21].

EXAMPLE 9.3

Airflow through a long rectangular heating duct that is 0.75 m wide and 0.3 m high maintains the outer duct surface at 45 C. If the duct is uninsulated and exposed to air at 15°C in the crawlspace beneath a home, what is the heat loss from the duct per meter of length?

SOLUTION

Known: Surface temperature of a long rectangular duct.

Find: Heat loss from duct per meter of length.

WVMP SAR Reference 3-31

"Natural-Convection Heat Transfer in Liquids Confined by Two Horizontal Plates and Heated from Below," Globe, S., and D. Dropkin, J. Heat Trans. – T. ASME, 81C, 24-28, 1959.

Natural-Convection Heat Transfer in Liquids Confined by Two Horizontal Plates and Heated From Below

SAMUEL GLOBE

Principal Scientist, Physics Section, Avco Research and Advanced Development Division, Wilmington, Mass.

DAVID DROPKIN

Professor of Mechanical Engineering, Department of Thermal Engineering, Cornell University, Ithaca, N. Y.; and consultant to Avco

This paper presents results of an experimental investigation of convective heat transfer in liquids placed between two horizontal plates and heated from below. The liquids used were water, silicone oils of 1.5, 50, and 1000 centistoke kinematic viscosities, and mercury.

The experiments covered a range of Rayleigh numbers between $1.51(10)^5$ and $6.76(10)^8$, and Prandtl numbers between 0.02 and 8750.

Tests were made in cylindrical containers having copper tops and bottoms and insulating walls. For water and silicone oils the container was 5 in. in diam and 2 in. high. For mercury, two containers were used, both 5.28 in. in diameter, but one 1.39 in. high and another 2.62 in. high. In all cases the bottom plates were heated by electric heaters. The top plates were air-cooled for the water and silicone-oil experiments and water-cooled for the mercury tests. To prevent amalgamation, the copper plates of the mercury container were chromium plated.

Surface temperatures were measured by thermocouples embedded in the plates.

The test results indicate that the heat-transfer coefficients for all liquids investigated may be determined from the relationship

$$Nu = 0.069(Ra)^{1/3}(Pr)^{0.074}$$

In this equation the Nusselt and Rayleigh numbers are based on the distance between the copper plates.

The results of this experiment are in reasonable agreement with the data reported by others who used larger containers and different fluids.

On certain engineering projects it is sometimes necessary to predict the heat-transfer rates by convection in liquids confined between two horizontal plates and heated from below. The search of published literature reveals that such information is scarce. The two important papers that are available on this subject are limited in their scope. They do not possess the desired range of physical properties to justify a derivation of a general equation. The work of Mull and Reiher, as reported by Jakob [1][1] was done on air, while Malkus [2] used water and acetone in his experiments.

In the first case, the Prandtl number was practically constant because it is known that for air the variation of Prandtl number with changes in temperature is negligible; in the second case, Malkus purposely kept the mean temperature of the water and acetone at a constant value.

The Prandtl number, however, may be an important factor in a mathematical expression from which heat-transfer rates are computed.

Thus this lack of confidence that an equation derived from the available data will apply to liquids with widely different physical properties suggested the work presented in this paper.

The main purpose of this investigation was to obtain data and, if possible, develop a mathematical relationship from which reliable heat-transfer coefficients for confined liquid heated from below could be determined.

To obtain this goal, five liquids with dissimilar properties were chosen for these tests.

[1] Numbers in brackets designate References at end of paper.

Contributed by the Heat Transfer Division of The American Society of Mechanical Engineers and presented at the Heat Transfer and Fluid Mechanics Institute, Berkeley, Calif., June 19–21, 1958.

Note: Statements and opinions advanced in papers are to be understood as individual expressions of their authors and not those of the Society. Manuscript received at ASME Headquarters, July 21, 1958.

Nomenclature

- C_p = specific heat at constant pressure, Btu/(lb)(F)
- C = constant, dimensionless
- f = function
- g = acceleration of gravity, ft/(hr)^2
- Gr = Grashof number, dimensionless, $L^3\rho^2 g\Delta t\beta/\mu^2$
- h' = special convective heat transfer coefficient, Btu/(hr)(ft^2)(F)
- k = thermal conductivity, Btu/(hr)-(ft)(F)
- L = height of container, ft
- m, n = exponents
- Nu = Nusselt number, dimensionless, $h'L/k$
- Pr = Prandtl number, dimensionless, $C_p\mu/k$
- q = rate of heat flow per unit area, Btu/(hr)(ft^2)
- Ra = Rayleigh number, dimensionless, Gr Pr
- β = coefficient of volumetric expansion, 1/F
- Δt = temperature difference between the top and bottom plate, F
- μ = dynamic viscosity, lb/(ft)(hr)
- ρ = liquid density, lb/ft^3

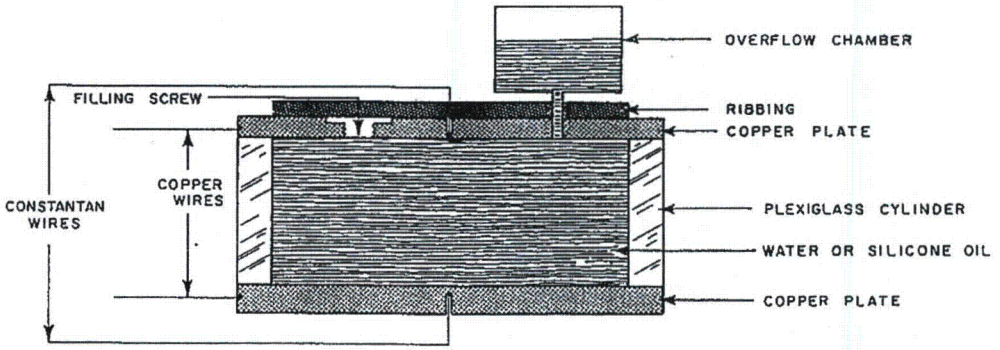

Fig. 1 Diagram of container for silicone oils and water

The liquids used were water, silicone oils of 1.5, 50, and 1000 centistokes kinematic viscosity, and mercury.

Procedure

The heat-transfer coefficient in geometrically similar containers was assumed to be subject to the generally accepted factors that influence convection, with the exception of L and Δt. The dimension L, the distance between the plates, was used as the characteristic distance, and Δt was used as the difference in temperature between the plates. Thus

$$h' = f[L, \rho, \mu, C_p, k, \Delta t, (\beta g)] \quad (1)$$

Without much difficulty we may derive by dimensional analysis the relationship

$$\frac{h'L}{k} = f\left(\frac{L^3\rho^2 g\beta\Delta t C_p}{\mu k}, \frac{\mu C_p}{k}\right) \quad (2)$$

Assuming the functional relationship to be given by a product of powers we get

$$\mathrm{Nu} = C\,\mathrm{Ra}^m\mathrm{Pr}^n \quad (3)$$

The Nusselt number here defined is an indicator of how effectively heat is transferred by convection as compared to that of conduction. When the Nusselt number is equal to 1, convection does not exist and heat is transferred by conduction.

The constant C and exponents m and n were determined from appropriate graphs of the test results.

The exponent m was determined from the plot of log Nu versus log Ra at a constant Prandtl number. Then all test data were plotted as log $\mathrm{Nu}/\mathrm{Ra}^m$ versus log Pr, and the exponent n and the constant C were found from the plot.

The physical properties of the liquids which were needed to compute the dimensionless numbers were determined at the mean temperatures of the upper and lower copper plates. For silicone oils, water, and mercury, the properties were taken from Dow Corning [3], Brown and Marco [4], and Liquid Metals Handbook [5], respectively.

All data were recorded when steady-state conditions were established. It was assumed that steady state was obtained when all readings remained constant for more than one hour.

For each run the electrical heat input to the lower plate, the temperatures of the two copper plates, and the temperature differences between the plates were measured.

The following experimental range was covered:

Prandtl number from 0.02 to 8750
Rayleigh number from $1.51(10)^5$ to $6.76(10)^8$
Nusselt number from 1.9 to 66.9
Temperature difference between the hot and cold copper plates from 2 to 80 F
Temperature of the hot copper plate from 75 to 198 F.

Apparatus

The test apparatus used in these experiments consisted of right-circular hollow cylinders with $^1/_4$-in-thick copper plates at the top and bottom, and insulating walls.

As shown in Fig. 1, the liquid container for the water and silicone-oil tests had an ID of 5 in. and a clear distance of 2 in. between plates. The cylindrical wall was made of plexiglas and attached to the plates with O-ring seals so that no leakage occurred. The heat from the upper plate was removed by blowing air over its surface. In order to improve the heat-transfer rate, the upper surface of the top plate was finned. The upper plate was also drilled and tapped, and connected with a $^1/_4$-in. nipple to an expansion chamber.

The temperatures of the plate surfaces were measured by copper-constantan thermocouples. The thermocouple junctions were located at the center of the plates and approximately 0.03 in. from the liquid surfaces. The wiring connections were such that the temperature differences as well as the individual temperatures of each plate could be determined. The thermocouples were connected to a recording potentiometer and a portable precision potentiometer. The recording potentiometer was used to indicate the time when steady state was established.

The mercury container is shown in Fig. 2. Two different heights were used: 1.39 and 2.62 in. The ID for both heights was 5.28 in. The side walls were made of pyrex glass and the copper-plate surfaces were chromium plated to prevent amalgamation of the copper. O-ring seals were used at the interface of the glass and copper plates, and the plates were bolted together through a transite ring. To remove the heat from the top plate a chamber was constructed above this plate and cold water was circulated through it. Provision was also made for the expansion of mercury. The overflow chamber, located off center, can be seen in Fig. 2.

As in the water and oil containers, temperatures were determined by the use of copper-constantan thermocouples and potentiometers. However, the thermocouples were connected so that only individual readings could be made. Direct reading of Δt was not possible because of the electrical path through the mercury.

An electric heater was used to supply the heat to the containers. In the early experiments a laboratory hot plate was used. Later, a heater was constructed from an element used in an electric cooking range and a $^3/_4$-in-thick aluminum plate attached at its top surface. The aluminum was used to assure even heat distribution.

The electrical input to the heaters was measured by a voltmeter and ammeter. A voltage regulator, connected in the electric circuit, insured constant voltage.

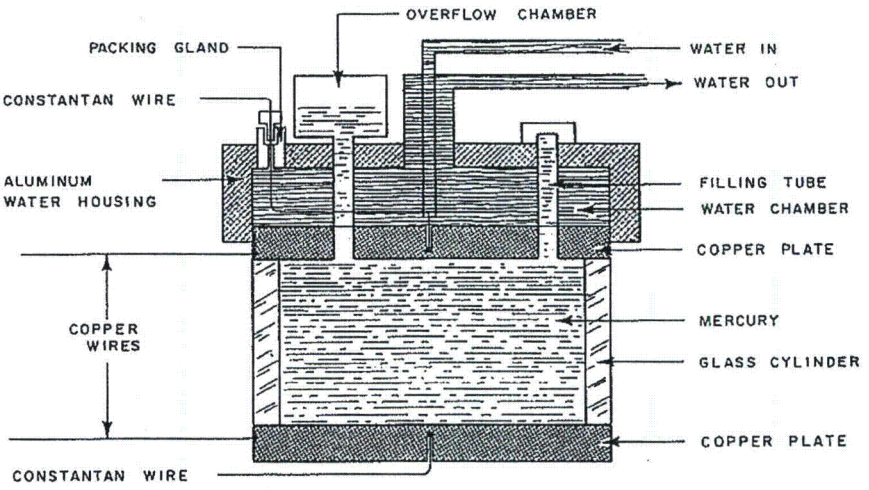

Fig. 2 Diagram of container for mercury

Method of Tests

The container was filled with the appropriate liquid and then placed in an evacuated chamber to eliminate any gas entrainment. When evolution of gas bubbles ceased, the container was put on the electric heater. This assembly was then placed in a large box and surrounded by about 3 in. of mineral wool.

The electrical input was adjusted to a predetermined value and the recording potentiometer connected to the thermocouples.

When the temperatures remained constant for one or more hours, the precision potentiometer was connected and used to determine the temperatures. For the experiments with mercury, in the region where the temperatures fluctuated, the recording potentiometer was used to estimate the average temperatures as well as the magnitudes of the fluctuations. The voltage and amperage to the heater were also recorded.

Results and Discussion

An analysis of the variation of the physical properties with temperature revealed that the Prandtl number for mercury remained practically unchanged within the experimental range of temperatures. This fact led to the logarithmic graph shown in Fig. 3. The straight line may be expressed by

$$\mathrm{Nu} = 0.051(\mathrm{Ra})^{1/3} \tag{4}$$

It should be noted that in Fig. 3, NuRa instead of Nu was used. This was done to improve the accuracy of the graph since the largest source of error is Δt. The convective-heat-transfer coefficient h' is determined from the relationship

$$q = h'\Delta t \tag{5}$$

The Nusselt number may be written as

$$\mathrm{Nu} = \frac{qL}{\Delta t k} \tag{6}$$

The Rayleigh number is

$$\mathrm{Ra} = \frac{L^3\rho^2 g\beta\Delta t C_p}{\mu k} \tag{7}$$

Thus an error in Δt creates errors of opposite sign in Nu and Ra. The product of the Nusselt and Rayleigh numbers is

$$\mathrm{Nu\ Ra} = \frac{qL^4\rho^2 g\beta C_p}{\mu k^2} \tag{8}$$

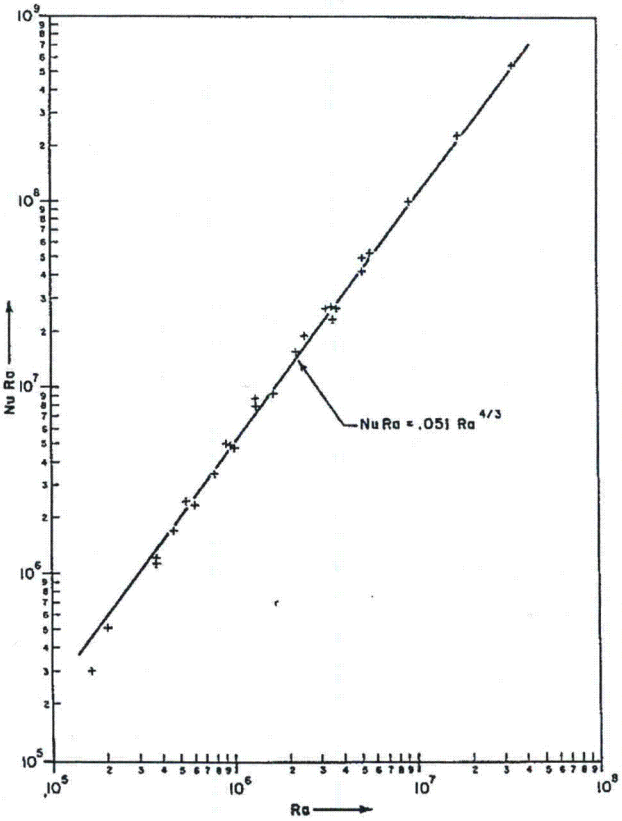

Fig. 3 Natural convection between horizontal plane surfaces in mercury

The Nu Ra may be considered a dimensionless heat flux while Ra is a dimensionless Δt. Nu Ra is independent of Δt, but dependent on q, which was known very precisely from the electrical readings. Fig. 3 is in effect a graph of heat transfer as a function of temperature difference and any possible error in Δt is not magnified because it appears only in Ra.

The fact that the exponent m is $1/3$ suggests that the natural convection is in the turbulent region. The point at which turbulence starts is a matter of some disagreement among various observers. Schmidt and Saunders [6], working with water, observed a transition to turbulence when Ra = 45,000. Jakob [1]

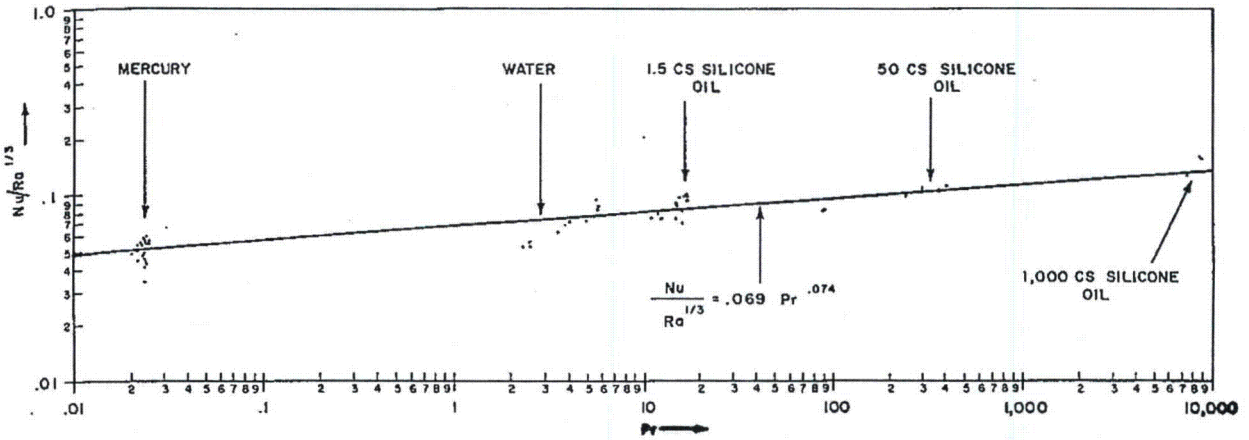

Fig. 4 $Nu/Ra^{1/3}$ versus Prandtl number for liquids

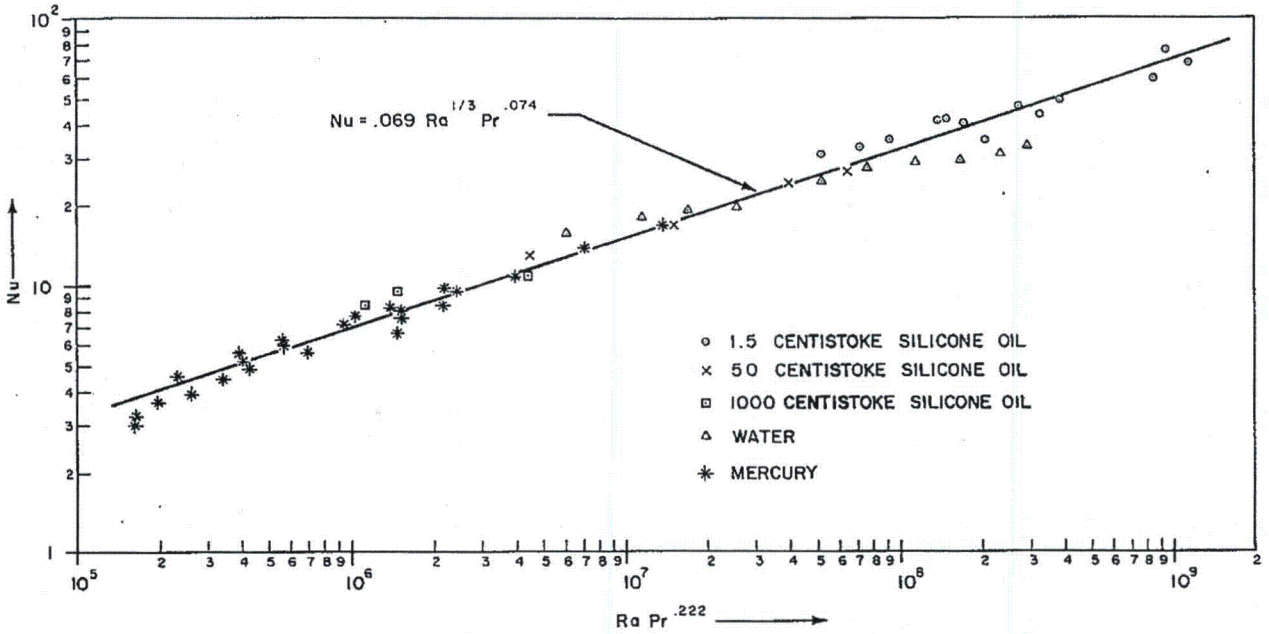

Fig. 5 Natural convection between horizontal surfaces in various liquids heated from below

correlating the data of Mull and Reiher on air sets the transition point at about Ra = 280,000. Malkus [2] in experiments with water and acetone observed changes at several different values of Rayleigh numbers. His lowest value of Ra is about 50,000.

The smallest value of Ra reported here is 151,000 and there were only two observations below 300,000. It may, therefore, be safely said that the results in this paper pertain to the turbulent region.

With the exponent m determined, we may now evaluate exponent n. This is done by plotting on logarithmic paper $Nu/Ra^{1/3}$ against Pr for all observations recorded in these tests.

The graph of this type is shown in Fig. 4. The slope of the line indicates that $n = 0.074$ and the resulting equation is

$$Nu = 0.069(Ra)^{1/3}(Pr)^{0.074} \quad (9)$$

The graph of equation (9) is shown in Fig. 5. The computed values for the five liquids are superimposed on this plot to show their deviations. It is seen that the points for water deviate slightly more than the points for other liquids. The reason for this is probably the sensitivity of physical properties to changes in temperature. We know that water is more temperature-sensitive than the other liquids tested. It is probable that determining physical properties at the arithmetic mean temperature of the two plates is only an approximation to the correct representation of convective heat transfer in a fluid whose properties change with temperature.

Equation (9) is in fairly good agreement with the results presented by the two previously mentioned observers. Jakob [1] in his analysis of the data of Mull and Reiher on air gives the relationship

$$Nu = 0.068(Gr)^{1/3} \quad (10)$$

Assuming for air a Prandtl number of 0.71, Equation (9) simplifies to

$$Nu = 0.060(Gr)^{1/3} \quad (11)$$

Malkus [2], basing his relationship on the data of water and acetone at room temperature, proposed the expression

$$Nu = 0.085(Ra)^{0.325} \quad (12)$$

for the turbulent region.

The Prandtl number for water at 70 F is 6.8. Using this value in Equation (9), we get

$$Nu = 0.080(Ra)^{1/3} \quad (13)$$

It is pertinent to point out here that the authors are convinced that the size of the containers used for the experiments reported in this paper had no bearing on the heat-transfer rates obtained. This conviction is based on the fact that for the mercury tests two containers were used with radically different ratios of diameter to height of liquid. Although the ratio was changed by a factor of almost two, in the region of overlap there appeared to be no difference in the results, and outside the overlap the observation fits the same relationship.

The data of Mull and Reiher and especially those of Malkus corroborate this conclusion. Malkus experimented with containers 4 in. in diam and from 0.05 to 3.2 in. in height. His conclusion was that the departure of the heat-transfer rate from a model of infinite horizontal extent is negligible.

In the experiments on mercury, turbulent fluctuations of temperature were observed at Rayleigh numbers above 10^5. These fluctuations appeared at both the upper and the lower plates. They increased in magnitude with increase in Rayleigh number and attained their largest value at $Ra = 3(10)^6$. Beyond this Rayleigh number, there was no increase of temperature fluctuation as a percentage of Δt. The largest possible fluctuation of Δt would occur when the individual plate fluctuations were out of phase. Thus the maximum difference between Δt for the lower-plate maximum temperature and upper-plate minimum temperature and Δt for the lower-plate minimum temperature and upper plate maximum temperature was found to be between ± 10 per cent of the average Δt. It is reasonable to assume that the net fluctuations in Δt were smaller than this, but since there was only one recorder, it was not possible to determine their true variations.

To investigate the possibility of lateral temperature gradients, a second thermocouple was attached to the lower plate. This thermocouple was located $1^1/_2$ in. away from the center of the plate and was used to determine temperatures at Rayleigh numbers above 10^6. The results showed that there was a negligible difference in temperature readings between the centrally located thermocouple and the one $1^1/_2$ in. away. The temperature fluctuations were similar in magnitude at the two points measured on the lower plate.

Conclusion

A mathematical expression has been developed for computing heat-transfer coefficients when liquids are heated from below. This equation is based on experimental data of liquids for a range of Prandtl numbers between 0.02 and 8750, and Rayleigh numbers between $1.5(10)^5$ and $6.8(10)^8$. The expression is

$$Nu = 0.069(Ra)^{1/3}(Pr)^{0.074}$$

The Nusselt and Rayleigh numbers include the thickness of the liquid layer as the characteristic geometric factor.

Acknowledgments

The authors gratefully acknowledge the efforts of Mr. R. Wetherby in the design of the containers, and Messrs. R. Levy and A. Kocsi for constructing and assembling the apparatus.

This work has been carried on under the financial support of the United States Air Force under contract No. AF-04(645)-30.

References

1 M. Jakob, "Heat Transfer," John Wiley & Sons, Inc., New York, N. Y., vol. 1, 1949, p. 534.

2 W. V. R. Malkus, "Discrete Transitions in Turbulent Convection," *Proceedings of the Royal Society (London)*, series A, vol. 225, 1954, p. 185.

3 "Dow Corning Silicone Notebook," Dow Corning Corporation.

4 A. I. Brown and S. M. Marco, "Introduction to Heat Transfer," McGraw-Hill Book Company, Inc., New York, N. Y., 1951, p. 243.

5 R. N. Lyons, "Liquid Metals Handbook," AEC and Bureau of Ships, Navy Department, second edition, 1952.

6 R. J. Schmidt and O. A. Saunders, "On the Motion of a Fluid Heated From Below," *Proceedings of the Royal Society (London)*, series A, vol. 165, 1938, p. 216.

7 R. C. L. Bosworth, "Heat-Transfer Phenomena," John Wiley & Sons, Inc., New York, N. Y., 1952, p. 104.

8 W. H. McAdams, "Heat Transmission," McGraw-Hill Book Company, Inc., New York, N. Y., 1954, p. 181.

WVMP SAR Reference 3-32

"Correlating Equations for Laminar and Turbulent Free Convection from a Vertical Plate," Churchill, S.W. and H. H. S. Chu, Int. J. Heat Mass Transport, 18(11), 1323-1329, 1975.

Int. J. Heat Mass Transfer. Vol. 18, pp. 1323–1329. Pergamon Press 1975. Printed in Great Britain

CORRELATING EQUATIONS FOR LAMINAR AND TURBULENT FREE CONVECTION FROM A VERTICAL PLATE

STUART W. CHURCHILL and HUMBERT H. S. CHU
Department of Chemical and Biochemical Engineering, University of Pennsylvania, Philadelphia, PA 19174, U.S.A.

(*Received* 2 *August* 1974 *and in revised form* 10 *February* 1975)

Abstract—A simple expression is developed for the space-mean *Nu* (or *Sh*) for all *Ra* and *Pr* (or *Sc*) in terms of the model of Churchill and Usagi. The development utilizes experimental values for *Ra* approaching zero and infinity, and the theoretical solutions obtained from laminar boundary-layer theory. The expression is applicable to uniform heating as well as to uniform wall temperature and for mass transfer and simultaneous heat and mass transfer. The correlation provides a basis for estimating transfer rates for non-Newtonian fluids and for inclined plates. Even simpler expressions are developed for restricted ranges of conditions. The general and restricted expressions are compared with representative experimental data. The structure of the correlating equation shows why the common power-law-type equations cannot be successful over an extended range of *Ra* and *Pr*.

NOMENCLATURE

a, arbitrary exponent;
A, dimensionless coefficient;
b, arbitrary exponent;
c, dimensionless coefficient;
$\mathscr{D}$, diffusivity [m^2/s];
$f\{Pr\}$, dimensionless function of Pr in equation (2);
$F\{m\}$, dimensionless function of power-law coefficient in equation (16);
g, acceleration due to gravity [m/s^2];
h, local heat-transfer coefficient [$J/m^2.s.°K$];
$\bar{h}$, mean heat-transfer coefficient over 0–z [$J/m^2.s.°K$];
k, thermal conductivity [$J/m.s.°K$];
k', local mass-transfer coefficient [s^{-1}];
$\bar{k}'$, mean mass-transfer coefficient over 0–z [s^{-1}];
K, coefficient defined by equation (15) [$kg/m\text{-}s^{2\text{-}m}$];
m, exponent defined by equation (15);
n, exponent in equation (1);
Nu, hz/k, local Nusselt number at z;
$\overline{Nu}$, $\bar{h}z/k$, mean Nusselt number over 0–z;
Pr, ν/α, Prandtl number;
q, heat flux density [$J/m^2\text{-}s$];
Ra, $g\beta(T_s-T_b)z^3/\nu\alpha$, Rayleigh number;
Ra', $g\gamma(\omega_s-\omega_b)z^3/\nu\mathscr{D}$, Rayleigh number for mass transfer;
Ra^*, $g\beta qz^4/k\nu\alpha$, modified Rayleigh number based on heat flux density;
Sc, $\nu/\mathscr{D}$, Schmidt number;
Sh, $k'z/\mathscr{D}$, local Sherwood number;
$\overline{Sh}$, $\bar{k}'z/\mathscr{D}$, mean Sherwood number over 0–z;
T, temperature [°K];
x, independent variable [m];
y, dependent variable [m];
z, distance up plate [m].

Greek symbols

α, thermal diffusivity [m^2/s];
β, thermal coefficient of expansion [$°K^{-1}$];
γ, dimensionless coefficient for expansion due to change in composition;
ω, mass fraction;
ν, kinematic viscosity [m^2/s];
$\varphi\{Pr\}$, dimensionless function of Pr in equation (8);
θ, angle of inclination of the plate from the vertical;
τ, shear stress [$kg/m\text{-}s^2$].

Subscripts

b, bulk;
s, surface;
0, limiting behavior for small z;
∞, limiting behavior for large z.

INTRODUCTION

A VARIETY of theoretical expressions, graphical correlations and empirical equations have been developed to represent the coefficients for heat and mass transfer by free convection from vertical plates. However, the discrepancies between the expressions proposed for correlation and the various sets of experimental data have still not been completely resolved or explained. The experimental anomalies are apparently due in part to physical property variations and undefined differences in the environment. The theoretical results are mostly limited to the intermediate range of Rayleigh number for which the postulates of laminar boundary-layer theory are applicable; a completely satisfactory theory has not been developed for either the diffusive regime (low Rayleigh numbers) or the turbulent regime (high Rayleigh numbers). The primary shortcoming of the empirical correlations is their failure to take into

proper account the *varying* dependence on the Rayleigh and Prandtl (or Schmidt) numbers.

This paper presents simple but very general correlations for the space-mean value of the transfer rate for free convection. The correlations are developed wholly in terms of the model of Churchill and Usagi [1]:

$$y^n\{z\} = y_0^n\{z\} + y_\infty^n\{z\} \tag{1}$$

and thus require appropriate expressions for the limiting behavior for both large and small values of the independent variable z.

Ede [2] provides a thorough review of the literature for heat transfer through 1964. In the interest of brevity, correlations, theoretical solutions and experimental data since that date will not be reviewed or analyzed except insofar as they are directly relevant to the derivations herein. The correlation is first developed in terms of heat transfer from an isothermal plate. Uniform heating, mass transfer, simultaneous heat and mass transfer, non-Newtonian fluids and inclined plates are subsequently considered.

LAMINAR REGIME

Boundary-layer theory has been utilized to derive relationships of the form:

$$Nu = Ra^{1/4} f\{Pr\} \tag{2}$$

where $f\{Pr\}$ represents a tabulation of values such as those summarized by Ede [2] for a number of values of Pr. Churchill and Usagi [1] derived an empirical expression in the form of equation (1) to provide a continuous approximation for these tabulated values of $f\{Pr\}$. This expression can be rewritten as follows in terms of $\overline{Nu}$:

$$\overline{Nu} = 0{\cdot}670 Ra^{1/4}/[1 + (0{\cdot}492/Pr)^{9/16}]^{4/9}. \tag{3}$$

Equation (3) represents the various computed values within 1 per cent from $Pr = 0$ to $Pr = \infty$ and is in general agreement for $10^5 < Ra < 10^9$ with the widely scattered experimental values compiled by Ede [2].

Equation (2) and hence equation (3) would be expected to become invalid for $Ra > 10^9$ owing to the onset of turbulence and as $Ra \to 0$ owing to thickening of the boundary layer relative to the distance from the starting edge of the plate. A generally accepted solution has not been derived for this latter regime. For pure conduction ($Ra = 0$) from an infinite strip $\overline{Nu} = 0$, but for a plate of finite dimensions $\overline{Nu}$ has a finite value. The experimental data of Saunders [5] indicate a limiting value of approximately 0·68, probably due to edge effects.

Utilizing 0·68 for $y_0\{z\}$ and the right side of equation (3) for $y_\infty\{z\}$ in equation (1) yields the following test expression for the entire laminar regime:

$$\overline{Nu}^n = 0{\cdot}68^n + \left(\frac{0{\cdot}670 Ra^{1/4}}{[1 + (0{\cdot}492/Pr)^{9/16}]^{4/9}}\right)^n. \tag{4}$$

A test plot of representative experimental data [2–13] in the form proposed by Churchill and Usagi [1] indicates that $n = 1$ is a reasonable choice, yielding

$$\overline{Nu} = 0{\cdot}68 + \frac{0{\cdot}670 Ra^{1/4}}{[1 + (0{\cdot}492/Pr)^{9/16}]^{4/9}}. \tag{5}$$

Equation (5) is seen in Fig. 1 to provide a good representation for all $Ra < 10^9$ while equation (3) is seen to be increasingly in error for $Ra < 10^5$.

LAMINAR PLUS TURBULENT REGIME

An asymptotic solution is not available for $Ra \to \infty$, but Churchill [14] has asserted on the basis of dimensional analysis that

$$Nu \to A Ra^{1/3} \varphi\{Pr\} \tag{6}$$

where A is an empirical constant and $\varphi\{Pr\}$ is a function which approaches unity for $Pr \to \infty$ and is proportional to $Pr^{1/3}$ for $Pr \to 0$. Equations (5) and (6) could be combined in the form of equation (1) to obtain a test expression for all Ra and Pr. However the limiting value of 0·68 proves to combine with equation (6) to produce a simpler and equally successful correlation. The resulting test expression is

$$\overline{Nu}^n = 0{\cdot}68^n + [A Ra^{1/3} \varphi\{Pr\}]^n. \tag{7}$$

Equation (7) provides a dependence of Nu on Ra for any positive n which increases continuously from the zeroth power to the 1/3-power as Ra increases. If equation (7) is to provide the same interrelationship between Ra and Pr in the laminar boundary-layer regime as equation (5) it is necessary that:

$$\varphi\{Pr\} = ([1 + (0{\cdot}492/Pr)^{9/16}]^{-4/9})^{4/3} = [1 + (0{\cdot}492/Pr)^{9/16}]^{-16/27} \tag{8}$$

The expression resulting from insertion of equation (8) in (7) also conforms to the asserted dependence for $Pr \to 0$ and ∞ as $Ra \to \infty$.

Bosworth [15] proposed an equation of the form of equation (7) with $\varphi\{Pr\} = 1{\cdot}0$ and $n = 1/2$ for $\overline{Nu}$ for free convection from horizontal cylinders in air. Trial plots indicate that $n = 1/2$ is a reasonable choice for the vertical plate as well. The straight line with a slope of 1/6 drawn in Fig. 2 through the same representative data as in Fig. 1 yields a value of $A = 0{\cdot}150$ and hence the final correlation:

$$\overline{Nu}^{1/2} = 0{\cdot}825 + \frac{0{\cdot}387 Ra^{1/6}}{[1 + (0{\cdot}492/Pr)^{9/16}]^{8/27}}. \tag{9}$$

This value of A is in reasonable accord with the value of $A\varphi\{Pr\} = 0{\cdot}10$, hence $A = 0{\cdot}12$, derived by Bayley [16] for air and also with the value of 0·13 proposed by Kutateladze [17] for a correlation in the form of equation (6) for turbulent free convection from vertical plates, cylinders and spheres to a number of fluids.

Equations (3) and (5) are plotted also in Fig. 2 for comparison and to indicate their limits of applicability. The undoubted superiority of equation (9) for $Ra > 19^9$ is somewhat obscured by the lack of data for truly high Ra, the scatter of the available data and the very condensed scale of the ordinate.

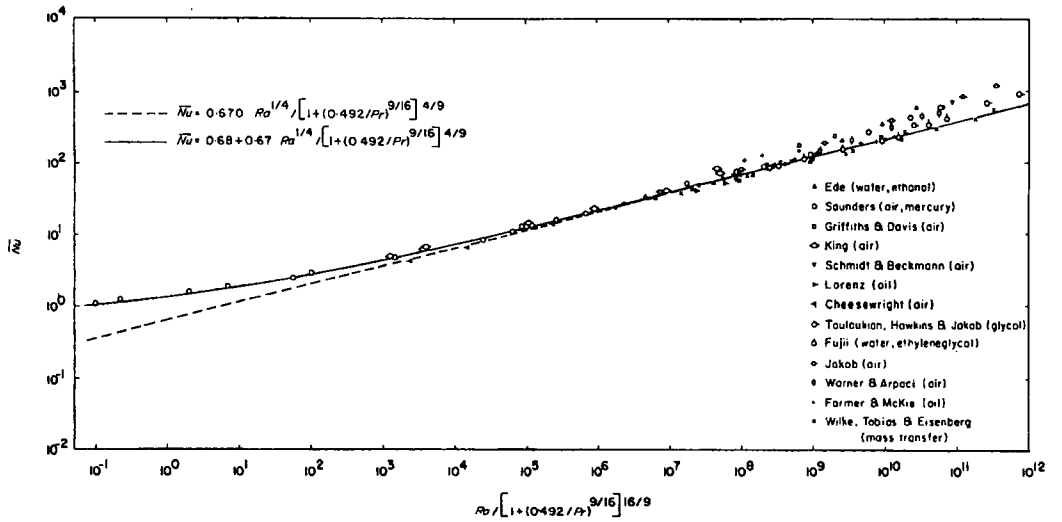

FIG. 1. Correlating equations for the laminar regime of isothermal, vertical plates.

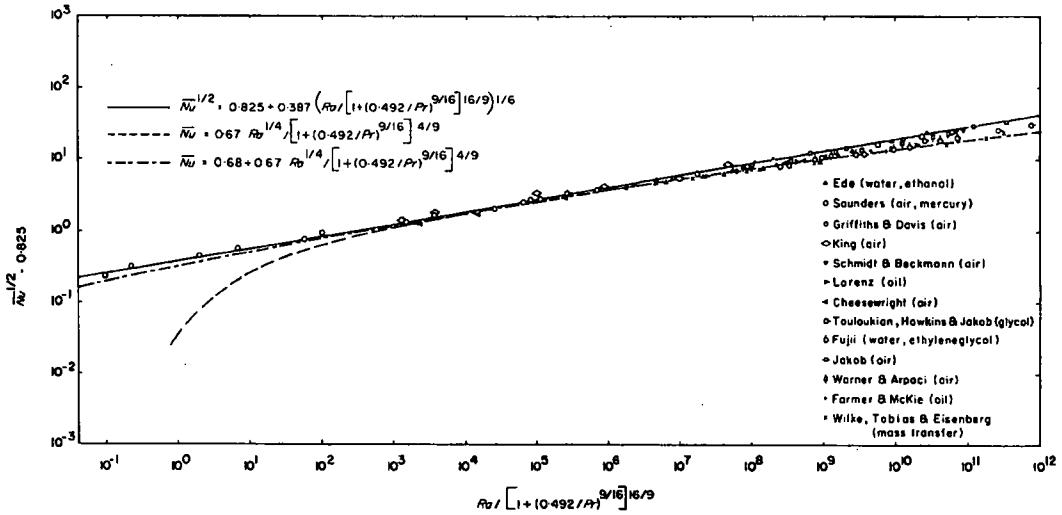

FIG. 2. Comparison of correlating equations with experimental data for isothermal, vertical plates.

INTERPRETATION

Computed values of $f\{Pr\}$ and $\varphi\{Pr\}$ for representative fluids are given in Table 1. The significant deviations for air and water from the limiting dependence for $Pr \to \infty$ indicate why the customary empirical equations of the form of equation (2) with $f\{Pr\} = 1{\cdot}0$ and equation (6) with $\varphi\{Pr\} = 1{\cdot}0$ have not proven satisfactory for a variety of fluids with a wide range of Pr. Table 1 also indicates that somewhat lesser but still significant discrepancies are to be expected with the simplified correlations for liquid metals based on the limiting form for $Pr \to 0$. A further variation in the dependence on Pr and Ra arises from the additive constant in equations (5) and (9). Thus empirical correlations of the form:

$$Nu = CRa^{a}Pr^{b} \tag{10}$$

cannot be expected to be successful over an extended range of Ra or Pr. Instead, the deviations from the correlations in the literature must be due in part to the choice of this form rather than wholly to experimental error. Such correlations appear to have outlived their usefulness.

Equation (9) provides a smooth transition from the laminar to the turbulent regime whereas the actual transition is known to be essentially discrete. The representation provided by equation (9) for this region is thus an oversimplification of reality and is numerically successful only because the effect of the transition is dampened by the integration which leads from the local to the mean Nusselt number. A correlation for the local Nusselt number extending through the transition from laminar to turbulent motion would need to be more complicated in structure than equation (9).

Table 1. Correction factor for various fluids from asymptotic behavior

Pr	Fluid	$f\{Pr\}$	$\varphi\{Pr\}$	$(0.492/Pr)^{1/4}f\{Pr\}$	$(0.492/Pr)^{1/3}\varphi\{Pr\}$
∞		1.000	1.000		
100	oil	0.978	0.971	0.259	0.165
7.0	water	0.914	0.887	0.471	0.366
0.70	air	0.766	0.701	0.702	0.623
0.024	mercury, 50°F	0.436	0.331	0.928	0.905
0.004	sodium, 1200°F	0.292	0.194	0.912	0.962
0				1.000	1.000

For large temperature differences such that the physical properties vary significantly, Ede [2] recommends that the physical properties be evaluated at the mean of the surface and the bulk temperature. Wylie [18] provides more detailed theoretical guidance for the laminar boundary-layer regime.

UNIFORM HEAT FLUX

The definition of the mean Nusselt number for uniform heating is somewhat arbitrary. However, Sparrow and Gregg [19] have shown that for a laminar boundary layer the use of the temperature difference at the midpoint of the plate yields values in better agreement with those for uniform wall temperature than the use of either the integrated mean temperature difference or the integrated mean heat-transfer coefficient. With this definition the following expression can be derived from the empirical representation of Churchill and Ozoe [20] for the local heat-transfer coefficient for uniform heating in a laminar boundary layer.

$$\overline{Nu} = 0.670Ra^{1/4}/[1+(0.437/Pr)^{9/16}]^{4/9}. \quad (11)$$

It may be noted that for $Pr \to \infty$ the coefficient of the Rayleigh number is indeed the same as that of equation (3) and that these expressions differ only by $((0.492/0.437)^{1/4}-1)100 = 3$ per cent even for $Pr \to 0$. [Equation (11) can be converted to one for the integrated mean temperature difference by multiplying the coefficient 0.670 by $(6/5)^{5/4}/2^{1/4}$ giving 0.708 and to the one for the integrated mean heat-transfer coefficient by multiplying by $(5/4)^{5/4}/2^{1/4}$ giving 0.745.]

Neither experimental data nor theoretical results appear to provide a limiting value of $\overline{Nu}$ for $Ra \to 0$. Hence the same value as for uniform wall temperature will arbitrarily be used. The exponent in equation (1) has generally been found to be the same for similar processes as illustrated by comparison of equations (3) and (11). Hence in the absence of experimental data the following expression is proposed for the entire laminar regime with uniform heating:

$$Nu = 0.68 + \frac{0.670Ra^{1/4}}{[1+(0.437/Pr)^{9/16}]^{4/9}}. \quad (12)$$

An equation of the form of equation (6) would be expected to hold for uniform heating as well as uniform wall temperature. Combining equation (6) with $\overline{Nu}_0 = 0.68$, forcing the same relationship between Ra and Pr as in equation (11) and assuming that 1/2 is again a satisfactory choice for n results in:

$$\overline{Nu}^{1/2} = 0.825 + \frac{A^{1/2}Ra^{1/6}}{[1+(0.437/Pr)^{9/16}]^{8/27}}. \quad (13)$$

A plot of a random selection from the limited sets of experimental data for uniform heating [21–24], in Fig. 3 in the form suggested by equation (13) again yields a value of $A = 0.15$, producing the following correlation for uniform heating for all Ra and Pr:

$$\overline{Nu}^{1/2} = 0.825 + \frac{0.387Ra^{1/6}}{[1+(0.437/Pr)^{9/16}]^{8/27}}. \quad (14)$$

Churchill [14] has asserted that Nu for fully developed turbulent motion ($Ra \to \infty$) should be the same for uniform heating as for wall temperature if a value independent of z, corresponding to a proportionality of Nu to $Ra^{1/3}$ is attained. This assertion is tested by plotting equation (9) for $Pr = 0.70$ in Fig. 3. Good agreement with the data may be noted as would be expected since equations (9) and (14) differ only slightly in one coefficient.

Free convection with uniform heating is often correlated in terms of Ra^* in order to avoid explicit inclusion of the surface temperature. Equations (11), (12) and (14) can be rewritten in terms of Ra^* simply by replacing $\overline{T_s - T_b}$ with $q/\bar{h}$, hence Ra with $Ra^*/\overline{Nu}$. However, this re-expression disguises the important result that the dependence of $\overline{Nu}$ on Ra is essentially the same as for uniform wall temperature.

INCLINED SURFACES

Vliet [25] has reviewed prior results for inclined surfaces and presented additional results for uniform heating. He concludes that for the laminar regime the solutions and correlations for a vertical plate may be used for a plate inclined up to at least 60° from the vertical if the component of gravity parallel to the surface is used in the Rayleigh number. However, the Rayleigh number for transition from laminar to turbulent motion is decreased drastically as the angle of inclination from the vertical is increased and his local results for the turbulent regime were better correlated in terms of g than in terms of $g \sin\varphi$.

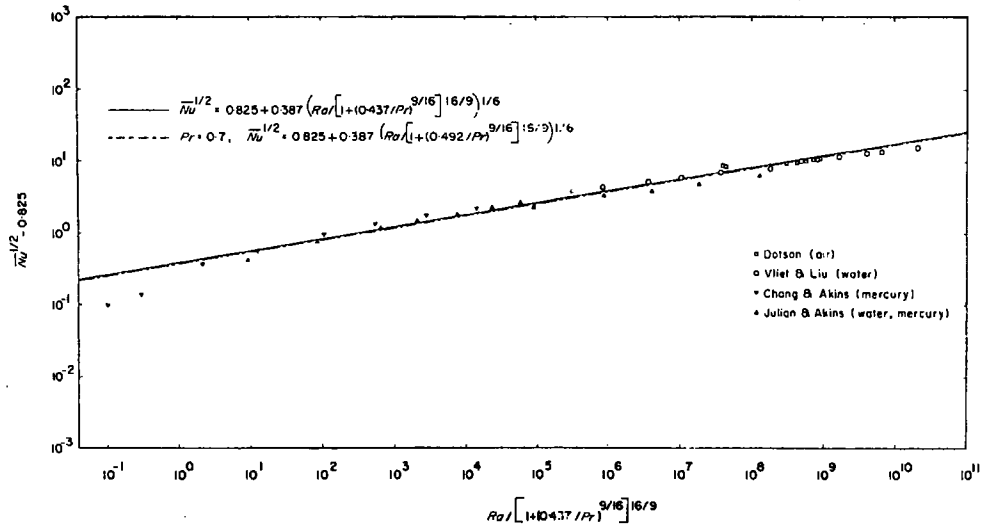

FIG. 3. Comparison of correlating equations with experimental data for uniformly heated, vertical plates.

MASS TRANSFER

Equations (5) and (9) with $\overline{Sh}$ substituted for $\overline{Nu}$, Sc for Pr, and Ra' for Ra are expected to hold for mass transfer as long as the net rate of mass transfer is not so high as to affect the velocity field significantly. Representative mass-transfer data [26] are included in Fig. 2 and reasonable agreement with equations (5) and (9) is apparent.

SIMULTANEOUS HEAT AND MASS TRANSFER

On the basis of the results of Saville and Churchill [27] and Lightfoot [28] for mass transfer due to a temperature gradient only $(\alpha(\omega_s-\omega_b)/\beta(T_s-T_b)\to 0$ and $Pr/Sc\to 0)$ $\overline{Sh}$ can be substituted for $\overline{Nu}$ and $Ra(Sc/Pr)^{4/3}$ for Ra in equation (9).

Also, on the basis of the results of Saville and Churchill [27] for simultaneous heat and mass transfer, $\overline{Nu}$ and Sh can be calculated from equation (9) for the special case of $Sc = Pr$ merely by substituting $Ra+Ra'$ for Ra. For $Sc \neq Pr$, the asymptotic solutions are not explicit and simple substitution in equation (9) is not possible [29].

NON-NEWTONIAN FLUIDS

For a power-law fluid such that:

$$\tau = -K\left|\frac{du}{dy}\right|^{m-1}\frac{du}{dy}. \tag{15}$$

Acrivos [30] has derived for $Pr\to\infty$ the following generalized form of equation (2):

$$Nu = F\{m\}\left(\frac{\rho g\beta(T_s-T_b)z^{2m+1}}{K\alpha^m\rho}\right)^{1/(3m+1)} \tag{16}$$

where $F\{m\}$ is a weak function of m and $F\{1{\cdot}0\} = 0{\cdot}670$. Equation (16) has been confirmed as a good representation for a number of fluids with $0{\cdot}6 \leqslant m \leqslant 1{\cdot}0$ by Agarwal *et al.* [30] for uniform wall temperature, and the analogue of equation (16) for uniform heating with $0{\cdot}4 < m < 1{\cdot}0$ by Chen and Wollersheim [32]. It follows that equation (5) with $f\{Pr\} = 1$ and equation (9) with $\varphi\{Pr\} = 1$ should be applicable for such fluids if $(\rho\beta(T_s-T_b)z^{2m+1}/K\alpha^m)^{4/3m+1}$ is susbsituted for Ra.

Fujii *et al.* [33] have obtained numerical solutions for a Sutterby fluid at finite Pr, and experimental results for aqueous solutions of polyethylene oxide. Their results indicate that Acrivos' solution may be a reasonable approximation for real fluids if the coefficients K and m are evaluated at the shear stress at the midheight of the heated plate.

CONCLUSIONS

1. Equation (9) based on the model of Churchill and Usagi provides a good representation for the mean heat transfer for free convection from an isothermal vertical plate over a complete range of Ra and Pr from 0 to ∞ even though it fails to indicate a discrete transition from laminar to turbulent flow.

2. Equation (14) provides an equivalent representation for heat transfer by free convection from a uniformly heated vertical plate. However, equation (9) is also an adequate representation for this boundary condition.

3. Equation (9) is applicable to mass transfer with $\overline{Sh}$, Ra' and Sc substituted for $\overline{Nu}$, Ra and Pr and can be applied for simultaneous heat and mass transfer for the special case of $Pr = Sc$ if $Ra+Ra'$ is substituted for Ra. Other such extensions are also possible.

4. More accurate representations for the laminar regime are provided by equations (5) and (12) and these simpler expressions should be used rather than equations (9) and (14) for $Ra < 10^9$. The expressions for the laminar regime are also applicable to mass transfer and simultaneous heat and mass transfer with the indicated substitutions.

5. Equations (5) and (12) are proposed as tentative representations for laminar convection from plates inclined up to at least 60° from the vertical if $g\sin\varphi$ is substituted for g. Based on the results of Vliet [25], equations (9) and (14) may be applicable for the turbulent regime without this modification. Fortunately

these equations are quite insensitive to the point of transition from laminar to turbulent motion.

6. Equations (9) with $Pr \to \infty$ is applicable to non-Newtonian fluids whose behavior can be represented by a power-law if $(\rho g \beta (T_s - T_b) z^{2m+1}/K\alpha^m)^{4/3m+1}$ is used for Ra.

7. The principal uncertainty in the correlations proposed herein arises from the uncertainty in the limiting solutions and experimental data for $Ra \to 0$ and ∞.

8. General correlations of the simple power-law type such as equation (10) are seen to be fundamentally unsound for any extended range of the variables and their use is no longer justified.

REFERENCES

1. S. W. Churchill and R. Usagi, A general expression for the correlation of rates of transfer and other phenomena, *A.I.Ch.E. Jl* **18**, 1121–1128 (1972).
2. A. J. Ede, Advances in free convection, in *Advances in Heat Transfer*, edited by J. P. Hartnett and T. F. Irvine, Jr., Vol. 4, pp. 1–64. Academic Press, New York (1967).
3. O. A. Saunders, Effect of pressure upon natural convection in air, *Proc. R. Soc.* **A157**, 278–291 (1936).
4. E. Griffiths and A. H. Davis, The transmission of heat by radiation and convection, DSIR Special Report No. 9, His Majesty's Stationary Office, London (1922).
5. W. J. King, The basic laws and data of heat transmission free convection, *Mech. Engng* **54**, 347–353 (1932).
6. E. Schmidt and W. Beckmann, Das Temperatur- und Geschwindigkeitsfeld vor einer Wärme abgebenden senkrechten Platte bei natürlichen Konvektion, *Tech. Mech. Thermo-dynam, Berlin* **1**, 341, 391 (1930).
7. N. H. Lorenz, Die Wärmeübertragung von einer ebenen senkrechten Platte an Öl bei natürlichen Konvektion, *Z. Tech. Phys.* **15**, 362–366 (1934).
8. R. Cheesewright, Turbulent natural convection from a vertical plane surface, *J. Heat Transfer* **90C**, 1–8 (1968).
9. Y. S. Touloukian, G. A. Hawkins and M. Jakob, Heat transfer by free convection from heated vertical surfaces to fluids, *Trans. Am. Soc. Mech. Engrs* **70**, 13–23 (1948).
10. T. Fujii, Experimental studies of free convection heat transfer, *Bull. J.S.M.E.* **2**(8), 555–558 (1959).
11. M. Jakob, Data as reported in Ede [2] above.
12. C. Y. Warner and V. S. Arpaci, An experimental investigation of turbulent natural convection at low pressure along a vertical heated flat plate, *Int. J. Heat Mass Transfer* **11**, 397–406 (1968).
13. W. P. Farmer and W. T. McKie, Natural convection from a vertical isothermal surface in oil, ASME Paper 64-WA/HT-12 (1964).
14. S. W. Churchill, An analysis of heat and component transfer by turbulent free convection from a vertical plate, *Proc. Chemeca '70*, Session 6A, pp. 1–16. Butterworths of Australia, Sydney (1970).
15. R. L. C. Bosworth, *Heat Transfer Phenomena*, p. 101. Wiley, New York (1952).
16. F. J. Bayley, An analysis of turbulent free convection heat transfer, *Proc. Instn Mech. Engrs* **169**(20), 361–370 (1955).
17. S. S. Kutateladze, *Fundamentals of Heat Transfer*, p. 294. Edward Arnold, London (1963).
18. R. G. Wylie, The transfer coefficients of a laminar boundary layer with variable fluid properties, *Chem. Engng* **6**, 1–14 (1973).
19. E. M. Sparrow and J. L. Gregg, Laminar free convection from a vertical plate with uniform surface heat flux, *Trans. Am. Soc. Mech. Engrs* **78**, 435–440 (1956).
20. S. W. Churchill and H. Ozoe, A correlation for laminar free convection from a vertical plate, *J. Heat Transfer* **95C**, 540–541 (1973).
21. J. P. Dotson, Heat transfer from a vertical plate by free convection, M.S. Thesis, Purdue University, Lafayette, Indiana (1954).
22. G. C. Vliet and C. K. Liu, An experimental study of turbulent natural convection boundary layers, *J. Heat Transfer* **91C**, 517–531 (1969).
23. B. H. Chang and R. G. Akins, An experimental investigation of natural convection in mercury at low Prandtl numbers, *Int. J. Heat Mass Transfer* **15**, 513–515 (1972).
24. D. V. Julian and R. G. Akins, Experimental investigation of natural convection heat transfer to mercury, *I/EC Fundamentals* **8**, 641–646 (1969).
25. G. C. Vliet, Natural convection local heat transfer on constant-heat-flux inclined surfaces, *J. Heat Transfer* **91C**, 511–516 (1969).
26. C. R. Wilke, C. W. Tobias and M. Eisenberg, Free convection mass transfer at vertical plates, *Chem. Engng Prog.* **49**, 663–674 (1953).
27. D. A. Saville and S. W. Churchill, Simultaneous heat and mass transfer in free convection boundary layers, *A.I.Ch.E. Jl* **16**, 268–273 (1970).
28. E. N. Lightfoot, Free-convection heat transfer: The limiting case of $Gr_{AB}/Gr \to 0$ and $Pr/Sc \to 0$, *Chem. Engng Sci.* **23**, 931 (1968).
29. J. W. Taunton, B. N. Lightfoot and W. E. Stewart, Simultaneous heat and mass transfer in laminar boundary layers, *Int. J. Heat Mass Transfer* **25**, 1927–1937 (1970).
30. A. Acrivos, A theoretical analysis of laminar natural convection heat transfer to non-Newtonian fluids, *A.I.Ch.E. Jl* **6**, 584–590 (1960).
31. B. K. D. Agarwal, K. S. Lieu and M. Adelman, Experimental verification of Acrivos' equation for laminar natural heat convection to non-Newtonian fluids, Personal communication.
32. T. Y. W. Chen and D. E. Wollersheim, Free convection at a vertical plate with uniform flux condition in non-Newtonian power law fluids, *J. Heat Transfer* **95C**, 123–124 (1973).
33. T. Fujii, O. Mujatake, M. Fujii, H. Tanaka and K. Murakami, Natural convective heat transfer from a vertical isothermal surface to a non-Newtonian Sutterby fluid, *Int. J. Heat Mass Transfer* **16**, 2177–2187 (1973).

LOIS DE CORRELATION EN CONVECTION NATURELLE LAMINAIRE ET TURBULENTE SUR UNE PLAQUE VERTICALE

Résumé—Une expression simple pour le nombre de Nusselt (ou de Sherwood) moyen est obtenue à l'aide du modèle de Churchill et Usagi pour tout nombre de Rayleigh et de Prandtl (ou de Schmidt). Au cours des développements il est fait usage de valeurs expérimentales du nombre de Rayleigh tendant vers zéro ou vers l'infini et de solutions théoriques obtenues en théorie de la couche limite laminaire. L'expression est applicable au transfert thermique à flux constant aussi bien qu'à température constante ainsi qu'au transfert de masse et au transfert simultané de chaleur et de masse. La loi de corrélation fournit une base de calcul des taux de transfert pour des fluides non newtoniens et pour des plaques inclinées. Des expressions tout aussi simples sont développées pour des domaines limités correspondant à des conditions particulières. Les expressions d'application générale et d'application restreinte sont comparées aux

données expérimentales représentatives. La structure de l'équation de corrélation fait apparaitre la raison pour laquelle les lois habituelles de type puissance ne peuvent s'appliquer sur un domaine étendu de nombres de Rayleigh et de Prandtl.

KORRELATIONEN FÜR LAMINARE UND TURBULENTE FREIE KONVEKTION AN EINER SENKRECHTEN PLATTE

Zusammenfassung—Nach einem Modell von Churchill und Usagi wurde eine einfache Beziehung für mittlere *Nu*-Zahlen (oder *Sh*) für alle *Ra* und *Pr* (oder *Sc*) entwickelt. Es sind dazu experimentelle Werte für *Ra* die gegen Null und unendlich gehen herangezogen und theoretische Lösungen, wie sie aus der Grenzschichttheorie erhalten werden. Die Beziehung ist anwendbar für gleichförmige Heizung, einheitliche Wandtemperatur, für Stoffübergang und gleichzeitigen Wärme- und Stoffübergang. Die Korrelation vermittelt eine Grundlage zur Bestimmung des Übergangs bei nichtnewtonischen Flüssigkeiten und für geneigte Platten. Für bestimmte Anwendungsbereiche werden einfachere Beziehungen angegeben. Die allgemeine Gleichung und die spezielle Beziehung werden vergliechen mit repräsentativen experimentellen Daten. Die Struktur der Korrelationsbeziehung gibt Aufschluß über das Versagen der allgemeinen Exponential-Gleichungen für einen ausgedehnten Bereich von *Ra* und *Pr*.

КОРРЕЛЯЦИОННЫЕ УРАВНЕНИЯ ДЛЯ ОПИСАНИЯ ЛАМИНАРНОЙ И ТУРБУЛЕНТНОЙ СВОБОДНОЙ КОНВЕКЦИИ ОКОЛО ВЕРТИКАЛЬНОЙ ПЛАСТИНЫ

Аннотация — С помощью модели Черчилля и Узаги получено простое выражение для осредненного по пространству значения числа *Nu* (или *Sh*) при любых значениях чисел *Ra* и *Pr* (или *Sc*). При выводе использовались экспериментальные данные для числа *Ra*, стремящегося к нулю и бесконечности, и аналитические решения, полученные на основе теории ламинарного пограничного слоя. Выражение применимо к случаям постоянного теплового потока, постоянной температуры стенки, а также для описания процессов массообмена и одновременного тепло- и массообмена. Корреляция дает возможность рассчитать скорости переноса в неньютоноских жидкостях и в случае наклонных пластин. Аналогичные, но более простые выражения получены для ограниченных диапазонов условий. Общее и частные выражения сравниваются на достоверных экспериментальных данных. Структура корреляционного уравнения позволяет объяснить тот факт, почему обычные уравнения типа степенных зависимостей не могут успешно применяться при больших диапазонах значений *Ra* и *Pr*.

WVMP SAR Reference 3-33

"Natural Convection Adjacent to Horizontal Surface of Various Platforms," Lloyd, J.R. and W. R. Moran, J. Heat Transf., 96(4), 1974.

Pages 443 through 447

J. R. Lloyd
Assoc. Professor.
University of Notre Dame.
Notre Dame, Ind.
Assoc. Mem. ASME

W. R. Moran[1]
Graduate Assistant.
University of Notre Dame.
Notre Dame, Ind.

Natural Convection Adjacent to Horizontal Surface of Various Planforms

Natural convection adjacent to horizontal surfaces of circular, square, rectangular, and right triangular planforms has been studied experimentally. Electrochemical techniques were employed involving a fluid with a Schmidt number of about 2200. The results encompass a wide range of Rayleigh numbers thus providing information on both the laminar and the turbulent regimes. The data for all planforms are reduced to a single correlation in the laminar and turbulent regimes using the characteristic length, as recommended by Goldstein, Sparrow, and Jones, $L^* = A/p$, where A is the surface area and p is the surface perimeter. The laminar data for all planforms are correlated by the expression

$$\mathrm{Sh} = 0.54\,\mathrm{Ra}^{1/4} \quad (2.2 \times 10^4 \leq \mathrm{Ra} \leq 8 \times 10^6)$$

and the data for the turbulent regime are correlated by the expression

$$\mathrm{Sh} = 0.15\,\mathrm{Ra}^{1/3} \quad (8 \times 10^6 \leq 1.6 \times 10^8)$$

Transition is found to occur at about $\mathrm{Ra} = 8 \times 10^6$. The present work thus significantly extends the Rayleigh number range of validity for the use of L^* through the 1/4 power laminar regime into the turbulent 1/3 power regime. It also demonstrates the validity of the use of L^* to correlate natural convection transfer coefficients for highly unsymmetrical planforms, which heretofore had not been demonstrated. Comparisons to analytical solutions and other experimental heat and mass transfer data are presented.

Introduction

This paper presents an experimental investigation of natural convection adjacent to horizontal surfaces of various planforms. The results encompass a wide range of Rayleigh numbers, including the laminar and turbulent flow regimes, for circular, square, rectangular, and right triangular planforms. An electrochemical technique was employed to obtain the natural convection mass transfer measurements. This technique has been used by many investigators in recent years to study mass transfer, as evidenced by the recently published review by Mizushina [1].[2] The electrolyte employed in the present investigation was an aqueous solution of cupric sulphate and sulphuric acid, wherein the Cu^{++} ions were the transferred ions and the sulphuric acid served as the supporting electrolyte. The boundary condition for these experiments was uniform concentration at the test surface, which is the counterpart of uniform surface temperature in the corresponding heat transfer problem. The Schmidt numbers were on the order of 2200 so that these results apply to the analogous high Prandtl number heat transfer problem. One of the advantages of using the present mass transfer technique over heat transfer experiments for high Prandtl number fluids is the fact that the property variations for the mass transfer experiments are essentially zero, whereas the corresponding heat transfer experiments exhibit large variation in properties. The present results apply to either the heated upward facing heat transfer surface or the cooled downward facing heat transfer surface.

A review of the literature reveals both analytical and experimental investigations of horizontal surfaces of various planforms. Analyses of the natural convection [2, 3, 4, 5] generally employ a boundary layer model applied to the two-dimensional problem of long thin rectangles. Suriano and Yang [6] solved the problem numerically for small and moderate Grashof numbers. It should be noted that the analyses give a 1/3-power dependence of the dimensionless transfer coefficients on the Rayleigh number for the laminar regime.

Experimentally, both heat and mass transfer investigations have been presented for horizontal surfaces e.g., [7-16]. The correlation between Nusselt number and Rayleigh number for the heat transfer problem which is the most widely accepted is that of Fishenden and Saunders [7]. Their experiments involved square planforms situated in air. The temperature differences involved were as high as 1000°F indicating extreme property variations and radiation corrections. Bosworth [8] provides very little information on his experiments, and Mikheyev [9] apparently used rectangular planforms, although this is not certain. Fujii and Imura [10] and Hassan and Mohamed [11] considered the horizontal upward facing surface as part of larger studies of heat transfer to inclined surfaces.

[1] Present address: Pratt and Whitney Aircraft, East Hartford, Conn.
[2] Numbers in brackets designate References at end of paper.

Contributed by the Heat Transfer Division and presented at the Winter Annual Meeting, New York, N. Y., November 17-22, 1974, of THE AMERICAN SOCIETY OF MECHANICAL ENGINEERS. Manuscript received by the Heat Transfer Division April 8, 1974. Paper No. 74-WA/HT-66.

Mass transfer natural convection experiments are provided by Fenech and Tobias [12], Wragg [13], Wragg and Loomba [14], Tobias and Boeffard [15], and Goldstein, Sparrow, and Jones [16]. References [12–15] used the same electrochemical technique employed herein. Fenech and Tobias [12] used electrodes embedded in the floor of the test cell. The electrodes had various widths and the length of each electrode stretched from one wall of the test cell to the other. Due to experimental difficulties only their wider test strips were used in their correlation and thus their results were only for the turbulent regime. Wragg [13] and Wragg and Loomba [14] used circular disks, but again embedded them flush in a surrounding collar. Tobias and Boeffard [15] studied both circular and rectangular horizontal electrodes surrounded by side walls. The side walls were both vertical and coplanar in nature. The object of this study was to determine the effect of the side walls and to determine the effect of electrode size on the mass transfer.

The work by Goldstein, Sparrow, and Jones [16] deserve special attention. They performed their experiments using naphthalene vapor sublimation. They investigated unshrouded circles, squares, and equilateral triangles, and proposed a characteristic length so that the results from these planforms could be correlated by a common expression. Heretofore this had not been possible. Unfortunately, their results did not span the full Rayleigh number range of the laminar flow regime, and did not contain any irregular or nonsymmetrical planforms.

The present results, to the best of the authors' knowledge, provide the only electrochemical mass transfer data for any free-standing, unshrouded planform. The results of the investigation are also the first for any mode of transfer involving the nonsymmetrical right triangle planforms. The Rayleigh numbers based on Goldstein, Sparrow, and Jones characteristic length range from 2.6×10^4 to 1.55×10^9, thus providing laminar, transition, and turbulent mass transfer information. By analogy, the results also apply to the corresponding isothermal horizontal surface heat transfer problem.

Data Analysis

In the present electrochemical mass transfer experiments, the total mass transfer rate of copper ions to the test surface was a result of three basic transfer mechanisms [21]: migration, convection, and diffusion

$$\dot{N} = \dot{N}_m + \dot{N}_c + \dot{N}_d \tag{1}$$

The three fluxes can be defined by the following relations which are all evaluated at the test surface

$$\dot{N}_m = Uc\frac{\partial \phi}{\partial y} \tag{2}$$

$$\dot{N}_c = vc \tag{3}$$

$$\dot{N}_d = -D\frac{\partial c}{\partial y} \tag{4}$$

The relative importance of each mechanism is revealed by examining their magnitudes under limiting current conditions. As explained in reference [1], under certain operating conditions, termed limiting current conditions, the concentration of the transferred species is essentially zero at the test surface.

Considering first the migration term, it is seen that $\dot{N}_m$ contains the transferred species conentration. Since this concentration is essentially zero at the surface, the entire term is, while in the presence of the supporting electrolyte where $\partial\phi/\partial y$ is small, negligibly small.

Next, consider the convection and diffusion terms together. Modeling the electrolyte solution as a binary mixture of copper ions as one component and the rest as the other component, reference [30] shows that $v = D/(1 - c/\rho)\,\partial(c/\rho)/\partial y$. Realizing that the concentration of the transferred species is approximately zero, the following is obtained

$$\dot{N}_c + \dot{N}_d = -\left(\frac{c/\rho}{1 - c/\rho} + 1\right) D\frac{\partial c}{\partial y} \cong -D\frac{\partial c}{\partial y} \tag{5}$$

Thus

$$\dot{N} \cong \dot{N}_d = -D\frac{\partial c}{\partial y} \tag{6}$$

The total rate of ion transfer is given in reference [21] as

$$\dot{N} = \frac{i}{n\mathrm{F}} \tag{7}$$

It is thus clear that the surface mass transfer is diffusive in nature which establishes the analogy between the present mass transfer experiments and the corresponding heat transfer problem.

It is possible now to define the mass transfer coefficient k in the same manner as is done in the analogous heat transfer problem

$$k = \frac{i}{n\mathrm{F}(c_\infty - c)} \cong \frac{i}{n\mathrm{F}c_\infty} \tag{8}$$

The dimensionless mass transfer number (analogous to the Nusselt number for the corresponding heat transfer problem) is given by the Sherwood number

$$\mathrm{Sh} = \frac{kL^*}{D} \tag{9}$$

Here D is the diffusion coefficient of the transferred species and L^* is the characteristic length. The characteristic length defined by Goldstein, Sparrow, and Jones [16] is

$$L^* = \frac{A}{P} \tag{10}$$

where A is the transfer area of the test surface and P is the perimeter. The Rayleigh number is

$$\mathrm{Ra} = \left[\frac{\zeta g(\zeta_\infty - \zeta_w)L^{*3}}{\mu^2}\right]\mathrm{Sc} \tag{11}$$

where Sc is the Schmidt number (analogous to the Prandtl num-

Nomenclature

A = surface area of transfer surface
c = transferred species concentration
D = diffusion coefficient of transferred species
F = Faraday number
g = gravitational acceleration
i = current density
k = mass transfer coefficient
L^* = characteristic length $L^* = A/p$
n = valence of transferred species
$\dot{N}$ = rate of mass transfer
p = perimeter of transfer surface
Pr = Prandtl number
Ra = Rayleigh number
Sc = Schmidt number
Sh = Sherwood number
t = transference number
U = ion mobility
v = convection velocity normal to test surface
y = distance normal to test surface
μ = viscosity
ζ = density
ϕ = electric field potential

Subscripts

c = due to convection
d = due to diffusion
m = due to migration
w = surface conditions
∞ = bulk conditions

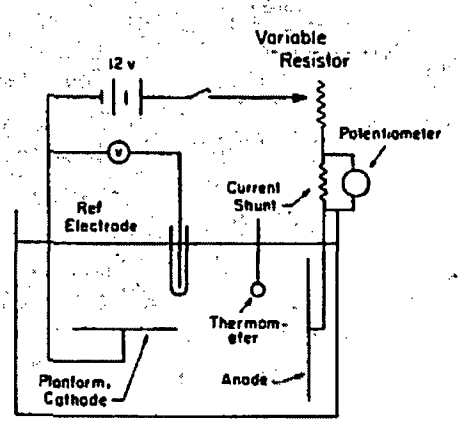

Fig. 1 Schematic of experimental apparatus

Table 1 Characteristic dimensions of various planforms

PLANFORM	CHARACTERISTIC DIMENSIONS, cm
CIRCLE (Diameter)	0.318
	0.592
	1.27
	5.08
	10.16
SQUARES (Length x Width)	0.635 x 0.635
	1.27 x 1.27
	12.7 x 12.7
RECTANGLES (Length x Width)	0.635 x 1.27
	2.54 x 1.27
	3.81 x 1.27
	6.35 x 1.27
	12.7 x 1.27
	12.7 x 2.54
	12.7 x 5.18
RIGHT TRIANGLES (Base x Height x Hypotenuse)	1.91 x 2.54 x 3.18
	1.27 x 1.91 x 3.29
	7.62 x 10.17 x 12.7
	15.25 x 20.3 x 25.4

ber) $\mu/\zeta D$; μ, ζ, and D are viscosity, density, and diffusion coefficient, respectively, at the average concentrations; and ζ_∞ and ζ_w are the fluid densities in the bulk and at the test surface, respectively. The properties were evaluated using the data of references [22-28], as described in reference [17]. As noted previously, property variations were practically nonexistent being 3 percent maximum. This is where this electrochemical technique has its major advantage over high Prandtl number heat transfer experiments.

Experimental Apparatus and Measurement Technique

A schematic of the experimental apparatus is presented in Fig. 1. A 30 gal polyethelene tank 61 cm × 45.6 cm × 45.6 cm (length × width × depth) served as the test chamber. The tank contained the electrolyte which was made up using reagent grade chemicals. The electrolyte solution was approximately 0.035 M $CuSO_4$ as the transferred species and 1.5 M H_2SO_4 as the supporting electrolyte.

The test surface was the cathode in the circuit. Table 1 provides a listing of the planforms tested and their characteristic dimensions. Each cathode was constructed of 0.635 cm thick copper. To the back side of each of the surfaces was attached a lead wire which connected to the main electrical circuit. The back and sides of the test pieces were carefully insulated with epoxy and Glyptal (an insulating paint). The test surface was held in position by a plexiglass holder. The lead wire was connected to a 12v automotive storage battery to provide the electric power. The potential of the cathode was measured relative to a reference electrode which consisted of a bare copper wire inserted into a glass tube. The glass tube had a small hole in the bottom to provide electrical contact between the reference electrode and the electrolyte solution. The potential was controlled with a series of precision variable resistors. The current flowing in the circuit, which is directly proportional to the mass transfer rate, was obtained by measuring the potential drop across a calibrated precision resistor, called a current shunt, with a Leeds and Northrup 8686 potentiometer. The anode was a large thin copper sheet 50 cm × 50 cm (length by width). It was purposely larger than the cathode so that the reaction would be totally controlled by conditions at the cathode.

To obtain a datum point the following procedure was followed. Prior to each test run the anode and cathode were carefully resurfaced and cleaned, essentially as described in reference [17], and then placed in the tank. The cathode was carefully leveled to provide a horizontal surface located about 15 cm off the bottom of the tank, and time was allowed for the system to come to complete equilibrium. Limiting currents, where the concentration of the transferred species is zero at the test surface [21], were determined in each run by noting the characteristic plateau in the current-potential curves in the voltage range between 0.40v and 0.50v as will be discussed further in a later section. The copper ion and sulphuric acid concentrations of the bulk solution were determined for each run by standard spectrometric and titration methods [18, 19]. Vertical bulk concentration gradients at the time of data acquisition were determined for each run to insure that all data would not be influenced by stratification. Finally, it should be noted that the length of each run was critical since it was necessary to operate long enough to insure steady operating conditions, but not so long as to generate any recirculation effects on the transfer at the surface. All data were taken so as to insure steady operating conditions without recirculation effects.

Results and Discussion

Before discussing the results of the experiments, a short discussion of the characteristic length is presented. The characteristic length employed in this investigation is that proposed by Goldstein, Sparrow, and Jones [16]. It was their "expectation" that this particular characteristic length would enable all horizontal planforms to exhibit a common correlation. Unfortunately, they investigated a more limited number of planforms and smaller Rayleigh numbers than in the present investigation. The present investigation should serve to prove or disprove their expectations.

As discussed earlier, limiting current-voltage curves as shown in Fig. 2 were generated in each run. Plotted in the figure on rectangular coordinates is the current density at the cathode versus the cathode voltage. As indicated in the figure, the plateau, signifying limiting current conditions, was reached in several steps. At each step, the system was allowed to reach steady conditions. All data were taken at cathode voltages of 0.40v to 0.50v to insure that limiting conditions had been reached. Current shunt signals for the laminar flow regime were very steady and could be read directly. In the turbulent regime the shunt signals fluctuated making it necessary to time average the data over a period of approximately two minutes, which was determined in the present investigation to be sufficient to obtain accurate time averages without encountering stratification effects. This time averaging was accomplished by recording the data digitally on the tape unit of a Hewlett Packard 2019A Data Acquisition System and then statistically averaging them on a computer.

Fig. 3 presents the data for the laminar flow regime. The Sher-

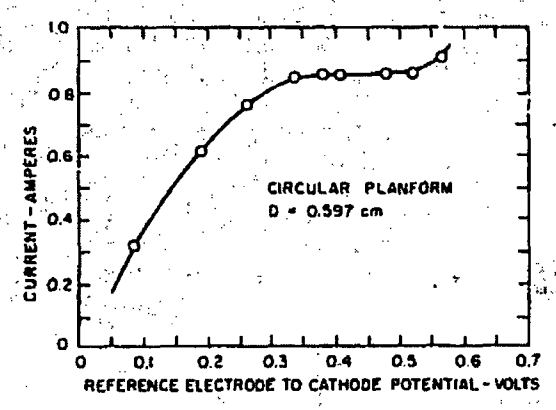

Fig. 2 Limiting current plateau

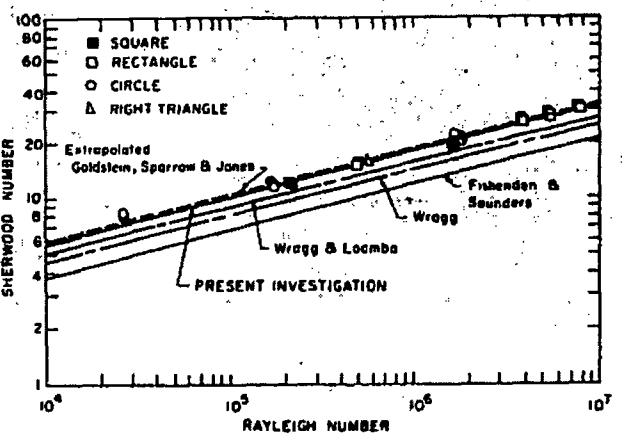

Fig. 3 Laminar mass transfer results

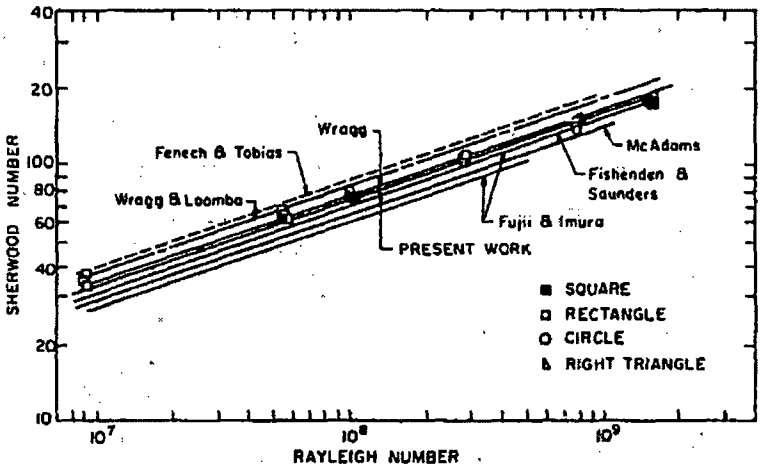

Fig. 4 Turbulent mass transfer results

wood number is plotted as a function of the Rayleigh number on logarithmic coordinates. The shape of the symbols reflect the planforms of the various surfaces as indicated in the upper left corner of the figure. It is immediately obvious that within the scatter of the data, approximately ± 5 percent, the data from all planforms are correlated through the use of L^*, including the nonsymmetric right triangle planform. This confirms the expectations of Goldstein, Sparrow, and Jones. A least squares fit through the data yields the relation

$$\mathrm{Sh} = 0.50\,\mathrm{Ra}^{0.255}$$

Forcing a slope of ¼, as has been reported in the literature for the heat transfer experiments, one finds the relation

$$\mathrm{Sh} = 0.54\,\mathrm{Ra}^{1/4}$$

for the data in the Rayleigh number range from 2.6×10^4 to 8×10^6.

Since L^* appears to correlate all the horizontal planforms, other published experimental results can be appropriately modified and compared to the present work. The data of Wragg and Loomba [14] and Wragg [13] can be compared directly to the present work since the same electrochemical technique was employed. Wragg and Loomba, it should be noted, is a revision of Wragg. They concerned themselves with circular surfaces which had a flush fitting collar surrounding their free-standing test surface. The revised data of Wragg and Loomba fall 10 percent below the present results. This difference could be a result, at least in part, from the presence of the surrounding collar.

The prediction of Goldstein, Sparrow, and Jones also involved mass transfer but at a much lower Schmidt number, approximately 2.5. Although their data only extended up to a Rayleigh number of 7×10^3, it is interesting that extension of their prediction into the Rayleigh number range covered in the present investigation falls very close to the present result. This would indicate that the Rayleigh number may be sufficient to account for Schmidt or Prandtl number variations.

Fig. 4 presents data for the turbulent flow regime. The Sherwood number is plotted as a function of the Rayleigh number on logarithmic coordinates. As in Fig. 3 the symbols reflect the planforms of the various surfaces. There does not appear to be any difference in the data for the various planforms. A least squares fit through the data for Rayleigh numbers greater than 8×10^6 provide the following correlation

$$\mathrm{Sh} = 0.169\,\mathrm{Ra}^{0.327}$$

If a ⅓ slope is enforced the best fit expression becomes

$$\mathrm{Sh} = 0.15\,\mathrm{Ra}^{1/3}$$

With the exception of two data points, the data scatter ±7 percent about this correlation.

The results of other investigators are also presented. The heat transfer correlations of Fishinden and Saunders [7] and McAdams [29] are seen to fall 4 to 12 percent lower than the present investigation. The data of Fujii and Imura [10] using water as the working fluid are perhaps the most interesting heat transfer data for comparison to the present work. They present two Nusselt num-

ber expressions, for the turbulent regime. Both have the form $Nu = C\ Ra^{1/3}$, but the value for C is 0.13 for Ra less than 5×10^8 and 0.16 for Ra greater than 2×10^8. The difference, they state, is due to edge effects on the surface. These experimental results using water as the surrounding medium have, within experimental scatter, essentially the same correlation as the present work when their edge effects are minimal. This would indicate again that the use of the Rayleigh number may be sufficient to account for Prandtl or Schmidt number effects.

The data of Fenech and Tobias [12], Wragg [13], and Wragg and Loomba [14] employed the same electrochemical techniques but with the previously discussed differences in the experimental setup. The data of Fenech and Tobias fall about 12 percent higher than the present data. This difference is in all probability due to the differences in the experimental setup as have been discussed earlier. The data of Wragg and Loomba are about 8 percent higher than the present work. It is important to note, however, that the correlation of Wragg and Loomba is a revised version of Wragg, due to the use of different physical properties, and that the correlation of Wragg, which uses almost the same values for properties as the present work, falls within the scatter of the present data. In this regime, the effect of the surrounding collar appears to be negligible, based on comparisons of Wragg's data to the present investigation.

Finally, the work of Tobias and Boeffard [15] deserves special mention. They considered the effect of both vertical and coplanar surrounding walls on the mass transfer to horizontal surfaces using the same experimental techniques. They found that the surrounding walls had no effect on the mass transfer correlation if the surfaces were large enough. For smaller electrodes their correlation underpredicts and it must be multiplied by a factor d_n, a number which is larger than one. When one considers their data in the light of the present investigation it appears that their size effect is related to the transition noted in the present work from the turbulent range to the laminar range. Indeed, if one takes Schmidt and Grashof numbers characteristic of the present data and use their expression to predict the Sherwood number for the turbulent regime, it is found that their prediction falls within the scatter of the present turbulent data. If one considers the small electrodes found in the laminar regime of the present work and applies the d_n correction discussed in their work, their Sherwood number prediction falls approximately within the scatter of the present work. Thus, it appears to be possible that their size effects, even with the surrounding walls, may be related to the difference between the laminar and turbulent flow regimes discussed in the present work.

Concluding Remarks

The present data are the first electrochemical mass transfer investigations of truly free-standing unshrouded horizontal surfaces. They also present the only data available for any mode of transfer involving right triangular planforms. The characteristic length as proposed by Goldstein, Sparrow, and Jones appears to bring all the data into a common correlation, even the nonsymmetrical surfaces such as the right triangles, for all Rayleigh numbers investigated. Special note should be made that the experimentally determined laminar correlation involves the ¼ power of the Rayleigh number whereas the laminar boundary layer analyses indicate a ⅕ power dependence. This is probably the result of using a boundary layer approach in the analyses.

It is highly encouraging to see data from circular, square, rectangular, and right triangular planforms exhibit a common correlation through the use of the characteristic length proposed by Goldstein, Sparrow, and Jones. There are indications that the use of the Rayleigh number in the mass or heat transfer relations is sufficient to account for Schmidt or Prandtl number variations. These observations, based on the experimental data, will enable calculation of transfer rates involving any shaped upward facing horizontal surface provided the transfer surface area and perimeter are known.

Acknowledgment

The authors gratefully acknowledge the support for this work provided by the National Science Foundation under Grant Number GK 32658.

References

1 Mizushina, T., "The Electrochemical Method in Transport Phenomena," *Advances in Heat Transfer*, Vol. 7, J. P. Hartnett and T. F. Irvine eds., Academic Press, New York, 1971.

2 Levy, S., "Integral Methods in Natural Convection Flow," *Journal of Applied Mechanics*, Vol. 77, No. 5, May 1955, pp. 515-525.

3 Stewartson, K., "On the Free Convection From a Horizontal Plate," *Z. Angew. Math. Phys.*, Vol. 9 a, 1958, p. 276.

4 Gill, W. N., Zeh, D. W., and del Casal, E., "Free Convection on a Horizontal Plate," *Z. Angew. Math. Phys.*, Vol. 15, 1965, p. 539.

5 Roten, Z., and Classen, L., "Natural Convection Above Unconfined Horizontal Surfaces," *Journal of Fluid Mechanics*, Vol. 39, Part I, Oct. 23, 1969, pp. 173-192.

6 Suriano, F. J., and Yang, K. T., "Laminar Free Convection About Vertical and Horizontal Plates at Small and Moderate Grashof Numbers," *International Journal of Heat and Mass Transfer*, Vol. 11, No. 3, Mar. 1968, pp. 473-490.

7 Pishenden, M., and Saunders, O. A., *An Introduction to Heat Transfer*, Oxford University Press, London, 1950.

8 Bosworth, R. L. C., *Heat Transfer Phenomena*, Wiley, New York, 1952.

9 Mikheyev, M., *Fundamentals of Heat Transfer*, Peace Publishers, Moscow, 1968.

10 Fujii, T., and Imura, H., "Natural Convection Heat Transfer From a Plate With Arbitrary Inclination," *International Journal of Heat and Mass Transfer*, Vol. 15, No. 4, Apr. 1972, pp. 755-767.

11 Hassan, K., and Mohamed, S. A., "Natural Convection From Isothermal Flat Surfaces," *International Journal of Heat and Mass Transfer*, Vol. 13, No. 12, Dec. 1970, pp. 1866-1873.

12 Fenech, E. S., and Tobias, C. W., "Mass Transfer by Free Convection at Horizontal Electrodes," *Electrochem. Acta*, Vol. 2, No. 3, Mar. 1960, pp. 311-321.

13 Wragg, A. A., "Free Convection Mass Transfer at Horizontal Electrodes," *Electrochem. Acta*, Vol. 13, No. 12, Dec. 1968, pp. 2159-2165.

14 Wragg, A. A., and Loomba, R. P., "Free Convection Flow Patterns at Horizontal Surfaces With Ionic Mass Transfer," *International Journal of Heat and Mass Transfer*, Vol. 13, No. 2, Feb. 1970, pp. 439-442.

15 Tobias, C. W., and Boeffard, A. L., "Ionic Mass Transport by Free Convection at Horizontal Electrodes," 17th General Meeting of CITCE, Sept. 5-9, 1966, Tokyo, Japan, pp. 23-24.

16 Goldstein, R. J., Sparrow, E. M., and Jones, D. C., "Natural Convection Mass Transfer Adjacent to Horizontal Plates," *International Journal of Heat and Mass Transfer*, Vol. 16, No. 5, May 1973, pp. 1025-1034.

17 Lloyd, J. R., Sparrow, E. M., and Eckert, E. R. G., "Local Natural Convection Mass Transfer Measurements," *J. Electrochem. Soc.*, Vol. 119, No. 6, June, 1972, pp. 702-707.

18 Sandell, E. B., *Colorimetric Determination of Traces of Metal*, Interscience Publishers, New York, 1950.

19 Kolthoff, I. M., and Sandell, E. B., *Textbook of Quantitative Inorganic Analysis*, Macmillan, New York, 1965.

20 Lloyd, J. R., Sparrow, E. M., and Eckert, E. R. G., "Laminar Transition and Turbulent Natural Convection Adjacent to Inclined and Vertical Surfaces," *International Journal of Heat and Mass Transfer*, Vol. 15, No. 3, Mar. 1972, pp. 457-473.

21 Wilke, C. R., Eisenberg, M., and Tobias, C. W., "Correlation of Limiting Currents Under Free Convection Conditions," *J. Electrochem. Soc.*, Vol. 100, No. 11, Nov. 1953, pp. 513-523.

22 Eisenberg, M., Tobias, C. W., and Wilke, C. R., "Selected Physical Properties of Ternary Electrolytes Employed in Ionic Mass Transfer Studies," *J. Electrochem. Soc.*, Vol. 103, No. 7, July 1956, pp. 413-416.

23 Vinal, G. W., and Craig, D. N., *J. Res. Nat. Bur. Std.*, Vol. 10, 1933, p. 781.

24 Cole, A. F. W., and Gordon, A. R., "The Diffusion of Copper Sulphate in Aqueous Solutions of Sulphuric Acid," *J. Phys. Chem.*, Vol. 40, No. 9, Sept. 1935, pp. 773-775.

25 James, W. A., Hollingshead, E. A., and Gordon, A. R., "The Differential Diffusion Constants of Hydrochloric and Sulphuric Acids," *J. Chem. Phys.*, Vol. 7, No. 2, Feb. 1939, pp. 89-92.

26 Hollingshead, E. A., and Gordon, A. R., "The Variation of the Differential Diffusion Constant of Sulphuric Acid With Temperature," *J. Chem. Phys.*, Vol. 8, No. 5, May, 1940, pp. 423-425.

27 Landolt-Bornstein, "Physikalish-Chemische Tabellen," *5 Auflage*, Vol. 1, 1936, pp. 248-397.

28 Dorsey, E. N., *Properties of Ordinary Water Substance in All Its Phases; Water Vapor, Water, and All the Ices*, Hafner Publishing Co., 1968.

29 McAdams, W. H., *Heat Transmission*, McGraw-Hill, New York, 1954.

30 Eckert, E. R. G., and Drake, Jr., R. M., *Heat and Mass Transfer*, McGraw-Hill, New York, 1959.

WVMP SAR Reference 3-34

Perry's Chemical Engineers' Handbook, 6th ed., McGraw-Hill, New York (1984).

Page 10-13

fluid friction, it has greater utility than other expressions for the heat-transfer coefficient.

The classical (and perhaps more familiar) form of dimensionless expressions relates, primarily, the Nusselt number hD/k, the Prandtl number $c\mu/k$, and the Reynolds number DG/μ. The L/D and viscosity-ratio modifications (for Reynolds number <10,000) also apply.

The **dimensional equations** are usually expansions of the dimensionless expressions in which the terms are in more convenient units and in which all numerical factors are grouped together into a single numerical constant. In some instances, the combined physical properties are represented as a linear function of temperature, and the dimensional equation resolves into an equation containing only one or two variables.

NATURAL CONVECTION

Natural convection occurs when a solid surface is in contact with a fluid of different temperature from the surface. Density differences provide the body force required to move the fluid. Theoretical analyses of natural convection require the simultaneous solution of the coupled equations of motion and energy. Details of theoretical studies are available in several general references (Brown and Marco, *Introduction to Heat Transfer*, 3d ed., McGraw-Hill, New York, 1958; and Jakob, *Heat Transfer*, Wiley, New York, vol. 1, 1949; vol. 2, 1957) but have generally been applied successfully to the simple case of a vertical plate. Solution of the motion and energy equations gives temperature and velocity fields from which heat-transfer coefficients may be derived. The general type of equation obtained is the so-called **Nusselt equation:**

$$\frac{hL}{k} = a\left(\frac{L^3\rho^2 g\beta\,\Delta t}{\mu^2}\,\frac{c\mu}{k}\right)^m \qquad (10\text{-}32a)$$

$$N_{Nu} = a(N_{Gr}N_{Pr})^m \qquad (10\text{-}32b)$$

Nusselt Equation for Various Geometries Natural-convection coefficients for various bodies may be predicted from Eq. (10-32). The various numerical values of a and m have been determined experimentally and are given in Table 10-1. Fluid properties are evaluated at $t_f = (t_s + t')/2$. For **vertical plates and cylinders** and $1 < N_{Pr} < 40$, Kato, Nishiwaki, and Hirata [*Int. J. Heat Mass Transfer*, 11, 1117 (1968)] recommend the relations

$$N_{Nu} = 0.138N_{Gr}^{0.36}(N_{Pr}^{0.175} - 0.55) \qquad (10\text{-}33a)$$

for $N_{Gr} > 10^9$, and

$$N_{Nu} = 0.683N_{Gr}^{0.25}N_{Pr}^{0.25}[N_{Pr}/(0.861 + N_{Pr})]^{0.25} \qquad (10\text{-}33b)$$

for $N_{Gr} < 10^9$.

Simplified Dimensional Equations Equation (10-32) is a dimensionless equation, and any consistent set of units may be used. Simplified dimensional equations have been derived for air, water, and organic liquids by rearranging Eq. (10-32) into the following form by collecting the fluid properties into a single factor:

$$h = b(\Delta t)^m L^{3m-1} \qquad (10\text{-}34)$$

Values of b in SI and U.S. customary units are given in Table 10-1 for air, water, and organic liquids.

Simultaneous Loss by Radiation The heat transferred by radiation is often of significant magnitude in the loss of heat from surfaces to the surroundings because of the diathermanous nature of atmospheric gases (air). It is convenient to represent radiant-heat transfer, for this case, as a **radiation film coefficient** which is added to the film coefficient for convection, giving the combined coefficient for convection and radiation ($h_c + h_r$). In Fig. 10-7 values of the film coefficient for radiation h_r are plotted against the two surface temperatures for emissivity = 1.0.

Table 10-2 shows values of ($h_c + h_r$) from single horizontal oxidized pipe surfaces.

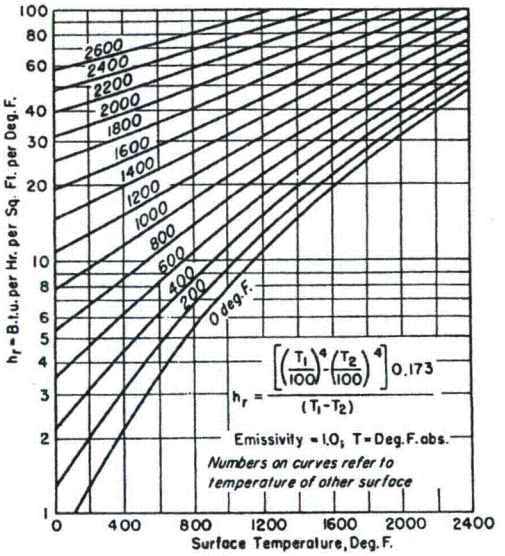

FIG. 10-7 Radiation coefficients of heat transfer h_r. To convert British thermal units per hour–square foot–degrees Fahrenheit to joules per square meter–second–kelvins, multiply by 5.6783; °C = (°F − 32)/1.8.

TABLE 10-1 Values of a, m, and b for Eqs. (10-32) and (10-34)

Configuration	$Y = N_{Gr}N_{Pr}$	a	m	b, air at 21°C	b, air at 70°F	b, water at 21°C	b, water at 70°F	b, organic liquid at 21°C	b, organic liquid at 70°F
Vertical surfaces	$<10^4$	1.36	1/6						
L = vertical dimension <3 ft	$10^4 < Y < 10^9$	0.59	1/4	1.37	0.28	127	26	59	12
	$>10^9$	0.13	1/3	1.24	0.18				
Horizontal cylinder	$<10^{-5}$	0.49	0						
L = diameter <8 in	$10^{-5} < Y < 10^{-3}$	0.71	1/25						
	$10^{-3} < Y < 1$	1.09	1/10						
	$1 < Y < 10^4$	1.09	1/6						
	$10^4 < Y < 10^9$	0.53	1/4	1.32	0.27				
	$>10^9$	0.13	1/3	1.24	0.18				
Horizontal flat surface	$10^5 < Y < 2 \times 10^7$(FU)	0.54	1/4	1.86	0.38				
	$2 \times 10^7 < Y < 3 \times 10^{10}$(FU)	0.14	1/3						
	$3 \times 10^5 < Y < 3 \times 10^{10}$(FD)	0.27	1/4	0.88	0.18				

NOTE: FU = facing upward; FD = facing downward. b in SI units is given in °C column; b in U.S. customary units, in °F column.